

# **ANALYSIS OF BRAZING EFFECTS ON HOT CORROSION BEHAVIOR OF AN AEROSPACE SUPERALLOY**

By

**NIYOUSHA ESMAEILI**

A thesis submitted to the Faculty of Graduate Studies of

The University of Manitoba

in partial fulfillment of requirements for the degree of

**Master of Science**

**Department of Mechanical and Manufacturing Engineering**

**University of Manitoba**

**Winnipeg**

Copyright © April 2017 by Niyousha Esmaili

## **Abstract**

Hot corrosion is a predominant type of degradation that takes place in gas turbine engine components. Wide-gap brazing is a commonly used method for joining extremely difficult-to-weld aerospace materials such as the superalloys used in gas turbine engines. Therefore, effects of brazing and use of different interlayer materials on hot corrosion resistance of brazed IN738 superalloy were studied. Brazing was observed to result in significant reduction in the hot corrosion resistance of the superalloy. However, application of composite powder mixture, which consists of additive superalloy powder, enhanced the hot corrosion resistance of brazed samples. It is also found that although the use of composite powder mixture increased hot corrosion resistance of brazed alloy, if the additive powder completely melts, which is possible during brazing, it can significantly reduce the hot corrosion resistance of the brazed joint. Elemental micro-segregation during solidification of the joint with completely melted powder mixture produces chromium depleted zones and consequently reduces hot corrosion resistance, since a uniform distribution and adequate chromium concentration is necessary to combat hot corrosion. This has not been previously reported in the literature and it is crucial to the use of composite powder mixture for enhancing the properties of brazed superalloys.

# Acknowledgement

I would like to express my deepest gratitude to my supervisor Dr. Olanrewaju Ojo, I am sincerely grateful to him for his precious guidance and encouragement throughout my Master program.

Special thanks to my department colleagues, specially, Dr. Lina Zhang, Olatunji Oluwadamilola, Gbenga Asala and my friend Kiana Amini. Their kindness and encouragement was invaluable. I would like to appreciate Mike Boskwick and Trevor Smith for their technical assistance and friendly manner.

I thank my mom, dad and my brother and best friend Shayan. I am grateful to them for their endless support and I acknowledge that I couldn't be the person I am now without them.

Above all, I am forever grateful to God for giving me wisdom and strength to complete this program.

# Dedication

I dedicate this master's thesis to

My parents

Words cannot express my appreciation

# Table of Contents

Abstract.....	i
Acknowledgement.....	ii
Dedication.....	iii
List of tables.....	vi
List of figures.....	vii
<b>CHAPTER 1 – INTRODUCTION.....</b>	<b>1</b>
<b>1.1 Background information.....</b>	<b>1</b>
<b>1.2 Research objective.....</b>	<b>3</b>
<b>1.3 Major findings.....</b>	<b>3</b>
<b>1.4 Thesis structure.....</b>	<b>4</b>
<b>CHAPTER 2 - LITERATURE REVIEW.....</b>	<b>5</b>
<b>2.1 Microstructure of Ni-base superalloys.....</b>	<b>6</b>
<b>2.1.1 Gamma matrix.....</b>	<b>6</b>
<b>2.1.2 Gamma prime precipitates.....</b>	<b>6</b>
<b>2.1.3 Carbides.....</b>	<b>7</b>
<b>2.2 Joining and repair techniques for Ni-base superalloys.....</b>	<b>7</b>
<b>2.2.1 Fusion welding.....</b>	<b>8</b>
<b>2.2.2 Diffusion brazing.....</b>	<b>11</b>
<b>2.2.3 Wide-gap brazing.....</b>	<b>11</b>
<b>2.3 Hot Corrosion.....</b>	<b>16</b>
<b>2.3.1 Formation of deposited salts on gas turbine components.....</b>	<b>16</b>
<b>2.3.2 Na<sub>2</sub>SO<sub>4</sub>–induced Hot Corrosion.....</b>	<b>22</b>
<b>2.3.3 Role of salt deposits in hot corrosion mechanisms.....</b>	<b>29</b>
<b>2.3.4 High temperature hot corrosion (Type I).....</b>	<b>32</b>
<b>2.3.5 Low temperature (Type II) hot corrosion.....</b>	<b>56</b>
<b>2.4 Scope of investigation.....</b>	<b>58</b>
<b>CHAPTER 3 – MATERIALS AND EXPERIMENTAL PROCEDURE.....</b>	<b>59</b>
<b>3.1 Experimental.....</b>	<b>59</b>
<b>3.2 Materials.....</b>	<b>59</b>
<b>3.2.1 Base material.....</b>	<b>59</b>

3.2.2 Composition of interlayer powders .....	59
3.3 Wide-gap brazing and microstructural analysis of brazed joints .....	62
3.3.1 Sample preparation and wide-gap brazing.....	62
3.3.2 Microstructural examination of brazed samples .....	62
3.4 Hot corrosion experiment.....	67
<b>CHAPTER 4 – RESULTS AND DISCUSSION.....</b>	<b>69</b>
4.1 Microstructure and Hot Corrosion Behavior of IN738 Base Alloy and Brazed Samples with 100% Conventional Brazing Filler Alloy.....	69
4.2 Microstructure and Hot Corrosion Behavior of Brazed Samples with (Nicrogap 108) Additive Powder .....	81
4.3 Microstructure and Hot Corrosion Behavior of Brazed Samples with other Additive Powders (IN738 and Haynes 282) .....	85
4.4 Microstructure and Hot corrosion Behavior of Brazed Samples with Completely Melted Additive Powder (IN738).....	90
4.5 Effect of Salt Mixture on Hot Corrosion Behavior of Brazed Samples with Completely and Partially Melted IN738 Additive Powder.....	95
4.6 Effect of Temperature on Hot Corrosion Behavior of Brazed Samples with Completely and Partially Melted IN738 Additive Powder.....	99
4.7 Effect of Completely Melted Additive Powder Containing High Amount of Cr (Haynes 282) on Hot Corrosion Behavior of Brazed Samples .....	102
4.8 Effect of Brazing Cycles on Hot Corrosion Behavior of IN738 Base Metal .....	105
<b>CHAPTER 5 - CONCLUSIONS AND SUGGESTIONS FOR FUTURE WORK .....</b>	<b>108</b>
5.1 Summary and conclusions.....	108
5.2 Suggestions for future work .....	109
<b>Bibliography .....</b>	<b>111</b>

## List of Tables

Table 3.1 – Chemical composition of IN 738 polycrystalline in as cast condition.....	60
Table 3.2 – chemical composition of regular brazing filler alloy.....	61
Table 3.3 – Chemical composition of additive powders used in this study.....	61
Table 4.1– SEM-EDS semi-quantitative metallic composition of eutectic constituents in the wide-gap brazed joint with 100% conventional brazing filler alloy.....	78

## List of Figures

Figure 2.1 – Illustration of different zones in fusion welded joint.....	10
Figure 2.2 – Schematic presentation of wide gap brazed joint with partially melted additive powders in the joint region.....	15
Figure 2.3 – General configuration of gas turbine engine [50].....	17
Figure 2.4 – Distribution of temperature on surface of first-stage blade from Rolls-Royce Conway engine [51].....	19
Figure 2.5 - Schematic presentation of hot corrosion stages.....	23
Figure 2.6 - Schematic presentation of phase stability diagram for Na-S-O system [57].....	31
Figure 2.7 - Schematic drawing indicating the situation that cause hot corrosion of metals and alloys [57].....	33
Figure 2.8 - Solubilities of various oxides in Na <sub>2</sub> SO <sub>4</sub> as a function of melt basicity [70].....	39
Figure 2.9 - Solubility of NiO in fused Na <sub>2</sub> SO <sub>4</sub> at 1200k [98].....	41
Figure 2.10 –Schematic indication of dissolution of protective oxide scale [106].....	44
Figure 2.11 - Schematic indication of Rapp and Gotto negative solubility criterion [106].....	45
Figure 2.12 - basicity and oxygen activity measured on a preoxidized Ni coupon with a Na <sub>2</sub> SO <sub>4</sub> film at 1173K in O <sub>2</sub> - 0.1% SO <sub>3</sub> gas [69].....	47
Figure 2.13 - solubility of Cr <sub>2</sub> O <sub>3</sub> in fused Na <sub>2</sub> SO <sub>4</sub> at 1200k for PO <sub>2</sub> = 1 atm [101].....	51
Figure 2.14 – Dominant chromium species in Na <sub>2</sub> SO <sub>4</sub> – Cr <sub>2</sub> O <sub>3</sub> system at 1200K [101].....	52



Figure 2.15 - Schematic presentation of the inhibiting action of chromium in hot corrosion attack by precipitation back on oxide grain boundaries and other defects [69].....	53
Figure 3.1 – configuration of samples.....	63
Figure 3.2 - The brazing cycle which was done at 1100°C for 1 hour.....	64
Figure 3.3–The brazing cycle used to obtain complete melting of Inconel 738 additive powder...	65
Figure 3.4 – Brazing cycle used to obtain complete melting of Haynes 282 additive powder.....	66
Figure 4.1 – SEM micrograph of MC carbide in cast IN738.....	70
Figure 4.2 – SEM micrograph of gamma prime precipitates on gamma matrix.....	70
Figure 4.3 - Hot corrosion behavior of IN738 base metal.....	71
Figure 4.4 – SEM-EDS X-ray mapping from oxide scale on IN738 base alloy.....	72
Figure 4.5 – Optical micrograph showing eutectic constituents in joint region of wide gap brazed sample with 100% regular brazing filler alloy.....	75
Figure 4.6 – (a and b) SEM micrographs of eutectic constituents in joint region of brazed sample with 100% filler alloy.....	76
Figure 4.7 - The hot corrosion behavior of IN738 samples which were brazed using the ‘100% filler alloy’ as the interlayer alloy.....	79
Figure 4.8 – Optical micrograph showing the uniform distribution of partially melted Nicrogap 108 additive powders in the joint region.....	83
Figure 4.9 - shows the hot corrosion curve for brazed samples with partially melted Nicrogap 108 as the additive powders.....	84

Figure 4.10 – Optical micrograph showing uniform distribution of partially melted IN 738 additive powder in joint region.....	87
Figure 4.11 - Optical micrograph showing uniform distribution of partially melted Haynes 282 additive powder in joint region.....	87
Figure 4.12 - shows the hot corrosion curve for brazed samples with partially melted IN738 as the additive powders.....	88
Figure 4.13 - shows the hot corrosion curve for brazed samples with partially melted Haynes 282 as the additive powders.....	89
Figure 4.14– Optical micrograph showing eutectic constituents in joint region of completely melted IN 738 additive powder.....	91
Figure 4.15 – Quant map analysis showing Cr distribution in the joint microstructure of completely melted IN 738 additive powder.....	92
Figure 4.16 – shows the hot corrosion curve for complete melting of Inconel 738 additive powder in joint region.....	93
Figure 4.17 - hot corrosion results for partially melted and completely melted Inconel 738 additive powder in 100% Na <sub>2</sub> SO <sub>4</sub> .....	96
Figure 4.18 – Hot corrosion results for partially melted and completely melted Inconel 738 additive powder in 50%NaCl + 50% Na <sub>2</sub> SO <sub>4</sub> .....	98
Figure 4.19 – Hot corrosion results for completely melted and partially melted Inconel 738 additive powder at 950°C.....	100

Figure 4.20 – Hot corrosion results for completely melted and partially melted Inconel 738 additive powder at 1000°C.....101

Figure 4.21 - Optical micrograph shows eutectic constituents in joint microstructure of completely melted Haynes 282 additive powder.....103

Figure 4.22 – Hot corrosion results for completely melted Haynes282 additive powder.....104

Figure 4.23–Hot corrosion results for base material without brazing for different heat treatment.....106

## **CHAPTER 1 – INTRODUCTION**

### **1.1 Background information**

Superalloys have been developed in response to the increasing demand for materials with higher resistance to corrosion and creep and also with higher mechanical strength at higher temperatures [1]. Superalloys contain nickel (Ni), cobalt (Co) or iron (Fe) as the base elements [2]. Among these, Ni-base superalloys are predominantly used in manufacturing hot sections of gas turbine engine components. This is due to their high strength and corrosion resistance in extremely high temperature service environments which is typical for hot sections of gas turbine engines [3]. Ni-base superalloys owe their high strength to precipitation hardening and solid solution strengthening mechanisms [4].

The continuous demand for higher efficiency and output has resulted in the use of higher operating temperatures and gas pressure in modern gas turbine engines [5] [6]. Consequently, this has caused thermal and mechanical stresses which result in severe degradation and damage of gas turbine engine components due to creep, fatigue and hot corrosion [7]. The decision to replace or repair damaged parts depends on the overall repair cost and expected life of the repaired components [6]. However, in most cases, it is more cost effective to repair damaged parts rather than use a full replacement [8].

Welding has been widely used to manufacture and repair turbine components [9]. However, this technique has been problematic when manufacturing or repairing parts with Ni-base superalloys, particularly, those that have high titanium (Ti) and aluminum (Al) contents. This is due to the high bonding temperature which causes microstructural changes and results in high susceptibility to

cracking in the heat affected zone (HAZ). Therefore, these superalloys are considered as difficult-to-weld materials.

To repair wide gaps or cracks in precipitation hardened Ni-base superalloy components used in gas turbine engines, wide-gap brazing has been the commonly applied method. The lower bonding temperature required produces a good quality joint with the least amount of detrimental effects on the substrate materials. The interlayer used in wide-gap brazing consists of a conventional filler alloy with a low temperature melting point mixed with an additive powder that has a high temperature melting point. The brazing temperature is higher than the melting point of the conventional brazing filler alloy powder but well below the melting point of the additive powder. Therefore, it is generally believed that the additive powder does not completely melt during brazing. However, recent studies show that it is possible to completely melt the additive powder during brazing [10] [11] [12].

It is important to mention that due to the significance placed on safety in the aerospace industries, the reliability of wide-gap brazed joints must be demonstrated to eliminate possible damage and degradation that may take place in the hot section components of gas turbine engines. It is well known that one of the most common types of degradation that takes place in the hot section components of gas turbine engines is caused by hot corrosion. Hot corrosion resistance of these components is very important because hot corrosion can result in the depletion of alloying elements (dealloying process), reduction in surface strength, initiation of cracks and eventually failure [13] [14] [15] [16] [17] [18] [19] [20] [21].

## **1.2 Research objective**

The objective of this research is to determine the effect of brazing on hot corrosion behaviour of wide-gap brazed joints, and how this is affected by the use of different interlayer materials.

## **1.3 Major findings**

To achieve the objective of this work, experimental investigations on the effect of brazing on the hot corrosion behavior of brazed samples are carried out. Brazing was found to result in significant reduction in the hot corrosion resistance of the alloy. The results also show that Inconel 738 joints brazed with a composite powder mixture (combination of conventional brazing filler alloy and additive powder) at a ratio of R<sub>7:3</sub> (70 wt.% conventional brazing filler alloy and 30 wt.% additive powder) have considerably better hot corrosion resistance compared to brazed samples that entirely use a conventional brazing filler alloy. Therefore, the addition of additive powder to conventional brazing filler alloy enhances the hot corrosion resistance. This is due to the uniform distribution of partially melted additive powder that contains a sufficient amount of chromium (Cr; 15%). In addition, despite the fact that the conventional brazing filler alloy used in this study also contains a large amount of Cr (15%), the brazed joints show reduced hot corrosion resistance compared to those that use the composite powder mixture. This is attributed to the high volume of liquid present in the joint during brazing which results in the segregation of the alloying elements and depletion of Cr in the Ni-rich boride phase. Therefore, the use of additive powder contributes to the hot corrosion resistance of a brazed joint. However, if the additive powder completely melts, which is possible during brazing [10] [11] [12], this can considerably reduce the hot corrosion resistance because there is a large volume of liquid in the joint due to the completely melted additive powder and consequently, the formation of phases which are depleted in Cr. This finding

has not been previously reported in the literature and it is crucial to the use of additive powder for enhancing the properties of brazed materials.

The results show that with increasing temperature and also the addition of sodium chloride (NaCl) to sodium sulphate ( $\text{Na}_2\text{SO}_4$ ) salt, the duration of the initiation stage is considerably reduced and the amount of weight loss is significantly increased correspondingly. Therefore, this condition provides a more severe hot corrosion environment which results in reduced hot corrosion resistance of the brazed samples.

It is important to note that in all of the experiments, hot corrosion attacks are localized in the joint region and the different brazing cycles used do not affect the hot corrosion resistance of the base metal.

## **1.4 Thesis structure**

The thesis is organized as follows.

- Chapter 1 is the introduction which contains background information, the research objective, major findings and details of the thesis structure.
- Chapter 2 provides a detailed literature review of Inconel 738 as the base material, and the different joining techniques; in particular, wide-gap brazing and hot corrosion mechanisms.
- Chapter 3 discusses in detail the experimental procedure, materials used, testing equipment as well as the preparation of the samples before and after brazing and hot corrosion testing.
- Chapter 4 provides the results and also a complete discussion of the results.
- Chapter 5 is the conclusion and outlines the recommendations for future work.

## **CHAPTER 2 - LITERATURE REVIEW**

The demand for stronger and more corrosion resistant alloys for high temperature applications has motivated engineers to develop stainless steel [9]. For many decades, stainless steel materials met high temperature engineering requirements; however, it was found that their high temperature strength capability is very limited [9]. Therefore, this led to the development of superalloys or high temperature heat resistant alloys [1]. These materials perform well in very high operating temperatures. Their operating temperatures can be as high as 25% less than their melting point and they maintain sufficient mechanical strength in the process [9]. Other properties of these alloys are their good oxidation and corrosion resistance and also excellent resistance to creep and rupture at high temperatures [1]. Generally, there are three types of superalloys: Fe-Ni-, Co-, or Ni-base superalloys [1]. Initially, Fe-base superalloys, which have a similar composition as modern austenitic stainless steel, were produced for high temperature applications [22]. However, the demand for greater efficiency resulted in the need for higher service temperatures, corrosion resistance and mechanical strength. Consequently, Co and Ni are used instead of Fe in these alloys [22]. Therefore, Fe-Ni-base superalloys are used at lower temperatures, while Co- and Ni-base superalloys are used according to the strength needed as well as the type of corrosive environment [9]. It is important to mention that the development of Ni-base superalloys has resulted in a significant increase in their strength at high temperatures, which have been increased almost sevenfolds in studies carried out between 1940 and 1970 [23]. As a result of this newfound increase in strength, Ni-base superalloys have been dominantly used in manufacturing hot sections of gas turbine engine components because of their unique ability to maintain high strength and corrosion



resistance in extremely high temperature service environments [3]. This desirable characteristic for manufacturing turbine engines is attributed to the microstructure of the Ni-base superalloys.

## **2.1 Microstructure of Ni-base superalloys**

### **2.1.1 Gamma matrix**

The microstructure of Ni-base superalloys consists of an austenitic face-centered cubic (FCC) crystal structure matrix, otherwise known as a gamma matrix, which can accommodate a considerable amount of solid solution strengthening elements, such as Cr, molybdenum (Mo), tungsten (W), Co, Fe, Ti and Al [1]. The 1 to 13 percent difference between the atomic diameter of these alloys and Ni provide considerable distortion of the lattice; therefore, dislocation movements are impeded and consequently, the strength of the matrix is increased through solid solution strengthening [1] [24].

### **2.1.2 Gamma prime precipitates**

The gamma prime phase can be precipitated into the gamma matrix through precipitation hardening heat treatment [1]. These FCC precipitates, which are an  $A_3B$ -type compound, have very low lattice mismatch with the gamma matrix, so they can coherently precipitate with very long-term stability [1]. In Ni-base superalloys, the large volume fraction of gamma prime precipitates, which is  $Ni_3(Al, Ti)$ , is the main reason for the high strength of the superalloys in high temperature environments [25] [26].

### **2.1.3 Carbides**

The microstructure of Ni-base superalloys also consists of carbides. These intermetallic compounds have the role of preventing dislocation movements and grain boundary sliding at high temperatures, consequently increasing high temperature strength and creep resistance of the materials [1] [22]. However, they can be detrimental if present in large quantities. They may also have an undesirable morphology and distribution which can cause material embrittlement [1] [27]. There are typically three types of carbides that form in Ni-base superalloys, namely: metal carbides (MC), and  $M_{23}C_6$ , and  $M_6C$  complex carbides. The metals include Ti, tantalum (Ta), niobium (Nb), and W.

The mentioned significant increase in the high temperature strength of Ni-base superalloys is not only achieved by increasing solid solution strengthening and precipitation hardening but also through the optimum distribution and morphology of carbides [1].

## **2.2 Joining and repair techniques for Ni-base superalloys**

With the advancement of science and technology, the operating temperature and gas pressure of modern gas turbine engines are continuously being increased due to the demand for higher efficiency and output [5] [6]. Consequently, turbine components are required to withstand higher temperatures and thermal and mechanical stresses which result in their rapid deterioration due to fatigue, creep and hot corrosion [7]. The decision to replace or repair the damaged parts depends on the overall repair cost and expected life of the repaired components [6]. However, in most cases, it is more cost effective to repair the damaged parts rather than put in a full replacement [8]. The complex microstructure of these improved materials accompanied with the increasing costs to

replace damaged components have resulted in the ongoing need to enhance manufacturing and repairing processes used on gas turbine engine components [28]. Among the various kinds of repairing and joining techniques, fusion welding and brazing are the most common methods used for joining high temperature materials.

### **2.2.1 Fusion welding**

Fusion welding, a method for joining materials, is used in many industries, such as ship building, automotive and power generation industries, and also for manufacturing and repairing gas turbine components in the aerospace industries [29] [30] [31]. Fusion welding involves the concentration of highly localised heat energy onto a comparatively small joint region during bond creation, which is followed by melting and subsequent solidification of the joint region [31]. Therefore, the base material remains at a lower temperature compared to the weld region. As a result, there is a substantial difference in temperature between the weld region and base metal during the fusion welding process [29]. The filler materials utilised have the same or similar composition as the base alloy being used, but for joints with a wide-gap size, a filler metal with lower melting point than the base material is used to ensure that the completely melted filler can flow between the faying surfaces [32].

There are three types of fusion welding which are differentiated based on the heat sources used:

1. gas welding (uses gas),
2. arc welding (uses electricity), and
3. laser beam welding (uses laser beams).

### **2.2.1.1 Limitations of fusion welding**

Fusion welding has been widely used for the fabrication and repair of turbine components [9]. However, this method has limitations when welding or repairing precipitation hardened Ni-base superalloys, particularly, those with high Ti and Al contents ( $> 6\%$  Al+Ti) due to the microstructural changes that result from localised heat input around the joint region which is known as the Heat Affected Zone (HAZ). The microstructural changes involve the dissolution and rapid precipitation of gamma prime precipitates in the HAZ during the period of cooling down from welding, which result in residual stress and consequently cracks in this region [33]. The high temperature gradient produced during welding results in stress concentration which significantly reduces the fatigue resistance of the HAZ compared to that of the base metal [11]. Therefore, fusion welding is not a suitable technique for joining or repairing gamma prime precipitation hardened Ni-base superalloys.

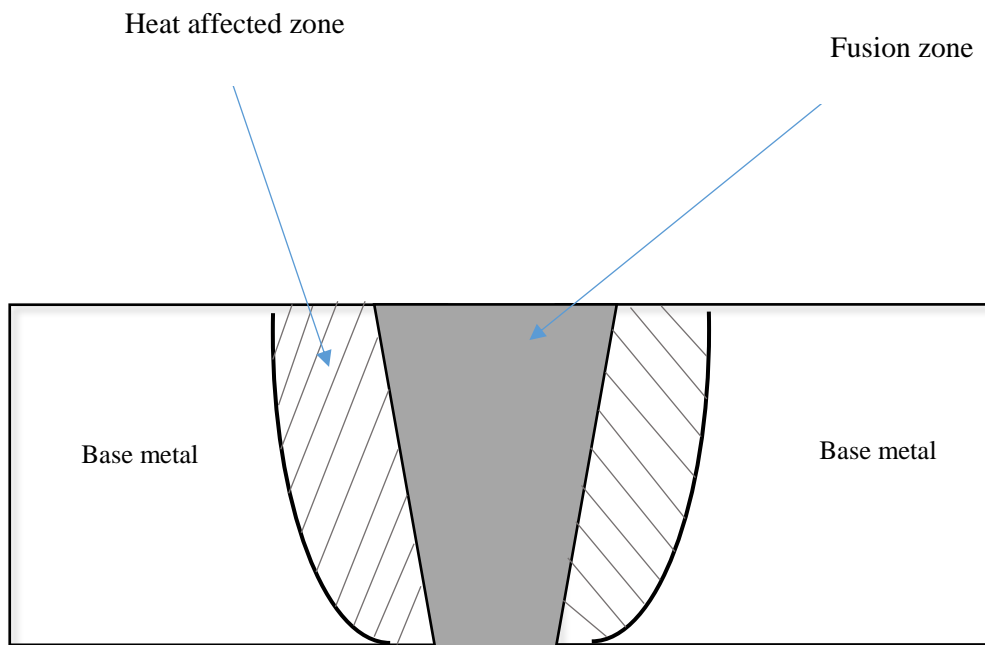


*Figure 2.1 – Illustration of different zones in fusion welded joint.*

### **2.2.2 Diffusion brazing**

To overcome some of the difficulties associated with fusion welding, diffusion brazing was carried to join precipitation hardened superalloys [34]. The high temperature and applied pressure utilised in diffusion brazing will melt the filler material so that it flows through capillary action between the joined surfaces, and there is interdiffusion of the atoms across the mating surfaces. Consequently, a bond with good mechanical properties will form [11] [34] [35]. The major advantage of using this technique over fusion welding is the relatively low temperature used in the process, and therefore high quality joints with the least amount of detrimental effects on the substrate materials are possible. However, one of the limitations in repair operations that use diffusion brazing is the need for high process tolerance so that it is necessary to prepare the surface and ensure that the size of the joint is appropriate but still be able to achieve the desired mechanical properties [28]. In this type of brazing, which is based on capillary action to work well, the clearance (or width) of the joint should be about 0.15 mm or less [36] [37]. However, this limits the extensive use of diffusion brazing in the aero engine component manufacture and repair sector because close tolerances are expensive to produce. In addition, cracks sustained in these components, due to service, are often much larger in width [38]. Therefore, a wide-gap is commonly used for these conditions which is difficult to meet the clearance requirement due to machining and assembly errors, and also when the parts to be joined have a complicated or non-uniform geometry [39].

### **2.2.3 Wide-gap brazing**

Wide-gap brazing has been widely used to repair and join the hot section components of aero engines which are manufactured from precipitation hardened Ni-base superalloys [38]. In the past

decades, this technique has invited much interest due to the extensive development of second generation aero engines made from materials that are hard-to-weld with more complex designs [39]. This technique is also well suited for situations where components are so severely degraded that welding alone is not sufficient and can also result in considerable mechanical distortion [39]. In diffusion brazing, the filler metal flows through the capillary attraction between the closely fitted surfaces of the joint [39]. For diffusion brazing to be successful, it is necessary that the molten filler alloy is drawn and retained in the joint gap through capillary forces [39]. However, wide-gap brazing of large components involves non-capillary gaps [40] [41] [42]. Consequently, the solution is to use conventional brazing filler alloy powder together with a second type of alloy powder in the joint gap for the brazing process [39].

In contrast to diffusion brazing where only conventional brazing filler alloy is used, wide-gap brazing involves the use of a composite powder mixture which consists of a conventional brazing filler alloy powder and a high temperature melting point base-alloy powder (additive powder) [8] [39]. The former contains a melting point depressant (MPD) which reduces the melting point and provides excellent wetting and flow performance [43] while the latter has no MPD solute. Consequently, the conventional brazing filler alloy powder has a much lower melting point than the additive powder [8]. In the wide-gap brazing process, the temperature is above the solidus of the conventional brazing filler alloy powder but lower than that of the additive powder. Therefore, the additive powder particles remain mostly unmelted. This provides the required capillary force to keep the molten brazing filler metal in the gap which would otherwise be too fluid to remain there [28] [39]. Consequently, this composite powder mixture behaves like slurry during brazing and has sufficient bridging power to fill wide cracks and gaps, and also to rebuild large surface areas of airfoils [44]. The additive powder is commonly used for its high melting temperature,

good environmental resistance and high strength [45]. Most of the time, its composition is similar to that of the base alloy material that is being repaired [45]. In addition, it reacts with the conventional brazing filler alloy through dissolution and an alloying reaction to enrich the joint region with the desirable alloying elements. Therefore, the additive powder enhances the mechanical and chemical properties of the joint region [8] [39]. During wide-gap brazing, as the temperature reaches the brazing temperature, the filler alloy powder melts and reacts with both the additive powder and base metal. At the same time, the MPD in the molten filler alloy diffuses into the additive powder and the base material which reduces its concentration in the liquid to an equilibrium liquidus value at the brazing temperature [8] [44]. This results in the partial melting of the additive powder and liquid phase erosion of the base material. It is important to note that unlike diffusion brazing, the utilisation of additive powder in wide-gap brazing means that it has sufficient capacity to act like a diffusive sink for MPD diffusion, so that there is minimal liquid phase erosion of the base material which is considered to be undesirable [8] [46] [47] [48].

It is generally believed that additive powder cannot be completely melted during brazing because the brazing temperature is well below its melting point, so only partial melting takes place due to the interaction with the liquid filler alloy and diffusion of MPD into the additive powder particles. However, Ghoneim et al. [10] performed numerical modeling to simulate the dissolution of additive powder particles by using a molten conventional brazing filler alloy and showed that it is possible to completely melt the additive powder depending on the parameters. The parameters in their study are:

1. the type of MPD solute,
2. the mixture ratio of filler alloy powder particles to additive powder particles,
3. the size of the additive powder particles,



4. the brazing temperature, and
5. the amount of MPD in the conventional brazing filler alloy.

In addition, Ojo [12] performed experiments at various temperatures and different powder mixture ratios. He also reported that it is practicable to obtain complete melting of the additive powder particles during brazing. Furthermore, Hunedy [11] investigated the factors that affect the dissolution of additive powder and indicated that its complete dissolution is beneficial in terms of reduction in the degree of porosity in the brazed joint. The three most important parameters that affect the dissolution of additive powder are: temperature, mix ratio of filler alloy to additive powder ( $R_{F:D}$ ) and the size of the additive powder particles. Hunedy [11] found that it is possible to have complete melting of IN 738 finely meshed additive powder particles during brazing with a mix ratio of  $R_{7:3}$  at  $1150^{\circ}\text{C}$  for 1 hour while the partially melted additive powders remained in the experiment at  $1100^{\circ}\text{C}$  for 1 hour. Consequently, it is possible to have complete melting of the additive powder during wide-gap brazing.

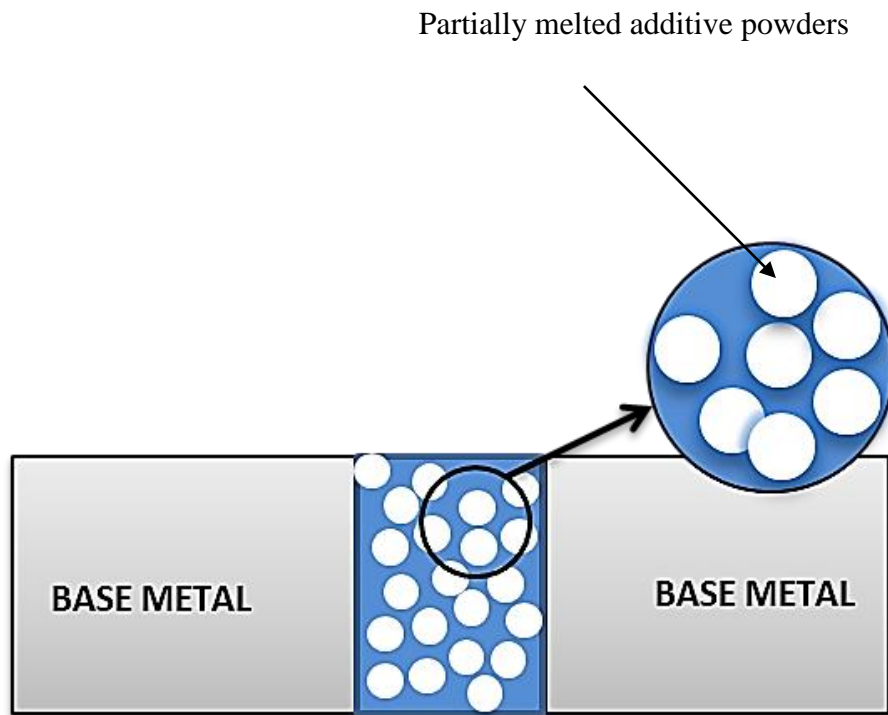


*Figure 2.2 – Schematic presentation of wide-gap brazed joint with partially melted additive powders in the joint region.*

Therefore, wide-gap brazing is a more desirable technique in terms of repairing and joining wide gaps and cracks in the hot section components of aero engines. However, the reliability of parts repaired through wide-gap brazing must be proven to determine any possible degradation that might take place in the hot section components of gas turbine engines. It is well known that one of the most common degradations in the hot section components of gas turbine engines is caused by hot corrosion. Hot corrosion resistance of such components is therefore very important since corrosion can cause their failure [13-21]. Therefore, the circumstances in which hot corrosion produces severe degradation of components are discussed in the next section.

## **2.3 Hot Corrosion**

### **2.3.1 Formation of deposited salts on gas turbine components**

To prevent hot corrosion, thorough knowledge of the reasons and conditions in which hot corrosion can take place is necessary. Hot corrosion is a serious issue for the hot sections of gas turbine engines. To better understand why, reference is made to Stringer [49] who discussed the working principle of gas turbine engines as follows.

In gas turbine engines, air enters the engine and is compressed. To obtain the desired temperature for the compressed air to enter the turbine, fuel is injected and burnt in the combustion sector. The combustion gas is always highly oxygenated due to the lower amount of fuel used in combustion in comparison to its stoichiometric reaction with air. Figure 2.3 [50] shows the primary components of a multi stage axial flow turbine. Hot and highly oxygenated gas then enters the turbine which can be composed of a series of fixed row of vanes and a revolving row of blades. These two components together are called a stage, and a turbine can have one or many stages.

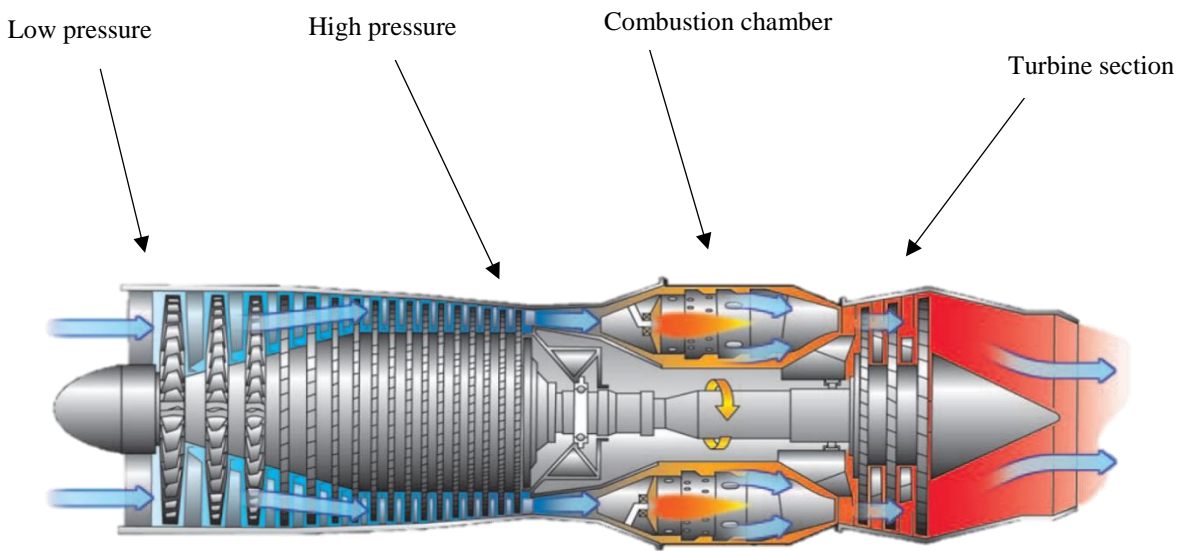


*Figure 2.3 – General configuration of gas turbine engine [50].*

Figure 2.4 [51] shows the temperature profile on the surface of the first stage blade which indicates that the pressure (concave) surface has the highest temperature. The greatest and the lowest temperatures in a cycle determine the efficiency of an engine. Although there are many factors that can affect the minimum temperature and in turn the efficiency, the main focus is on the maximum temperature or the turbine entry temperature which is relevant to this study. The industry has been favoring higher efficiency, which means that a gas turbine engine will run at a higher entry temperature. In the 1940s, the highest entry temperature for a Whittle engine was 700°C, but with the considerable development of the high temperature properties of the materials such as hot corrosion resistance and high temperature strength, the entry temperature in today's engines can be as high as 1350°C. During the Vietnam war in the late 1960s, the gas turbine engines of military aircrafts experienced intense hot corrosion due to the coastal climate [14]. Examination of the failed components showed the deposition of Na<sub>2</sub>SO<sub>4</sub> rich deposits on the turbine vanes and blades [14]. Severe hot corrosion can take place in conditions where these Na<sub>2</sub>SO<sub>4</sub> rich deposits are molten [52]. To prevent hot corrosion, it is therefore essential to understand the source and the mechanisms in which these deposits are produced [52]. Bornstein and Allen [53] provided two explanations for the salt deposition mechanisms on turbine airfoils: one involves the condensation of salt from the gas phase, and the other is direct spallation and impaction of salt particles onto the turbine components.

### **2.3.1.1 Condensation of salt from gas phase**

In the combustion sector of the engine, one of the most common fuel impurities is sulfur, which is oxidized into sulphur dioxide (SO<sub>2</sub>) and/or sulphur trioxide (SO<sub>3</sub>). It then reacts with gaseous NaCl

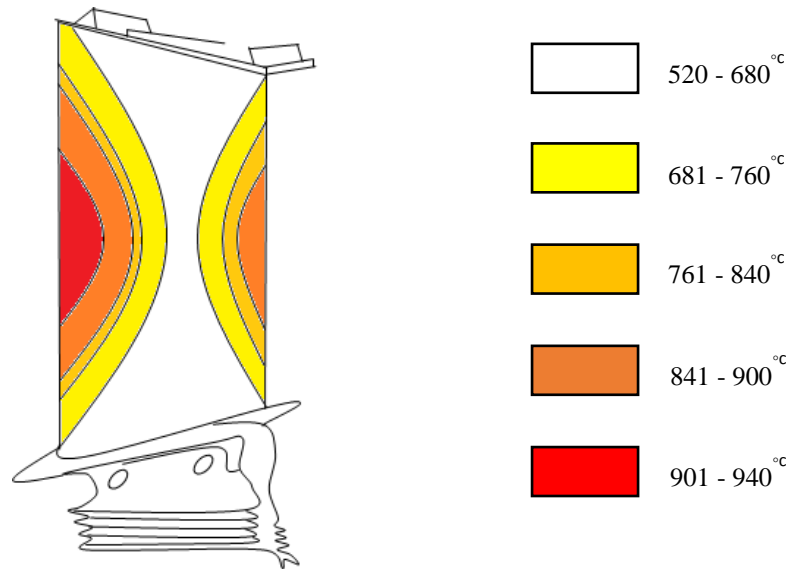
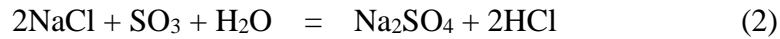
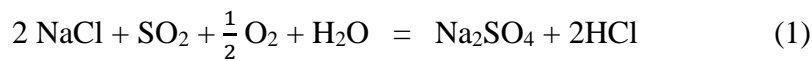


*Figure 2.4 – Distribution of temperature on surface of first-stage blade from Rolls-Royce Conway engine [51].*

and oxygen [52]. NaCl is found in the ingested air or the fuel [52]. In order for condensation of Na<sub>2</sub>SO<sub>4</sub> to take place on turbine components, their surface temperature must be lower than the dew point of Na<sub>2</sub>SO<sub>4</sub> [52]. However, the temperature required for condensation of salt can be affected by the concentration of ingested salt and the amount of sodium in the fuel [52].

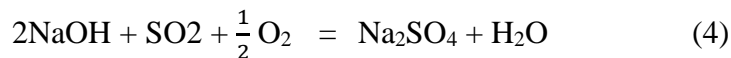
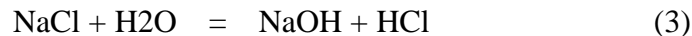
To better understand this process, Decrescent and Bornstein [54] assumed that there is 1 ppm of NaCl and 0.4 wt.% sulfur in the fuel, and determined these two reactions:



Both are in the gas phase.

They found that with 1 atm of total pressure and at a temperature of 1000°C, the conversion of NaCl to Na<sub>2</sub>SO<sub>4</sub> and HCl was 75% complete. The degree that NaCl is converted into Na<sub>2</sub>SO<sub>4</sub> can be increased with an increment in the overall pressure. Therefore, due to the high pressure found in gas turbine engines, Decrescent and Bornstein [54] concluded that complete conversion to Na<sub>2</sub>SO<sub>4</sub> can take place.

Hanby and Beer [55] further studied condensation as the mechanism of deposition and indicated that the conversion of NaCl into Na<sub>2</sub>SO<sub>4</sub> can be realized by using sodium hydroxide (NaOH) as the intermediate species if the temperature is adequately high enough:



They also concluded that the process very much depends on the temperature.

### **2.3.1.2 Direct spallation and impaction of salt particles**

The mechanism of deposition through the direct spallation and impaction of salt particles is realized when “some solid or liquid salt could detach from an upstream component (e.g. an air filter) and attach to a hot substrate upon impact” [14].

Bornstein and Allen [53] examined the actual mechanism in which salt is deposited onto the surface of gas turbine components. They conducted a series of experiments in the various turbine stages which involved different gas and surface temperatures. Based on their observations, the amount and composition of deposited salt is equal on the surface for the first 3 turbine stages. In addition, their analysis also revealed that the composition of the deposited salt on the internal and external surfaces of the first and second stage blades were comparable. Considering the fact that the surface temperature of turbine components decreases in the latter stages, and also as Figure 2.4 shows, the inner surface of a blade has a lower temperature than the outer surface, so if salt deposition was predominantly due to condensation, the amount of salt and its chemistry (composition) would be different in various parts of the turbine components because of the temperature gradient, but this was not observed. Therefore, Bornstein and Allen [53] concluded that spallation and impaction of salt are probably the main mechanism for salt deposition.

McCreath [56] further elaborated by clarifying that salt shedding from the compressor is more evident when the engine is operating under cyclic conditions (transition from standby to full power). He noted that for a gas turbine engine operating under constant engine load conditions in coastal regions, around 96 wt.% of the salt in the intake air is filtered in the compressor, while during the transition from standby to full power acceleration, there is significant salt shedding observed from the compressor.



Although it is generally believed that improved air filtration with the use of high quality fuel or redesigned air intake systems can significantly reduce the amount of deposited salt [49], it is worthwhile to mention that the presence of molten salt even in very small amounts and regardless of the deposition mechanism, can result in severe hot corrosion attacks [49].

### **2.3.2 Na<sub>2</sub>SO<sub>4</sub>–induced Hot Corrosion**

Hot corrosion is a “deposit-induced accelerated oxidation” [57] which is mostly observed in the hot sections of gas turbine engines. This environmental attack is called hot corrosion due to its common features with aqueous corrosion which involves degradation with an aqueous medium at room temperature [57]. In aqueous corrosion, the diffusion of dissolved oxygen in the aqueous medium is the controlling factor, while the soluble oxidant in hot corrosion is SO<sub>3</sub> (S<sub>2</sub>O<sub>7</sub><sup>-2</sup>) in fused salt [58] [59] [60] [61]. Hot corrosion can take place as a result of different deposits, such as sulfates of sodium, calcium, potassium, magnesium and also carbonates and vanadates [57] [62], but Na<sub>2</sub>SO<sub>4</sub> is commonly deposited onto gas turbine engines [57]. Regardless of the composition of the deposited salt, if the deposits on the surface of the alloy are liquid, it can separate the alloy from the gas environment and cause reactions between the liquid deposit and the alloy, and also reduce the transportation of some of the oxidants through the deposit. Consequently the oxidation features of alloys can be greatly affected by most deposits [57].

Hot corrosion is generally found in two forms based on the different mechanisms and environmental conditions under which hot corrosion can take place. When the temperature is higher than the melting point of Na<sub>2</sub>SO<sub>4</sub> (T<sub>m</sub>=884°C [63]), the deterioration is called high temperature hot corrosion or Type I hot corrosion [52]. The metallography of the corroded

components in this type of hot corrosion consists of internal sulfidation and an alloy depleted layer [49]. A liquid  $\text{Na}_2\text{SO}_4$  deposit can also form with temperatures lower than the melting point of  $\text{Na}_2\text{SO}_4$  due to the chemical reaction with combustion gases [52]. This form of hot corrosion is called Type II and highly accelerated and self-sustaining. It is characterised by pitting attacks with little or no internal sulfidation [64] [65].

### 2.3.2.1 Hot corrosion stages

It has been observed that the hot corrosion degradation of a metal or alloy always takes place first at a comparatively slow rate but then moves to another phase at a remarkably high rate of impairment, in which the component must be replaced due to very severe hot corrosion attacks [62] [66]. Therefore, the first stage, which has slower degradation, is called the initiation stage, which is followed by a significantly more severe attack called the propagation stage [62].

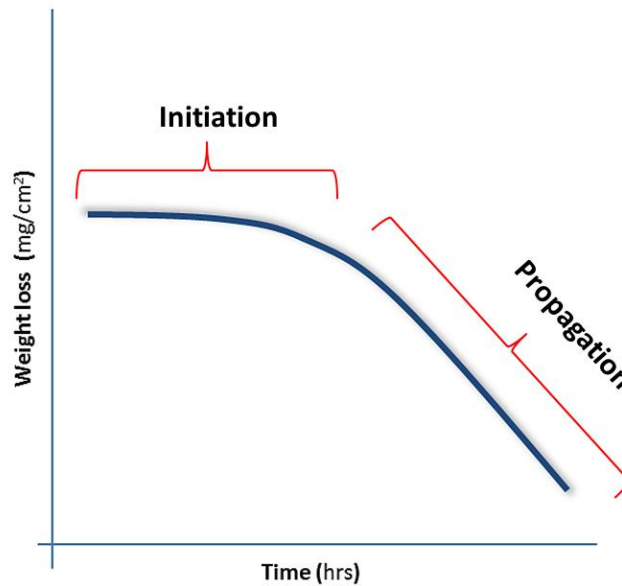


Figure 2.5 - Schematic presentation of hot corrosion stages.

### 2.3.2.1.1 Initiation Stage

The initiation (incubation) stage refers to the initial period of time in which little or no weight gain or slight weight loss is observed during hot corrosion tests [67]. During this stage, metals and alloys act as they do in the absence of deposits and their behavior is identical to simple oxidation [57]. This means that the chemical reactions and rate in which hot corrosion takes place in this stage are completely similar to those of simple oxidation [62] [52]. Therefore, it is obvious that to obtain a better resistance to hot corrosion, it is necessary to increase the time of the initiation stage for as long as possible [62]. Thus, it is important to determine the factors that can affect the length of the initiation stage. These factors not only can determine the length of the initiation stage but also at the same time reveal the type of reaction products that are produced during the propagation stage [62].

The factors that have been found to be the most important and influential for prolonging the initiation stage are listed below [52] [57] [62] [68].

#### 1) Alloy composition

It is generally accepted that the most beneficial alloying element that prevents hot corrosion is Cr [66], due to the formation of highly protective chromium oxide ( $\text{Cr}_2\text{O}_3$ ) scales which can resist  $\text{Na}_2\text{SO}_4$  induced hot corrosion attacks [14] [69].  $\text{Cr}_2\text{O}_3$  scales are much more preferable than other types of oxide scales because of their faster growth rate which allows protection of the alloys with more rapid recovery after a scale failure [70]. However, if the Cr content in a Ni-base alloy is less than 10-15%,  $\text{Cr}_2\text{O}_3$  will no longer form on the alloy [49]. In addition Rapp [71] noted that  $\text{Cr}_2\text{O}_3$  will oxidize into a gaseous species [ $\text{CrO}_3$ ] in

high temperatures and the chromia forming alloys can be only used in temperatures below 1000°C.

Another important alloying element is Ti. Ti can play a very important role by catching the released sulfur from Na<sub>2</sub>SO<sub>4</sub> deposits which can penetrate into the substrate of the alloy during hot corrosion attacks and reduce the resistance of the material to hot corrosion [72] [73]. Consequently, at least 15 wt.% Cr along with about 3 wt.% Ti or more is necessary for hot corrosion resistant superalloys [72] [74] [75] [76].

The effects of alloying elements on hot corrosion resistance can change considerably and reversed behavior have been observed depending on the experimental conditions and the alloy system [77]. For instance, there is considerable inconsistency in work on the effects of Mo on hot corrosion but the majority believe that it is harmful [66]. Stringer [49] indicated that when the amount of Mo is greater than a critical value, severe hot corrosion degradation in aggressive environments can result due to the acidic oxides which can significantly accelerate hot corrosion attacks [62] [78] [79]. Stringer [49] also mentioned that, specifically, for Cr<sub>2</sub>O<sub>3</sub> forming alloys, the critical amount of Mo can be increased with increases in the Cr content. The effects of Mo on the hot corrosion resistance of superalloys have been further reported in Misra [80] Pettit and Meier [62], Peters et al. [78] and Fryburg et al. [81] , who determined that alloys that contain Mo suffer severe degradation due to the reduction in oxide ion activity which results in acidic fluxing of the protective oxide scales.

Nb has been found to be beneficial for hot corrosion resistance due to formation of the NaNbO<sub>3</sub> phase which reduces oxide ion activity in fused Na<sub>2</sub>SO<sub>4</sub> [82] [83] while it has

been mentioned that in multi-component superalloys, Nb might promote acidic fluxing and consequently severe degradation of the material [82] [83] [84] [85] [86].

W is known to behave in the same way as Mo but is less harmful [66].

In contrast to  $\text{Cr}_2\text{O}_3$ , the scales in  $\text{Al}_2\text{O}_3$  forming alloys do not oxidize into gaseous species in high temperatures and the growth rate of the  $\text{Al}_2\text{O}_3$  scales on the surface of the alloy is significantly slower than that of chromia scales [49]. Approximately 15 wt. % of Cr and 5 wt.% of Al contributes to the unique oxidation resistance of Ni-base superalloys due to the formation of alumina scales at high temperatures [49].

Generally, Co-base alloys demonstrate better resistance to high temperature hot corrosion (Type I) than Ni-base superalloys. Stringer [49] indicated that there are three different reasons for this phenomenon: it is the result of the inherent properties of Co in contrast to Ni, presence of generally more Cr in Co-base alloys, or the fact that the solid solution strengthener in Co-base alloys is W but in Ni-base alloys is Mo.

Therefore, alloying elements have a remarkable role and determine the life of superalloys under hot corrosion conditions [87].

## 2) Production process

The process in which an alloying material is produced, i.e. cast, equiaxed grain or single crystal superalloys, can very much affect the hot corrosion properties. For example, in the cast condition, some alloying elements solidify more quickly than others, so segregation of the alloying elements takes place which can cause local Cr or Al depleted zones thus resulting in an overall reduction of corrosion resistance [52].

### 3) Gas composition

Gas composition can severely affect the duration of the initiation stage for both types of hot corrosion but especially Type II which occurs at temperatures lower than the melting point of  $\text{Na}_2\text{SO}_4$  [52]. Although Type I hot corrosion can occur in the presence of air or pure oxygen, Type II hot corrosion requires  $\text{SO}_3$  in a gas environment [88]. The influence of these gaseous species are significantly noticeable on the chemical and physical states of salt depositions and consequently on the hot corrosion of materials [52] which will be discussed later.

### 4) Deposit composition and physical state

The physical state of the deposited salt has a very important role in causing deposit induced accelerated oxidation, in a way that the same composition of deposit can cause severe hot corrosion attacks if present as a liquid while no attacks have been observed when the deposition is in the gas phase [89]. The reason is that the required interaction between substrate and deposit and consequent condition which is necessary for hot corrosion to take place, cannot develop when the deposition is in a gas form [57].

Another factor that can significantly affect the hot corrosion process is the composition of the salt. Pettit [57] stated that the addition of  $\text{NaCl}$  to  $\text{Na}_2\text{SO}_4$  at  $900^\circ\text{C}$  in air for both Ni-30Cr and Ni-25Cr-6Al alloys will increase the likelihood of hot corrosion attacks, while the Ni-30Cr alloy will suffer more severe attacks. Pettit [57] also added that the attacks will increase as the amount of  $\text{NaCl}$  is increased.

Stringer [49] noted other elements, such as vanadium (V), which is found in many fuel oils, also have a significant contribution to hot corrosion damage. In addition, the combination

of V and sodium can cause more severe degradation than when each element is solely found. Furthermore, lead, phosphorus and carbon can also accelerate hot corrosion attacks.

#### 5) Temperature

The influence of temperature has been well established in the literature due to the fact that one of the main factors for classifying hot corrosion into two Types I and II is due to the exposure temperature. If the temperature is above the melting point of  $\text{Na}_2\text{SO}_4$ , Type I hot corrosion takes place, while Type II occurs at lower temperatures with the presence of  $\text{SO}_2/\text{SO}_3$  gas mixtures [66]. Patnaik [66] noted increasing temperatures can increase the degradation caused by Type I hot corrosion up to a critical maximum value; beyond this value, the degradation tends to decrease due to the volatilization of the molten sulfates.

All of the mentioned factors can affect the protectiveness of the oxide scales that form on the substrate during the initiation stage and correspondingly greatly influence the length of the initiation stage [57]. The duration of the initiation stage determines the susceptibility of an alloy to hot corrosion attacks, and eventually, transition from the initiation to the propagation stage takes place due to the breakdown of the protective oxide scales [52].

#### **2.3.2.1.2 Propagation Stage**

The propagation stage takes place when the depositions significantly reduce the protectiveness of the oxide scales; therefore, small holes appear in the oxide scales and molten deposits penetrate them. Then, the protective oxide scales which were formed by selective oxidation are considered to be ineffective [79]. The propagation stage is characterized by a very severe hot corrosion attack of the alloy [66]. As a result, the component must be removed from service because the rate of

degradation at this point is much greater than that in the initiation stage [62]. This stage includes three different propagation modes: basic fluxing, and alloy-induced and gas-induced acidic fluxing [62]. The first two take place in high temperatures. Consequently, they are considered Type I hot corrosion while gas phase-induced acidic fluxing takes place at lower temperatures, and therefore is Type II hot corrosion [52].

Task said, "...The way in which the alloy and salt are preconditioned during the initiation stage" [52] will determine the propagation mode. Therefore, all the factors discussed in Section 2.3.2.1.1 are highly influential.

### **2.3.3 Role of salt deposits in hot corrosion mechanisms**

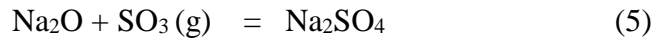
Before proceeding to the discussion on hot corrosion mechanisms and the propagation modes, it is important to once again emphasize the definition of hot corrosion which is deposit-induced accelerated oxidation. The interaction between the deposited salt and alloy eventually produces highly corrosive conditions because of the gradual shift to locally high base or acidic salt compositions [52]. These highly corrosive conditions can cause the protective scales to break down, so that the alloy becomes severely degraded (propagation occurs).

This explanation clearly highlights the critical role of salt deposits in hot corrosion mechanisms, so it is necessary to have a good understanding of their nature and properties.



### 2.3.3.1 Acid-base chemistry and oxide solubility

$\text{Na}_2\text{SO}_4$  is an oxyanion salt that is characterized by acid-base chemistry, just like pH for aqueous solutions. The acid-base character is described with gaseous  $\text{SO}_3$  as the acidic component, and oxide ions present as  $\text{Na}_2\text{O}$ , the basic component [14] [90].



Consequently,  $\log a_{\text{Na}_2\text{O}}$  can be quantitative data that represent the melt basicity and  $\log a_{\text{SO}_3}$  can be defined as the melt acidity [14]. To reconstruct a hot corrosion condition and measure the melt basicity during an experiment, two solid electrolyte reference electrodes, ( $\text{Na}^+$  and  $\text{O}^{2-}$  ion conductors) are simultaneously used to measure the activities of Na and  $\text{O}_2$  in the salt which can lead to particular values for  $\log a_{\text{Na}_2\text{O}}$  [14]. Therefore, the magnitude of the primary melt properties can be precisely established: its basicity ( $\log a_{\text{Na}_2\text{O}}$ ) and its oxidation potential ( $\log \text{PO}_2$ ) [14]. Based on these two parameters, thermodynamic stability diagrams are constructed that allow the phases to be illustrated, which are supposed to be stable during hot corrosion [52]. These phase stability diagrams show the changes in composition that can take place in  $\text{Na}_2\text{SO}_4$  deposits due to their interaction with the alloy. Therefore, the composition of salt can become more basic (higher  $a_{\text{Na}_2\text{O}}$ ) or more acidic (lower  $a_{\text{Na}_2\text{O}}$ ) [52].

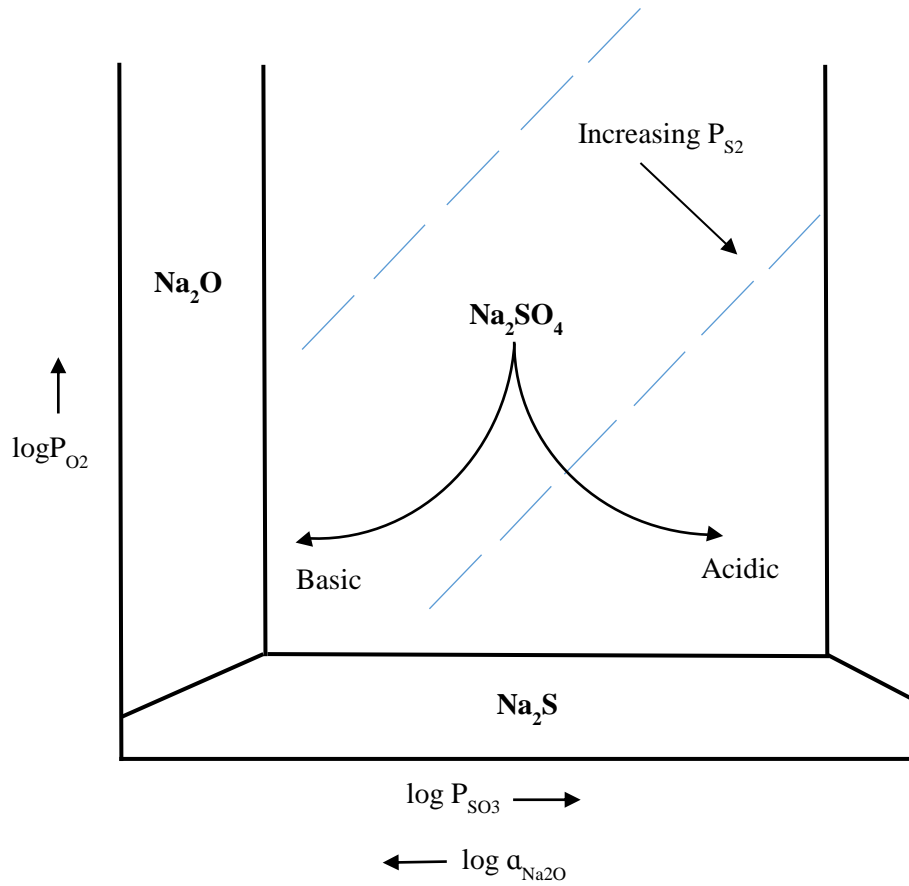


Figure 2.6 - Schematic presentation of phase stability diagram for Na-S-O system [57]. It shows that the composition of  $Na_2SO_4$  can change because of the reactions between salt and alloy. Alloy can remove oxygen and sulfur from the salt, so basic conditions can establish. Oxidation of refractory metals in alloy can establish acidic conditions [57].

### **2.3.3.2 Deposition induced effects**

It is important to study the effect of the deposits on the surface of the alloys on their hot corrosion behavior [62]. Figure 2.7 schematically shows a deposition of  $\text{Na}_2\text{SO}_4$  on the surface of a superalloy. The salt deposit prevents the free contact of the superalloy with gas and considering that the alloying elements in superalloys have a very high affinity to react with oxygen, oxygen is consumed in the region close to the alloy surface to produce oxide scales. Consequently, an oxygen gradient is established across the salt deposit due to the low diffusion rate of oxygen in the deposited  $\text{Na}_2\text{SO}_4$ . This situation causes a reduction in the oxygen activity over the surface of the alloy compared to what would have been established in the absence of a salt-deposit [79]. The oxygen activity is increased by moving towards the salt/gas interface.

The other effect of salt deposits on the hot corrosion behavior of superalloys is that the protective oxide scales, formed on the superalloy, may dissolve in a liquid salt deposit. This is due to the formation of highly acidic or basic conditions in the liquid deposit. In certain cases, conditions can exist where the protective oxide scales dissolve into the liquid deposit at the oxide/salt interface and precipitate at the salt/gas interface as a non-protective layer. This process is called fluxing reaction or dissolution of the protective oxide scales by the deposited salt [89] [91] [92].

### **2.3.4 High temperature hot corrosion (Type I)**

As mentioned before, Type I hot corrosion takes place at temperatures higher than the melting point of  $\text{Na}_2\text{SO}_4$  and is characterized by internal sulfidation. Due to the interaction between the material and liquid salt, the composition of the deposited salt can either form into a highly basic

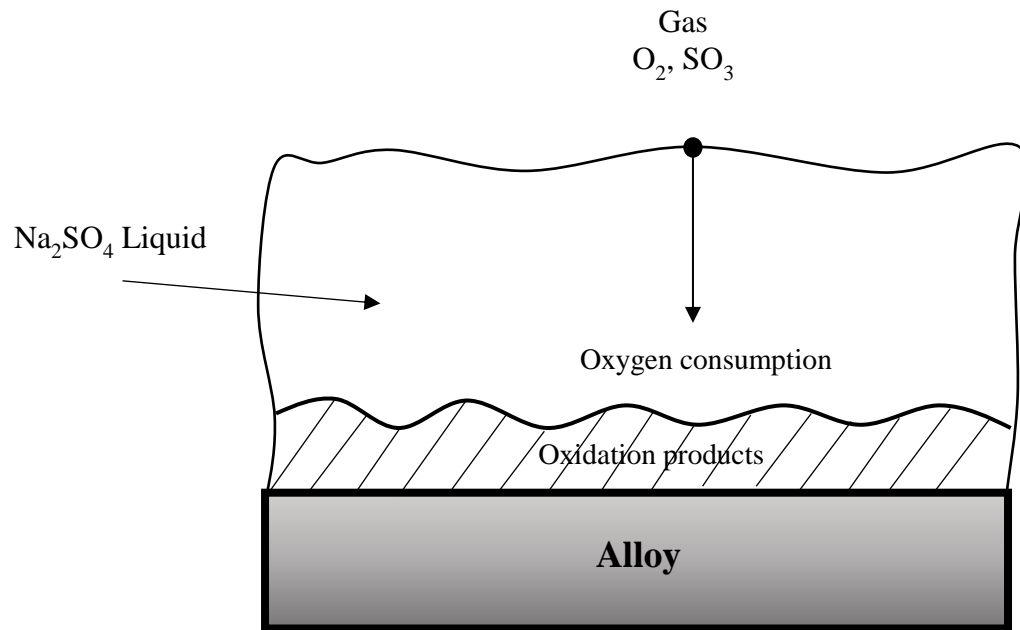


*Figure 2.7 - Schematic drawing indicating the situation that cause hot corrosion of metals and alloys [57]. Oxygen is consumed in the region close to the alloy surface to produce oxide scale.*

melt (high  $a_{\text{Na}_2\text{O}}$ ) or highly acidic melt (high  $P_{\text{SO}_3}$ ) [52]. This localized and highly corrosive melt composition can cause the dissolution of the protective oxide scales [52]. If the dissolution of the protective oxide scales is due to the highly basic melt (high  $a_{\text{Na}_2\text{O}}$ ), this is called basic fluxing (basic dissolution) [52]. If the dissolution is the result of a highly acidic melt (high  $P_{\text{SO}_3}$ ), this is called acidic fluxing (acidic dissolution) [52].

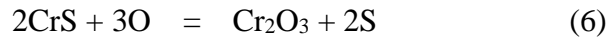
The primary factor that can determine whether acidic or basic fluxing is dominant, are the alloying elements found in the material [52].

#### **2.3.4.1 Basic fluxing**

Type I hot corrosion was first found in aircraft gas turbines at a temperature of 900°C with  $\text{Na}_2\text{SO}_4$  deposits [57]. The attack was named sulfidation because it "...appeared to be related to the oxidation of sulfides in the alloys where the sulfur came from the  $\text{Na}_2\text{SO}_4$  deposits" [93]. Simons et al. [94] were among the pioneers to find that sulfidation attacks are due to the accelerated oxidation of the sulfide phases and these sulfide phases can form when a reducing constituent in the material reacts with the salt deposit.

Danek [95] and Seybolt [96] suggested that the reason for reduced oxidation resistance is the Cr-depleted zones in the substrate alloy. Seybolt [96] proposed that the precipitation of the  $\text{Cr}_x\text{S}_y$  particles in an alloy can result in Cr-depleted zones in the substrate which reduces hot corrosion resistance and consequently, the material can be severely corroded. The hypothesis was investigated through experiments on ternary Ni-Cr-X alloys and different Ni-base superalloys. Seybolt [96] also oxidized some Ultimec 500 samples. These samples were altered in a way that the amount of Cr was reduced. This reduction in Cr content was done to obtain an equal amount

of Cr to areas close to the Cr sulfides in their earlier experiment. Seybolt [96] indeed observed reduced oxidation resistance of these materials and also added that the Cr sulfides react with oxygen, which results in releasing sulfur that can diffuse into the material and react with Cr. Consequently, more Cr sulfides form and the process will continue.



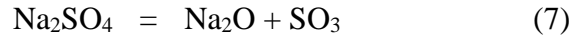
Therefore, for many years, it was believed that the main reason that hot corrosion (sulfidation) took place is due to sulfur, which can come from the deposited salt and react with the alloying elements in the material e.g. Cr, to form Cr sulfides. This sulfidation and the oxidation of sulfides were believed to be the reason for hot corrosion degradation.

Bornstein and Decrescent [89] took the first step to examine the accepted hot corrosion basic fluxing mechanism. They performed a series of experiments to investigate the role of sulfur in hot corrosion mechanisms. They used three types of superalloys, U-700, B-1900 (both  $\text{Al}_2\text{O}_3$  scale formers) and Waspaloy ( $\text{Cr}_2\text{O}_3$  former) at  $900^\circ\text{C}$  with and without deposits of  $\text{Na}_2\text{SO}_4$  and  $\text{Na}_2\text{NO}_3$ . They observed that the amount of degradation caused by hot corrosion is the same for both types of salts. The only difference is the microstructure. In the case of  $\text{Na}_2\text{SO}_4$ , sulfide phases were found in the microstructure but not observed in  $\text{Na}_2\text{NO}_3$ . Although the microstructures were different in terms of sulfide formation, for all of the salt-induced hot corrosion microstructures, a porous external oxide layer and an alloy depleted region beneath the scales were observed [89]. Bornstein and Decrescent [89] also performed experiments by using B-1900 alloy, and in one case, they used the same amount of sulfur found in  $1 \text{ mg/cm}^2$  of  $\text{Na}_2\text{SO}_4$  and in the other case,  $1 \text{ mg/cm}^2$   $\text{Na}_2\text{SO}_4$  or  $\text{Na}_2\text{NO}_3$  was deposited onto the surface of the alloy. No hot corrosion occurred when only sulfur was deposited onto the surface of the alloy while the material considerably corroded in the presence of the salts. Therefore, they concluded that the reason for hot corrosion attacks is not due

to sulfur or formation and oxidation of sulfides, but the oxide ions in the salt ( $\text{Na}_2\text{SO}_4$  or  $\text{Na}_2\text{NO}_3$ ) which react with the normally protective oxide film and results in the degradation of the material due to dissolution of the protective oxide scales [57]. Bornstein and Decrescent [89] added that basically the interaction between the salt (here  $\text{Na}_2\text{SO}_4$ ) and alloying elements such as Cr, can remove the sulfur from the salt which results in the formation of Cr sulfides in the substrate and oxide ions in the melt. So, the reason for the accelerated oxidation is the accumulation of these oxide ions (found as  $\text{Na}_2\text{O}$ ) in the melt and their interaction with the protective oxide scales [89].

Geobel and Pettit [97] further studied the mechanism while considering two important factors. The first factor is the phase stability diagram for the Na-Ni-S-O system at  $1000^\circ\text{C}$  which indicates no combination of conditions (melt basicity and  $P_{\text{O}_2}$ ) where Ni is stable when in contact with fused  $\text{Na}_2\text{SO}_4$  [14]. This can be extended to M-Na-O-S systems where the metal can be Ni, Co, Fe, Al or Cr [98] [99] [100] [101] [102] at 1200 k. So, if a metal or alloy comes into contact with the fused salt, a metal sulfide will form, even as a result of sulfur penetration along the grain boundary of the protective oxide scales [14]. The other important factor is that a fused salt deposit is required for hot corrosion attacks - gaseous  $\text{Na}_2\text{SO}_4$  Even though it has the same composition as fused  $\text{Na}_2\text{SO}_4$  salt deposit, accelerated oxidation does not result. This means that it is necessary to develop a concentration gradient across the salt deposit; but this cannot be developed in the case of gaseous salt because of the rapid rate of transport [52]. Geobel and Pettit [97] oxidized pure Ni at  $1000^\circ\text{C}$  in a molten  $\text{Na}_2\text{SO}_4$  deposit. In the beginning, they observed accelerated oxidation. After 6 hours, the oxidation slowed down to a normal parabolic growth kinetic. In addition, the microstructure comprised an internal NiS layer below the protective dense NiO scales and precipitation of non-protective NiO precipitates within the salt film [97]. The authors interpreted their results as follows.

Based on the phase stability diagram for Na-Ni-S-O system, NiO should be stable on the surface of Ni in the presence of fused Na<sub>2</sub>SO<sub>4</sub> at 1000°C. The oxygen required for the formation of NiO can be supplied either by the dissolved gaseous oxygen in the salt or the decomposition of Na<sub>2</sub>SO<sub>4</sub>.

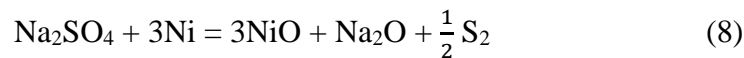


An oxygen gradient will develop across the salt film due to three reasons.

- 1) The fused Na<sub>2</sub>SO<sub>4</sub> film separates the Ni specimen from the oxygen gas (atmosphere).
- 2) The solubility and diffusion of molecular oxygen in fused Na<sub>2</sub>SO<sub>4</sub> are very low.
- 3) The oxygen is consumed on the Ni/salt interface to form NiO, so this interface has the least amount of oxygen.

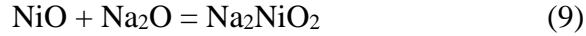
As a result of establishing a positive oxygen gradient across the molten Na<sub>2</sub>SO<sub>4</sub>, from the Ni interface to the gas interface, sulfur activity is increased such that it could penetrate the NiO oxide scales to the Ni interface which has very low oxygen activity and form NiS deposits under the NiO scales.

The removal of sulfur and oxygen from the fused Na<sub>2</sub>SO<sub>4</sub> salt to form NiS and NiO respectively resulted in Na<sub>2</sub>O (oxide ion) activity in the Na<sub>2</sub>SO<sub>4</sub> towards high local basicity as shown for the reaction in Equation (8).



The oxide ion activity (Na<sub>2</sub>O activity) is the greatest at the NiO/salt interface and decreases towards the salt/gas interface. Due to the high oxide ion activity at the NiO/salt interface, NiO reacts with the oxide ions in the melt based on the reaction below to form nickelate ions (NiO<sub>2</sub><sup>2-</sup>) which are soluble in molten Na<sub>2</sub>SO<sub>4</sub>.





Therefore, the nickelate ions diffused to a region with less oxide ion activity which is the salt/gas interface and the reverse of the above reaction occurred. This produced oxide ions at the salt/gas interface which eventually resulted in stabilizing the oxide ion concentration by removing the oxide ion gradient across the molten salt. Moreover, this reverse reaction can produce non-protective NiO scales which were observed in the molten salt. Consequently, the dissolution of NiO at the oxide/salt interface ceased, which stabilized the protective NiO scales on the metal surface. This is the reason that acceleration of oxidation stopped which was observed after approximately 6 hours. However, this pioneering study by Geobel and Pettit [97] was subjected to criticism because the results were only interpreted through phase stability diagrams which are not precise enough to make any definite conclusions. To identify and explain hot corrosion mechanisms, it is important to measure the degree to which a given oxide will dissolve over a range of quantitatively measured salt film basicities [14].

#### **2.3.4.1.1 Solubility plots for NiO, Co<sub>3</sub>O<sub>4</sub>, Al<sub>2</sub>O<sub>3</sub>, Fe<sub>2</sub>O<sub>3</sub> and Cr<sub>2</sub>O<sub>3</sub> in Na<sub>2</sub>SO<sub>4</sub>**

High temperature reference electrodes were used to measure the solubility of NiO, Co<sub>3</sub>O<sub>4</sub>, Al<sub>2</sub>O<sub>3</sub>, Fe<sub>2</sub>O<sub>3</sub> and Cr<sub>2</sub>O<sub>3</sub> in Na<sub>2</sub>SO<sub>4</sub> as a function of the melt basicity at P<sub>O<sub>2</sub></sub>=1 atm and T= 1200 k [70] [98] [102] [103] [104]. The compiled results are presented in Figure 2.8 [70].

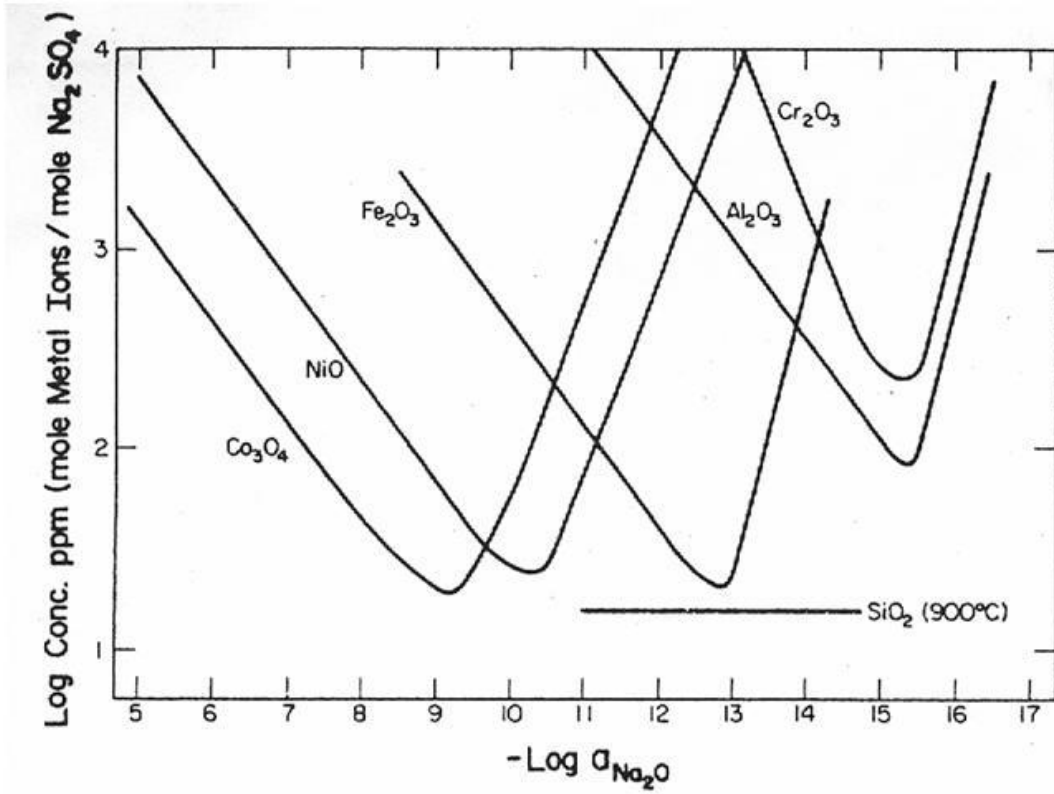
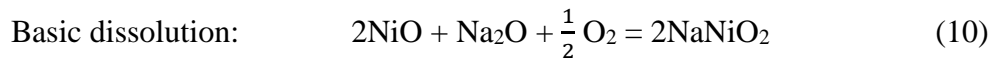


Figure 2.8 - Solubilities of various oxides in Na<sub>2</sub>SO<sub>4</sub> as a function of melt basicity [70].

### 2.3.4.1.2 Solubility of NiO in fused Na<sub>2</sub>SO<sub>4</sub> at 1200 k

Information on the solubility of the relevant oxides in Na<sub>2</sub>SO<sub>4</sub> as a function of the activity of the oxide ions (Na<sub>2</sub>O) in Na<sub>2</sub>SO<sub>4</sub> can provide a better understanding on the fluxing (dissolution) of the protective oxide scales during hot corrosion [98].

The steps to obtain the solubility curve of NiO at T= 1200 k which is shown in Figure 2.9 [98] are provided as an example. By using simple thermodynamic calculations, Gupta and Rapp [98] measured the Ni oxide solubility levels and formulated the corresponding curve. The reactions for the basic and acidic dissolution of NiO are shown for the reactions in Equations (10) and (11) respectively.



The equilibrium constant for the basic dissolution of NiO is based on consideration of the unit activity of NiO:

$$K = \frac{a_{\text{NaNiO}_2}^2}{a_{\text{Na}_2\text{O}} p_{\text{O}_2}^{1/2}} \quad (12)$$

Taking the logarithm of both sides, solving for  $a_{\text{NaNiO}_2}$ , and differentiating with respect to  $-\log a_{\text{Na}_2\text{O}}$  will give:

$$\frac{\partial \log a_{\text{NaNiO}_2}}{\partial (-\log a_{\text{Na}_2\text{O}})} = -\frac{1}{2} \quad (13)$$

This equation provides the slope of the NiO solubility curve for basic fluxing (left part). The acidic dissolution equation can be derived in a similar fashion, so that the slope of the acidic fluxing (dissolution) of NiO (right part) is provided by Equations (14) and (15):

$$K = a_{\text{NiSO}_4} a_{\text{Na}_2\text{O}} \quad (14)$$

$$\frac{\partial \log a_{\text{NiSO}_4}}{\partial (-\log a_{\text{Na}_2\text{O}})} = 1 \quad (15)$$

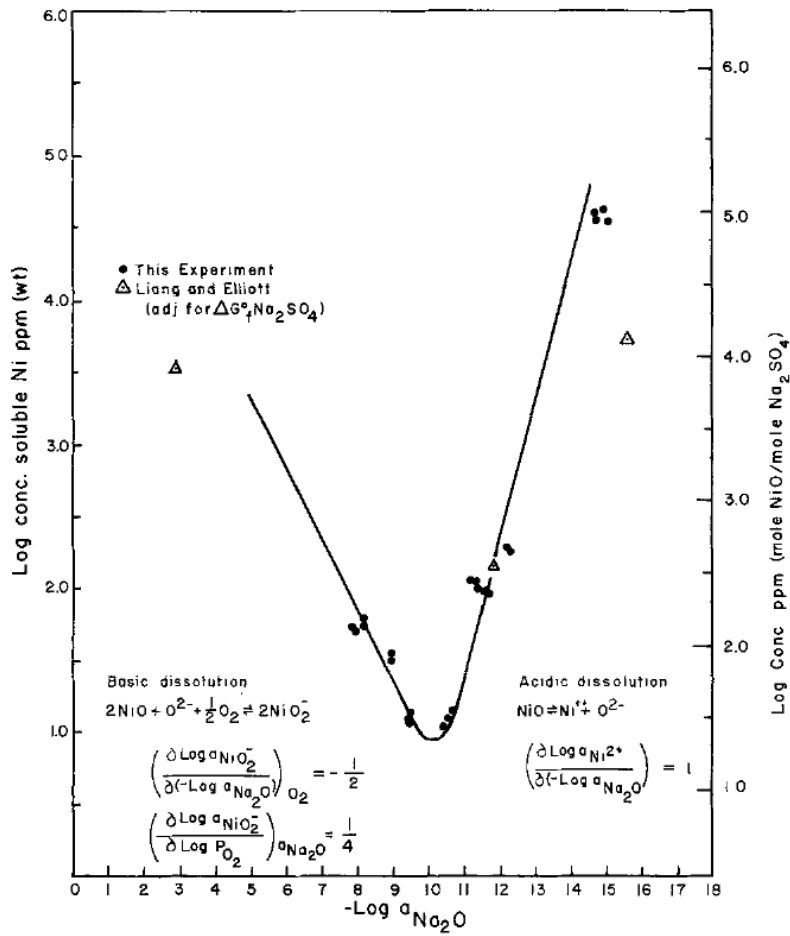
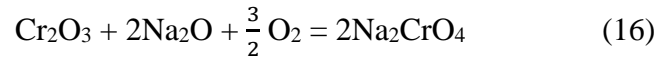


Figure 2.9 - Solubility of NiO in fused  $\text{Na}_2\text{SO}_4$  at 1200k [98].

It is important to mention that these solubility plots (Figure 2.8) are constructed at a constant  $PO_2$ , while the solubility of some of the oxides depends on the oxygen potential [52]. For example, consider the basic dissolution of  $Cr_2O_3$  and  $Al_2O_3$  in  $Na_2SO_4$  [105]:



Based on the above equations, Cr is oxidized from  $Cr^{3+}$  into  $Cr^{6+}$  but no change in valence can be observed in the case of the  $Al^{3+}$  ions [52]. This change in valence in the basic dissolution of Cr results in the dependence of the solubility of  $Cr_2O_3$  in  $Na_2SO_4$  on the oxygen pressure. This means that the solubility of  $Cr_2O_3$  will increase with increased  $PO_2$  [52]. Therefore,  $Cr_2O_3$  oxide scales are very important, which will be discussed later.

#### **2.3.4.1.3 Rapp and Goto criterion for occurrence of self-sustained hot corrosion attacks**

Based on Figure 2.8 and taking into consideration that oxide solubility would generally follow individual basic and acidic behaviors with respect to their solubility dependence on the melt basicity and in some cases on the  $PO_2$ , a general criterion proposed by Rapp and Goto [106] was applied. This criterion, as shown below, can determine the possibility that self-sustained hot corrosion attacks will occur.

$$\left[ \frac{d[\text{oxidesolubility}]}{dx} \right]_{x=0} < 0 \quad (18)$$

where X is the distance from the oxide/salt interface to the molten salt film. If a negative solubility gradient occurs, which means that the solubility of the protective oxide scales is greater at the oxide/salt interface and decreases towards the salt/gas interface, then the Rapp and Goto criterion will be satisfied. Therefore, the protective oxide scales will dissolve at the oxide/salt interface and precipitate as non-protective oxide scales at the salt/gas interface, where the solubility is lower (see figure 2.10 [106]).

Figure 2.11 [106] shows oxide solubility as a function of the basicity gradient in the salt which is plotted for a constant PO<sub>2</sub>. Three situations are shown in Figure 2.11 which can satisfy the “negative solubility gradient criterion” or the Rapp and Goto criterion [106]. In all three cases, I represents the oxide/salt interface and II represents the salt/gas interface [106]. It is obvious that whether the dissolution is basic (Case A) or acidic (Case C), the solubility of the oxide must be higher at Interface I as opposed to Interface II [52]. In order for oxide dissolution to continue in Case B, the location of the two interfaces must be on either side of the solubility minimum for the oxide [52]. On the contrary, if a specific condition exists in which a “positive solubility gradient” is established across the salt film, then the oxide dissolution and continuing hot corrosion will cease [14].

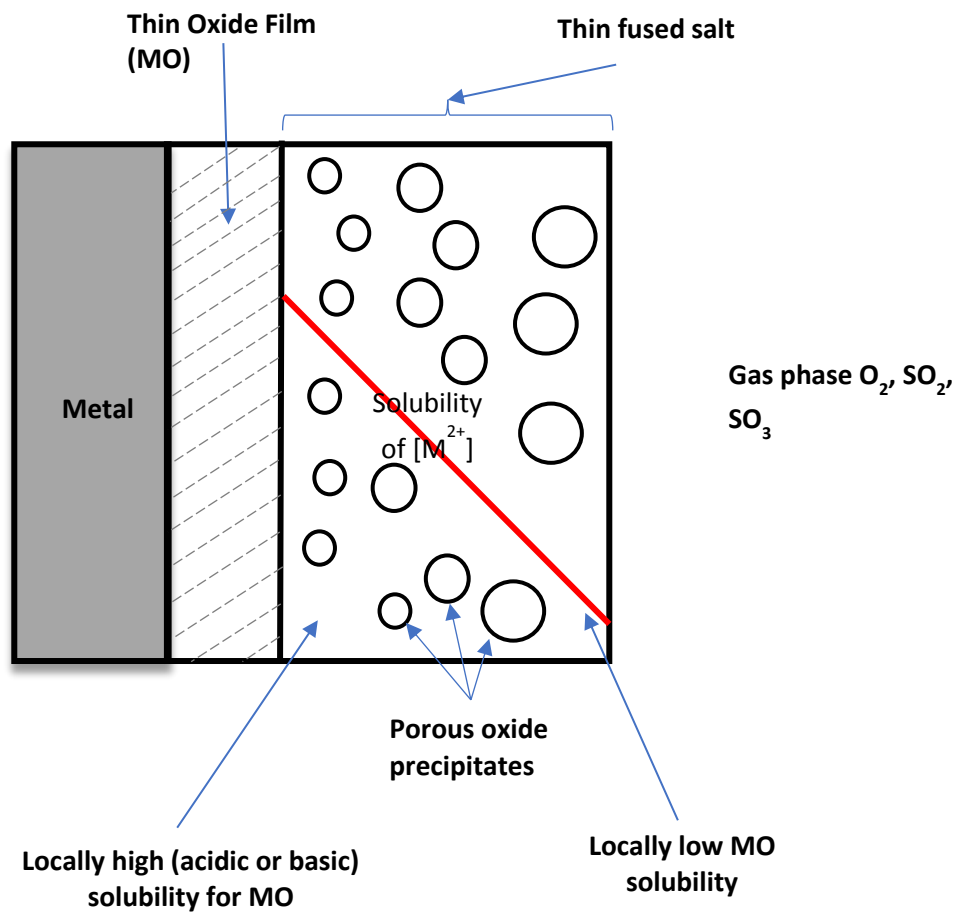
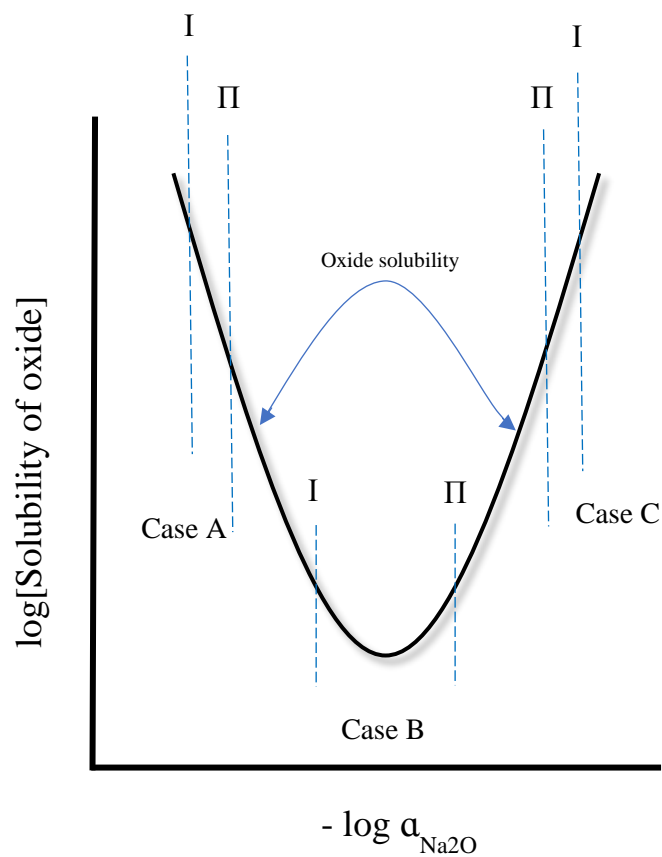


Figure 2.10 –Schematic indication of dissolution of protective oxide scale. Negative solubility gradient established across the salt (red line), so protective MO dissolved at oxide/salt interface due to high acidic or basic melt and porous MO precipitated at salt/gas interface [106].



*Figure 2.11 - Schematic indication of Rapp and Gotto negative solubility criterion [106]. I represents the oxide/salt interface and II represents the salt/gas interface. The solubility of the oxide must be higher at Interface I compared to Interface II, to satisfy Rapp and Gotto negative solubility criterion.*



Now the results of Goebel and Pettit [97] can be evaluated by using the Rapp and Gotto criterion. During the period of accelerated oxidation, the oxide ion activity ( $\text{Na}_2\text{O}$ ) is higher at the oxide/salt interface than the salt/gas interface. Considering that higher oxide ion activity will dissolve the NiO at the oxide/salt interface, it is therefore the same as saying that the NiO solubility is greater at the oxide/salt interface than the salt/gas interface. Therefore, a negative solubility gradient is maintained across the salt (see Figure 2.11, Case A). Consequently, hot corrosion attacks can take place, as observed by Goebel and Pettit [97]. After approximately 6 hours, the formation of NiS ceases and the oxide ion activity is stabilized throughout the salt, so that the negative solubility gradient is no longer present. Consequently, accelerated oxidation stops [52]. Rapp and Goto [106] also mentioned that, not only will the removal of sulfur from  $\text{Na}_2\text{SO}_4$  for forming sulfide phases increase the local melt basicity (higher oxide ion activity), but also the reduction of peroxide ions at the oxide/salt interface increases the basicity based on the following reaction:



Most of the experiments for examining Type I hot corrosion mechanisms and specifically, the Rapp-Goto criterion for negative solubility have been performed in air or pure oxygen while in real situations, sulfur containing combustion product gases are often found in gas turbine engines [57]. Otuska and Rapp [69] therefore conducted an experiment to observe the hot corrosion behavior of Ni in an oxygen-sulfur containing gas mixture at 1173 k. They determined the basicity and oxygen activity at the metal/salt interface by using a potentiometric measurement technique. The results were then plotted as a function of time on a Ni-Na-S-O phase stability diagram as shown in Figure 2.12 [69].

The NiO scales interacted with  $\text{Na}_2\text{SO}_4$ , thus resulting in a substantial reduction in the oxygen pressure, so that the values fell within the sulfide stability region. This means that the NiS

stabilized. After 16 minutes, the local melt basicity shifted considerably to the more basic region due to sulfur and oxygen removal from  $\text{Na}_2\text{SO}_4$ . The sample was significantly corroded at the end of the experiment, with the presence of  $\text{NiS}$  and precipitation of  $\text{NiO}$  in the salt film.

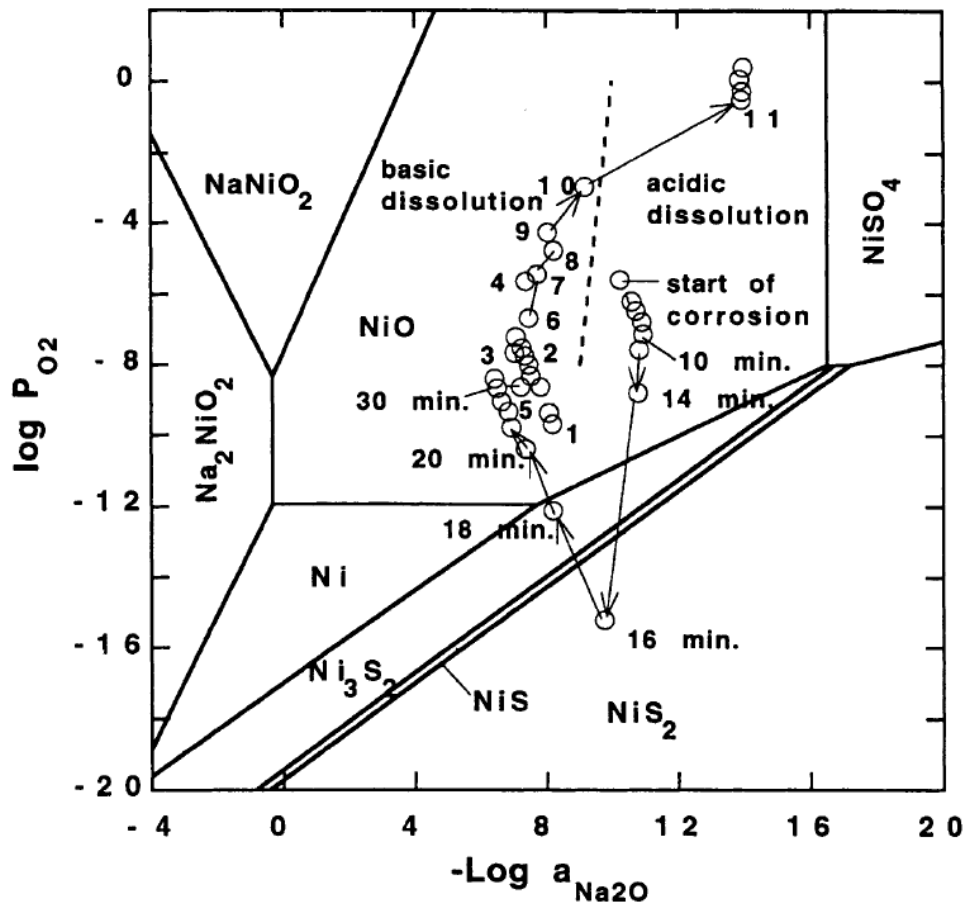


Figure 2.12 - basicity and oxygen activity measured on a preoxidized Ni coupon with a  $\text{Na}_2\text{SO}_4$  film at 1173K in  $\text{O}_2$  - 0.1%  $\text{SO}_3$  gas. The central dashed line in the NiO stable field indicates the minimum in NiO solubility [69]. Reproduced by permission of The Electrochemical society.

There are therefore three important contributions from this experiment.

- 1) The starting point of the hot corrosion experiment is in a region more basic than the ambient gas phase. This means that the reaction of Ni with  $\text{Na}_2\text{SO}_4$  overrides the salt/gas interaction. Therefore, in the case of Ni, Type I hot corrosion attacks are not dependent on the composition of the gas.
- 2) This experiment quantitatively validated the Rapp and Goto criterion for a negative solubility gradient condition. The significant shift to the more basic region during the experiment satisfies the negative solubility gradient condition and results in severe hot corrosion of the sample.
- 3) If the chemistry of the metal/salt interface is maintained in the acidic dissolution region, hot corrosion could be prevented because the acidic dissolution of Ni does not satisfy the negative solubility gradient criterion. Therefore, this study also suggested that hot corrosion can be prevented by buffering the chemistry of the metal/salt interface such that the negative solubility gradient criterion cannot be satisfied.

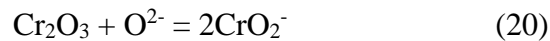
#### **2.3.4.1.4 Role of chromium in reducing hot corrosion attacks**

Bornstein and Decrescente [107] conducted hot corrosion experiments for different binary Ni-Cr and Ni-Al alloys,  $\text{Cr}_2\text{O}_3$ -forming wasp alloy and  $\text{Al}_2\text{O}_3$ -forming B-1900 with deposition of  $\text{Na}_2\text{SO}_4$  and  $\text{Na}_2\text{CO}_3$  at  $800^\circ\text{C}$  -  $1000^\circ\text{C}$ . The results showed that the oxidation of  $\text{Al}_2\text{O}_3$ -forming B-1900 and Ni-Al alloys is equally accelerated by both salts while in the case of the  $\text{Cr}_2\text{O}_3$ -forming wasp alloy and Ni-Cr alloys, oxidation is not accelerated by either salt. Consequently, they concluded that Cr can enhance hot corrosion resistance because the formation of  $\text{Cr}_2\text{O}_3$  and its

basic dissolution can reduce oxide ion levels (activity) at the oxide scale/salt interface based on the reaction provided in Equation (16). They also observed Cr in the water which was used to wash the corroded samples.

The basic dissolution of  $\text{Cr}_2\text{O}_3$  depends on the oxygen activity due to the valence change in Cr in the reaction provided in Equation (16) [101]. This dependence of basic chromate ( $\text{CrO}_4^{2-}$ ) solute on oxygen activity has been considered an important factor in determining the role of Cr in reducing hot corrosion attacks [108]. Zhang [101] determined the solubility of  $\text{Cr}_2\text{O}_3$  in fused  $\text{Na}_2\text{SO}_4$  at 1200 K for  $\text{PO}_2 = 1$  atm (Figure 2.13) to further understand the role of Cr in hot corrosion.  $\text{Cr}_2\text{O}_3$  was dissolved into  $\text{Na}_2\text{CrO}_4$  in the basic dissolution region as a chromate ( $\text{CrO}_4^{2-}$ ) solute.

It can be seen from Figure 2.13 that the slope of the basic dissolution of  $\text{Cr}_2\text{O}_3$  deviates from Equation (16). This indicates the presence of chromite ( $\text{CrO}_2^-$ ) solute near the solubility minimum region by using the equation below [101]:



Since no valence changes are involved in this reaction, there is no dependence of the solubility on the oxygen activity expected here [101]. The compiled results in Zhang [101] are plotted in Figure 2.14 which show the dominant Cr solutes based on basicity and  $\text{PO}_2$ . The plot shows that the solubility of the chromite ( $\text{CrO}_2^-$ ) solute is higher at a low  $\text{PO}_2$ , while the chromate ( $\text{CrO}_4^{2-}$ ) solute is more soluble with high oxygen activity (at the salt/gas interface). Moreover, the chromia ( $\text{Cr}_2\text{O}_3$ ) solubility increases with increasing oxygen activity [108]. This means that chromia is always more soluble at a more oxidizing (salt/gas) interface than at a more reduced (oxide/salt) interface [108]. In the words of Rapp and Otsuka [108]: "...unlike most other oxides, chromia presents a **positive** solubility gradient in the salt film, and is not subject to the Rapp-Goto "negative solubility

gradient” criterion for sustained hot corrosion caused by dissolution of the oxide at the oxide/salt interface with reprecipitation of particulate oxide in the salt film”. This special characteristic of chromia is even more evident when Cr is added to reactive base metals like Ni, Fe and Co. The oxides of these metals have the tendency to form an acidic solute (which releases oxide ions and increases the local basicity of salt). This is balanced by the tendency of  $\text{Cr}_2\text{O}_3$  to react with these oxide ions to create chromate or chromite ions. The chromate or chromite ion formation buffers the solution and prevents the shift to a more basic condition [108]. Consequently, the basic dissolution of Ni, Fe and Co oxides as well as their acidic dissolution do not satisfy the Rapp-Goto criterion for a negative solubility gradient, so sustained hot corrosion attacks cannot take place.

Shi and Rapp [109] further investigated the role of Cr through various electrochemical experiments. Their results showed that in the cathodic polarization of  $\text{Na}_2\text{SO}_4\text{-Na}_2\text{CrO}_4$  at 1200 K, a direct conversion of chromate to chromite was not observed, while based on the results in Zhang [101], the chromite ions are more stable in reducing conditions. They observed that after more reduction, an intermediate species is formed which results in the precipitation of solid  $\text{NaCrO}_2$  or  $\text{Cr}_2\text{O}_3$  in the basic and neutral solutions respectively. Therefore, the inability of chromate ions to reversely convert into chromite ions after more reduction signifies that considerable chromate solubility exists even near the oxide/salt interface. Consequently, during hot corrosion, these chromate ions are able to precipitate back to solids of  $\text{NaCrO}_2$  or  $\text{Cr}_2\text{O}_3$  which deposit and block reducing sites (oxide grain boundaries and flaws) at the metal/salt interface. Therefore, this can seal the alloy and provide protection as shown in Figure 2.15 [69].

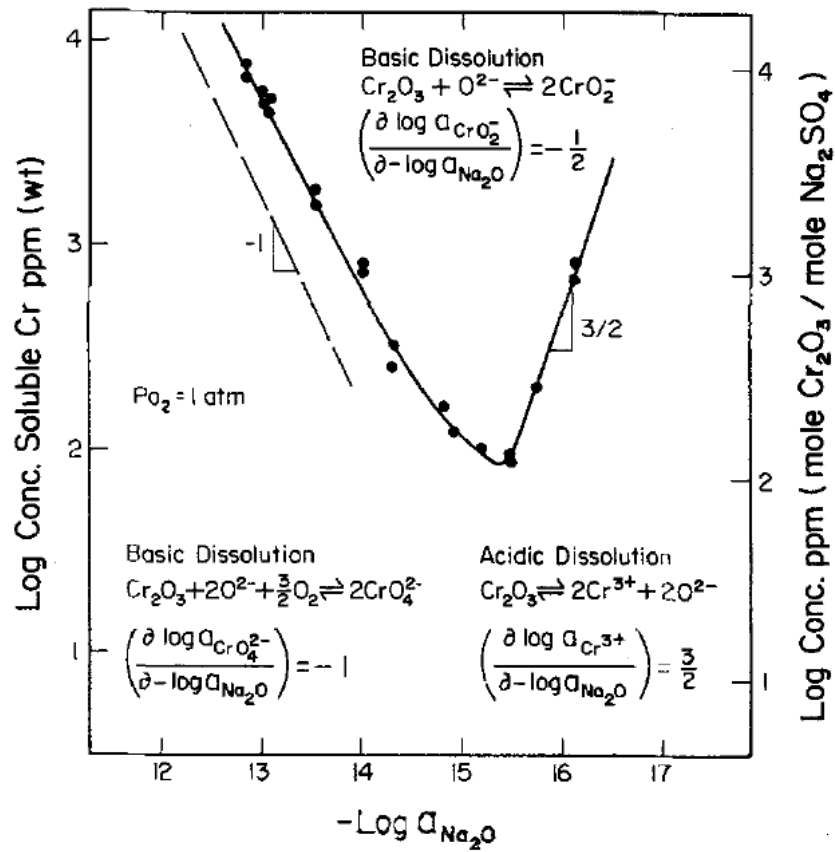


Figure 2.13 - solubility of  $Cr_2O_3$  in fused  $Na_2SO_4$  at 1200k for  $PO_2 = 1 \text{ atm}$  [101]. Reproduced by permission of The Electrochemical society.

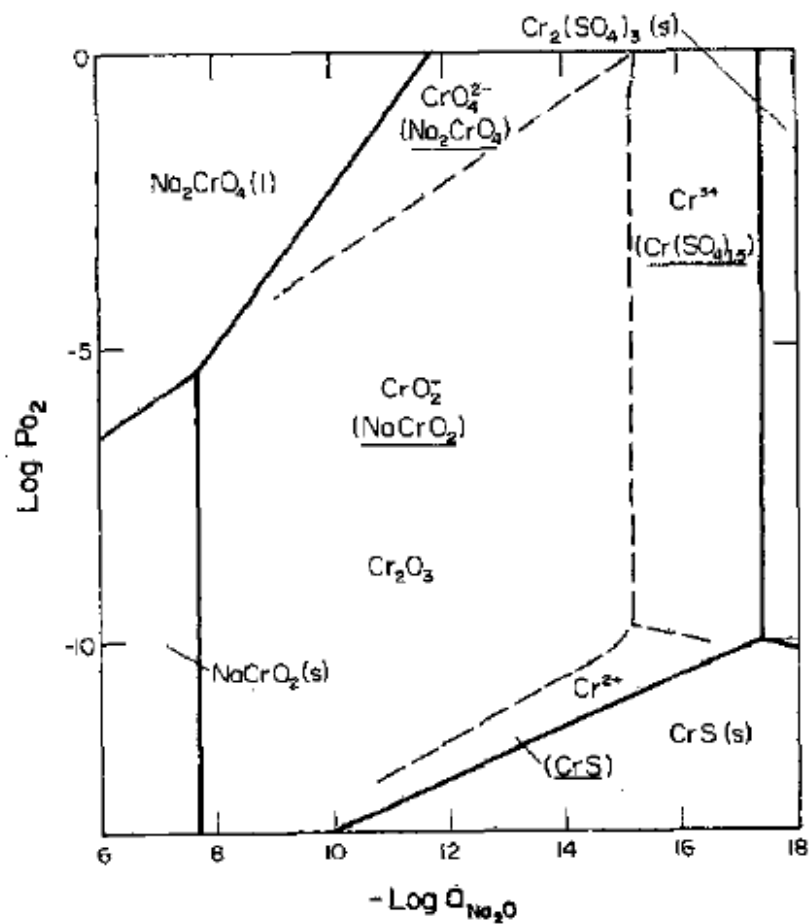


Figure 2.14 – Dominant chromium species in Na<sub>2</sub>SO<sub>4</sub> – Cr<sub>2</sub>O<sub>3</sub> system at 1200K [101].  
 Reproduced by permission of The Electrochemical society.

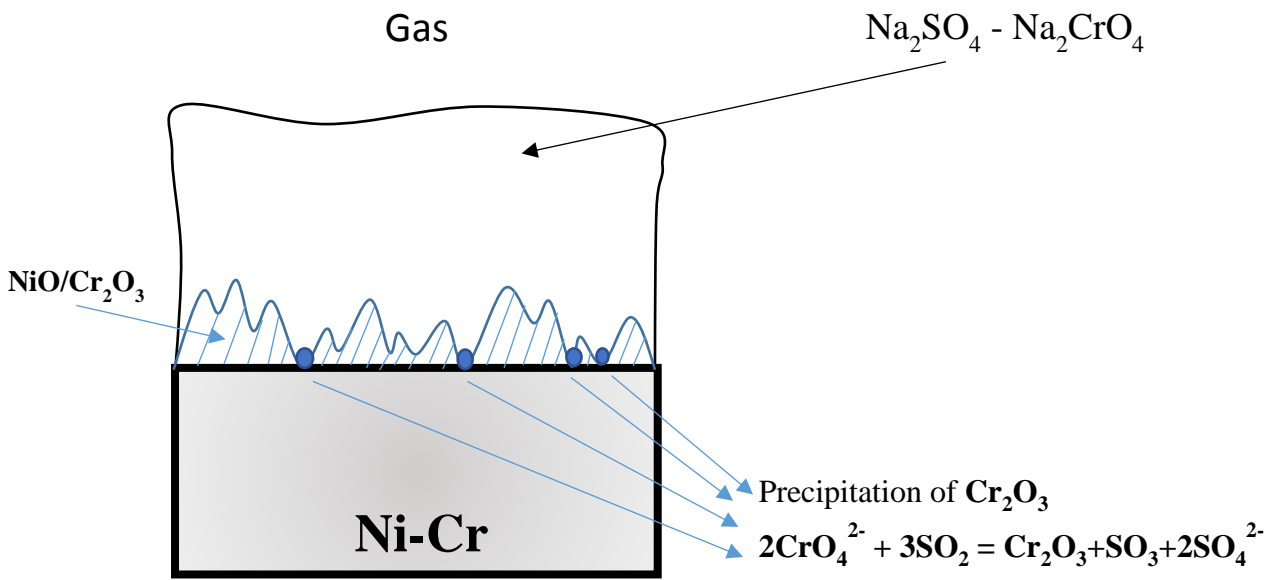


Figure 2.15 - Schematic presentation of the inhibiting action of Chromium in hot corrosion attack by precipitation back on oxide grain boundaries and other defects [69].

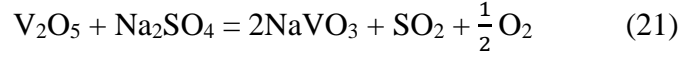


### 2.3.4.2 Alloy induced acidic fluxing

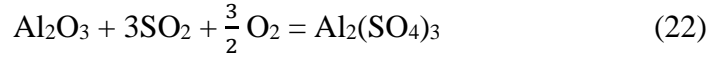
Goebel et al. [92] performed many experiments to determine the effects of different alloy compositions that contain Cr, Al, Mo, W and V on the hot corrosion caused by  $\text{Na}_2\text{SO}_4$ . They concluded that in general, there are two types of high temperature hot corrosions (Type I):  $\text{Na}_2\text{SO}_4$  induced accelerated oxidation and  $\text{Na}_2\text{SO}_4$  induced catastrophic oxidation. In the former, a basic fluxing mechanism is observed and takes place when an alloy does not contain Mo while the latter takes place when alloying elements such as Mo are found in the alloy.  $\text{Na}_2\text{SO}_4$  induced accelerated oxidation has been discussed in Section 2.3.4.1, and therefore the focus here will be on catastrophic oxidation.

In Section 2.3.4.1, it was shown that due to a shift towards a locally higher basic melt at the oxide/salt interface, a negative solubility gradient is found across the salt. Consequently, basic fluxing can take place. However, this attack is not self-sustaining [52]. In Figure 2.8, the oxide solubility plots show that acidic melts can also considerably dissolve the protective oxide scales. Generally, acidic conditions can be generated in  $\text{Na}_2\text{SO}_4$  salt either by  $\text{SO}_3$  in gas or alloying elements such as W and Mo which are added to superalloys as a solid-solution strengthener or V which is often an impurity in low-grade heating oils [4]. The oxides of these elements have the tendency to complex with oxide ions in salt to form tungstate, molybdate or vanadate ions [14].

Bornstein, Decrescente and Roth [110] investigated the effects of various alloying elements on the  $\text{Na}_2\text{SO}_4$  induced hot corrosion of Ni-base alloys at temperatures of  $800^\circ\text{C}$  -  $1000^\circ\text{C}$ . In the case of  $\text{Al}_2\text{O}_3$ -forming alloys, the hot corrosion rate is significantly increased when Mo or V is present in the alloys or  $\text{Na}_2\text{SO}_4$  is co-deposited with  $\text{MoO}_3$  or  $\text{V}_2\text{O}_5$ . Equation (21) shows the reaction of acidic oxides with oxide ions and formation of  $\text{SO}_2$ .



The released  $\text{SO}_2$  then dissolves into the  $\text{Al}_2\text{O}_3$  protective oxide scales in accordance with Equation (22) and result in the formation of soluble sulfate:



Bornstein, Decrescente and Roth [110] attributed the accelerated attack to the low melting point of  $\text{MoO}_3$  and  $\text{V}_2\text{O}_5$  as opposed to their respective binary oxides. Therefore, this contributes to a reduction in the liquidus temperature for their solutions with  $\text{Na}_2\text{SO}_4$ . A reduction in the liquidus temperature of film in hot corrosion means that the temperature for the hot corrosion attack is reduced to lower temperatures [14]. These molten, corrosive oxides can cause fluxing of the protective  $\text{Al}_2\text{O}_3$  oxide scales which result in the rapid degradation of the material (formation of soluble  $\text{Al}_2(\text{SO}_4)_3$  in reaction provided in Equation (22)) [110].

Goebel et al. [92] performed many hot corrosion experiments on a number of Ni-Al and Ni-Cr-Al alloys that contain W, Mo and V in air with thin  $\text{Na}_2\text{SO}_4$  deposits. All of the materials were substantially corroded. They observed an enrichment of the oxide scales in the refractory elements. Furthermore, attacks were initiated at phases rich in refractory elements, e.g. Mo-carbide. The following mechanism was then developed for Ni-Al-Mo alloys. However, based on their observations, it can be applicable to any alloy that contains refractory elements. During the initiation stage, the oxides of  $\text{Al}_2\text{O}_3$ , NiO and  $\text{MoO}_3$  form on the alloy surface.  $\text{MoO}_3$  reacts with the oxide ions in the salt based on reaction given in Equation (23):



This reaction reduces the oxide ion activity in the melt and consequently, prevents the occurrence of basic fluxing. The reduction in oxide ion activity in the melt adjacent to the scales can continue through the above reaction until the reaction in Equation (22) becomes possible. This means that  $\text{Al}_2\text{O}_3$  scales can dissolve through acidic dissolution. These strong acidic solutes greatly increase the solubility of the protective oxide scales ( $\text{Al}_2\text{O}_3$ ). Moreover, these acidic solutes show a high gas pressure which results in their evaporation from the salt/gas interface. The continual formation of  $\text{MoO}_3$  at the alloy/salt interface and its evaporation at the salt/gas interface result in the presence of a negative solubility gradient of this acidic solute and consequently sustains acidic fluxing.

### **2.3.5 Low temperature (Type II) hot corrosion**

Type II hot corrosion takes place at comparatively low temperatures, or approximately  $650^\circ\text{C}$  -  $750^\circ\text{C}$ . One would expect negligible corrosion in this temperature range because  $\text{Na}_2\text{SO}_4$  is a solid ( $T_m=884^\circ\text{C}$  [63]). However this type of hot corrosion is known to be perhaps the most severe form of hot corrosion attacks.

Conde and Wareham [111] were among the first to demonstrate hot corrosion at these low temperatures. They observed a Nimonic 105 blade attacked by pitting corrosion after operating in a coastal region at about  $750^\circ\text{C}$ . The degraded microstructure was completely different from those caused by high temperature hot corrosion and included pits that extended into the alloy [57].

Many mechanisms have been introduced to explain for Type II hot corrosion [112] [113] [114]. It is generally agreed that at temperatures of  $650^\circ\text{C}$  to  $750^\circ\text{C}$ , solid  $\text{Na}_2\text{SO}_4$  is converted into a liquid eutectic of  $\text{Na}_2\text{SO}_4/\text{MSO}_4$ , which has a considerably lower melting point than that of pure  $\text{Na}_2\text{SO}_4$ . This conversion happens because of the reaction with  $\text{SO}_3$  in the gas [57]. Therefore, it has been

considered that in order to stabilize this eutectic melt, an  $\text{SO}_3$  pressure of about  $10^{-5}$  is necessary [115]. This  $\text{SO}_3$  pressure is commonly used in the gas stream of marine or industrial gas turbines [52].

Wortman et al. [116] observed that CoCrAlY coatings are very vulnerable to this type of hot corrosion. Therefore, Type II hot corrosion studies have focused on Co-base materials. In the case of CoCrAlY alloys, the mechanism suggested by Luthra [112] is considered as the most reliable [57].

Luthra [112] proposed that a liquid  $\text{Na}_2\text{SO}_4\text{-CoSO}_4$  solution forms on the alloy surface and  $\text{SO}_3$  is transported from the gas via  $\text{S}_2\text{O}_7^{2-}$  ions through the  $\text{Na}_2\text{SO}_4\text{-CoSO}_4$  liquid. Co ions go into the liquid sulfate at the scale/sulfate interface as  $\text{Co}^{2+}$  and  $\text{Co}_3\text{O}_4$  is precipitated out into the liquid sulfate near the gas interface. In the case of a high  $\text{SO}_3$  pressure,  $\text{CoSO}_4$  precipitates rather than  $\text{Co}_3\text{O}_4$ . The dissolution of Co from the alloy results in the formation of porous and non-protective  $\text{Cr}_2\text{O}_3$  and  $\text{Al}_2\text{O}_3$  oxide layers. Therefore, severe hot corrosion attacks can take place. This proposed mechanism to address Type II is applicable to some alloys but not all of them.

## **2.4 Scope of investigation**

As previously discussed, wide-gap brazing is considered to be the preferred technique over the other repairing and joining methods when it comes to repairing or joining wide gaps or cracks in precipitation hardened Ni-base superalloy components used in gas turbine engines. A composite powder mixture is used which consists of an additive powder with a high melting point and a conventional brazing filler alloy powder. It is generally believed that additive powder does not completely melt during brazing because the temperature used during brazing is always well below its melting point. However, recent studies show that it is possible to have complete melting of additive powder in brazed joints, depending on the combination of different brazing parameters used.

On the other hand, these repaired parts must have sufficient resistance to possible damage and degradation that are commonly found in gas turbine engines, particularly, hot corrosion. Unfortunately, only a few scientific investigations have studied the effects of brazing on the hot corrosion resistance of wide-gap brazed Inconel 738 joints. Therefore, the objective of this work is to investigate the influence of brazing and use of different interlayer materials on hot corrosion resistance of brazed IN738 superalloy. In addition, the effect of additive powder in composite powder mixture on hot corrosion resistance of the wide-gap brazed Inconel 738 joints are also investigated.

## **CHAPTER 3 – MATERIALS AND EXPERIMENTAL PROCEDURE**

### **3.1 Experimental**

In this study, the experimental investigation is carried out in two stages:

1. Wide-gap brazing and microstructural analysis of the brazed joints, and
2. A study of the hot corrosion of brazed joints by using the immersion method.

### **3.2 Materials**

#### **3.2.1 Base material**

The Ni-base superalloy used in this research is IN 738 polycrystalline in the as cast condition. Its chemical composition is shown in Table 3.1.

#### **3.2.2 Composition of interlayer powders**

AMDRY 775, which is a conventional filler alloy powder with a melting temperature of 1055°C, was used as the filler alloy powder in all of the experiments, see Table 3.2. Different additive powders were then added to the filler alloy with a constant mix ratio of R<sub>7:3</sub> for all the experiments, or 70 wt.% conventional brazing filler alloy powder + 30 wt.% additive powder. The additive powders used in this study are IN 738 (AMDRY 7380-fine powder), Nicrogap 108 and Haynes 282. Their respective compositions are shown in Table 3.3.

*Table 3.1 – Chemical composition of IN 738 polycrystalline in as cast condition.*

<b>Elements</b>	<b>Wt%</b>
<b><i>Chromium</i></b>	<b><i>16.02</i></b>
<b><i>Cobalt</i></b>	<b><i>8.38</i></b>
<b><i>Molybdenum</i></b>	<b><i>1.78</i></b>
<b><i>Titanium</i></b>	<b><i>3.5</i></b>
<b><i>Aluminum</i></b>	<b><i>3.6</i></b>
<b><i>Tantalum</i></b>	<b><i>1.77</i></b>
<b><i>Tungsten</i></b>	<b><i>2.53</i></b>
<b><i>Niobium</i></b>	<b><i>0.89</i></b>
<b><i>Iron</i></b>	<b><i>0.07</i></b>
<b><i>Carbon</i></b>	<b><i>0.15</i></b>
<b><i>Boron</i></b>	<b><i>0.013</i></b>
<b><i>Zirconium</i></b>	<b><i>0.05</i></b>
<b><i>Sulphur</i></b>	<b><i>0.001</i></b>
<b><i>Manganese</i></b>	<b><i>0.01</i></b>
<b><i>Nickel</i></b>	<b><i>Bal</i></b>

*Table 3.2 – Chemical composition of regular brazing filler alloy*

<b>Regular Brazing Filler Alloy</b>	<b>Chemical Composition Wt.%</b>
AMDRY 775	15.0 Cr, 3.5 B, Bal. Ni

*Table 3.3 – Chemical composition of additive powders used in this study.*

<b>Additive powder</b>	<b>Chemical Composition Wt.%</b>
AMDRY 7380	Same as IN738 (Table 3.1)
Nicrogap 108 (M <sub>T</sub> : 1800°C)	15 Cr, 0.75 Si, 7 Fe, 0.2 B, Bal. Ni
Haynes 282 (M <sub>T</sub> : 1300°C)	20 Cr, 10 Co, 8.5 Mo, 2.1 Ti, 1.5 Al, 1.5 Fe, 0.3 Mn, 0.15 Si, 0.06C, 0.005 B, Bal. Ni



### **3.3 Wide-gap brazing and microstructural analysis of brazed joints**

#### **3.3.1 Sample preparation and wide-gap brazing**

The as-received Inconel 738 base material was sectioned into coupons with a dimension of 13.70 mm × 9.30 mm × 4.54 mm by using a numerical controlled DS-2 travelling wire electro-discharge machine ((EDM), Hansvedt). The EDM was also used to create 0.32 mm gap sizes (see Figure 3.1), and the machined surfaces were subsequently sanded by using 180, 400, 600, and 1200 grade silicon-carbide (SiC) papers to remove the oxide layers and then ultrasonically cleaned in acetone for 20 minutes. The non-mating surfaces of the samples were given a ceramic coating, Nicrobraz Green Stop-off, to avoid the liquated interlayer from flowing out of the joint area during bonding. An adequate amount of interlayer powder was placed between the mating surfaces to fill the gap.

The wide-gap brazing was carried out in a LABVAC 11 vacuum furnace with a vacuum pressure of approximately  $5 \times 10^{-5}$  torr. Various brazing cycles were performed as shown in Figures 3.2, 3.3, 3.4. The brazing cycle shown in Figure 3.2 was used for brazed samples with 100% conventional brazing filler alloy and also to obtain partial melting of IN738, Nicrogap 108 and Haynes 282 additive powders. The brazing cycle in Figure 3.3 was used to obtain complete melting of IN738 additive powder and the brazing cycle in Figure 3.4 was used for complete melting of Haynes 282 additive powder.

#### **3.3.2 Microstructural examination of brazed samples**

The brazed samples were perpendicularly sectioned to their bonding surfaces with the EDM and then mounted on Bakelite, grounded with 180, 400, 600 and 1200 grade SiC papers and

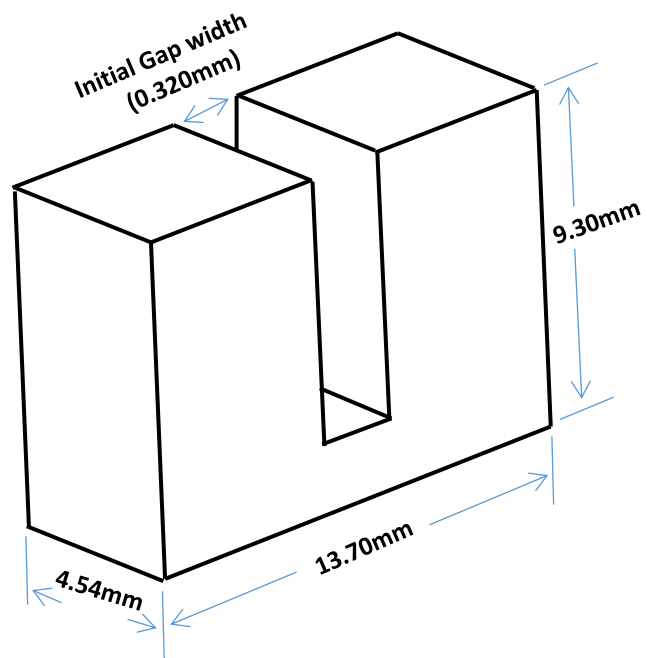


*Figure 3.1 – Configuration of samples.*

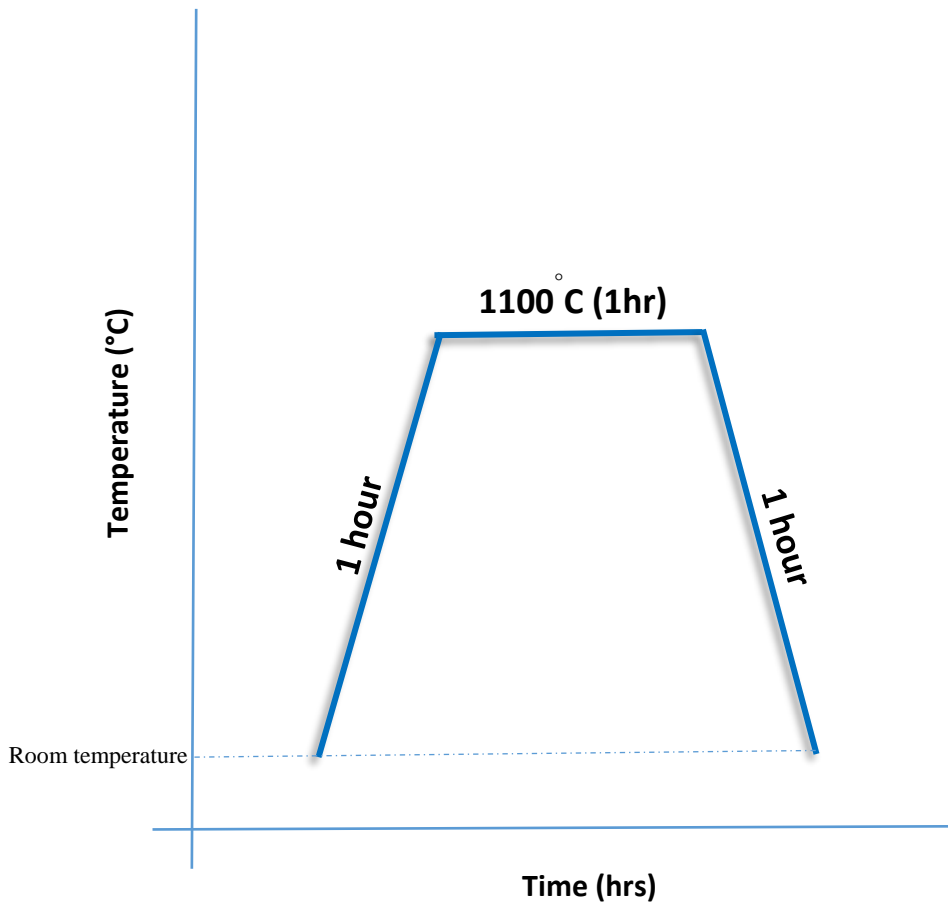


*Figure 3.2 - The brazing cycle which was done at 1100°C for 1 hour.*

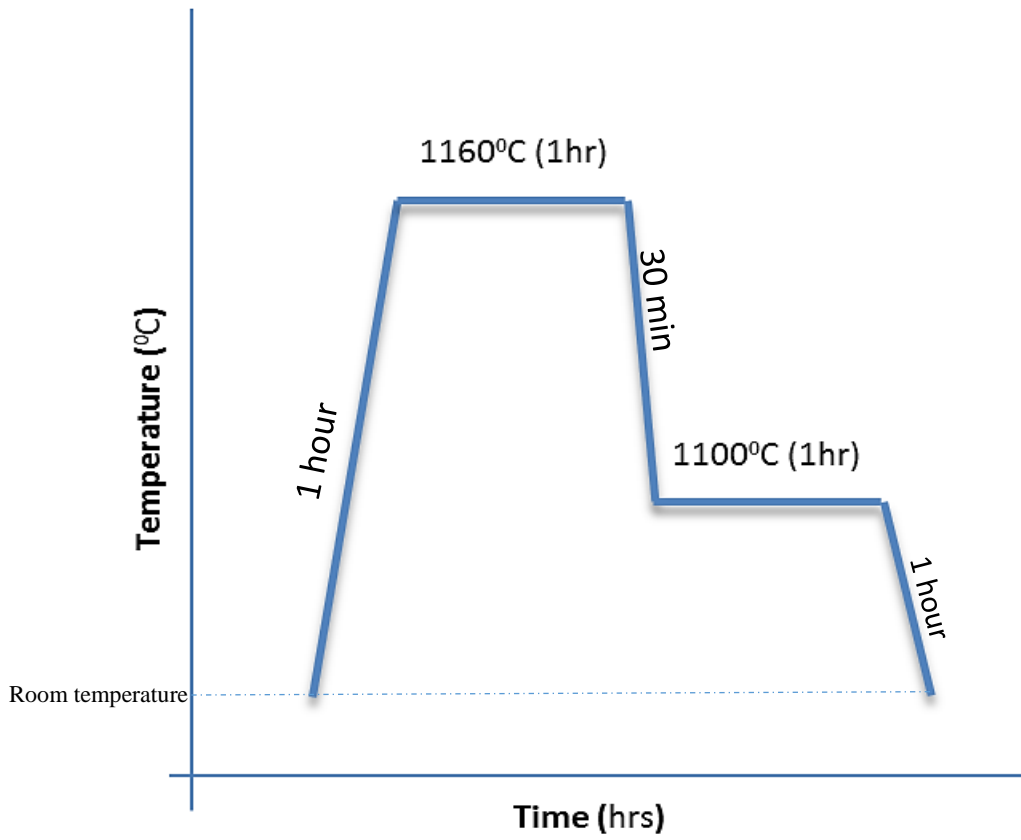


Figure 3.3 – The brazing cycle used to obtain complete melting of Inconel 738 additive powder.

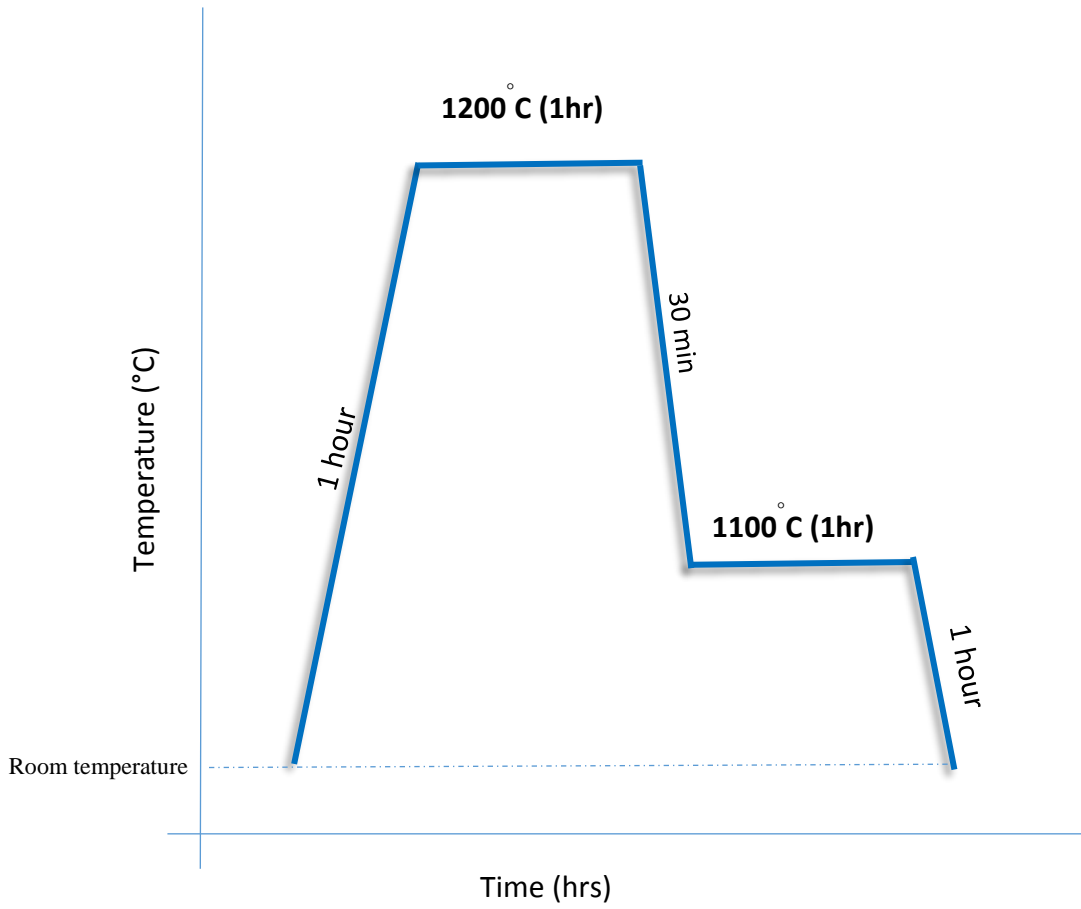


Figure 3.4 – Brazing cycle used to obtain complete melting of Haynes 282 additive powder.

subsequently polished with 6 mm silica paste and finally 1  $\mu\text{m}$  diamond paste. The samples were etched by using electro-etch with 48 mL of sulfuric acid, 40 mL of nitric acid and 12 mL of phosphoric acid solution. The examination of the joint microstructure was preliminarily done by using a ZEISS Axiovert25 optical microscope and an inverted reflected light microscope equipped with CLEMEX Vision 3.0 image processing software. For better detection of the phases and their composition in the joint microstructure, a JEOL JSM 5900LV scanning electron microscope (SEM) equipped with an ultra-thin window energy dispersive spectrometer (EDS; Oxford) was used. The SEM was also used to obtain better images of the surface morphology and characterize the phases and their composition in the joint microstructure.

### **3.4 Hot corrosion experiment**

All of the brazed samples were grinded with the 180, 400, 600, and 1200 SiC papers and then cleaned for 20 minutes in acetone. The dimensions and weight of each sample were determined prior to carrying out the hot corrosion experiment. The samples were weighed by using a digital microbalance (Denver Instrument) at a resolution of  $\pm 0.01$  mg. Different salt mixtures, namely, 100 wt.%  $\text{Na}_2\text{SO}_4$ , 25 wt.%  $\text{NaCl}$  + 75 wt.%  $\text{Na}_2\text{SO}_4$  and 50 wt.%  $\text{NaCl}$  + 50 wt.%  $\text{Na}_2\text{SO}_4$  and also different temperatures, that is,  $900^\circ\text{C}$ ,  $950^\circ\text{C}$  and  $1000^\circ\text{C}$  were used in the hot corrosion experiments. Hot corrosion was carried out by using the immersion method, in which the sample was immersed into a crucible full of salts and then placed into the furnace [13] [16] [20] [77] [94] [116] [117] [118] [119] [120] [121] [122] [123] [124] [125] [126] [127] [128] [129] [130] [131]. Therefore, the samples were immersed into 15 mL ceramic crucibles that contained salts and then

placed into a Carbolite furnace with an air atmosphere and temperature variation of ( $\pm 5^\circ\text{C}$ ) for different holding times. The crucibles were then removed from the furnace after a specific holding time and cooled in air. The samples were subsequently washed to remove the salts and placed in boiling distilled water for a minimum of 1 hour. A brush was used to remove the corrosion products and after that, the samples were ultrasonically cleaned in acetone and dried with a hair dryer. The samples were weighed after descaling and the weight loss was measured by using  $\Delta W = \frac{W_2 - W_1}{A}$  ( $\text{mg}/\text{cm}^2$ ), where  $W_1$  is the weight of the specimen before testing,  $W_2$  is the weight of the specimen after testing (after removing the corrosion products) and  $A$  is the total surface area of the sample. The hot corrosion data were plotted as weight loss ( $\text{mg}/\text{cm}^2$ ) versus exposure time (hour).

## **CHAPTER 4 – RESULTS AND DISCUSSION**

### **4.1 Microstructure and Hot Corrosion Behavior of IN738 Base Alloy and Brazed Samples with 100% Conventional Brazing Filler Alloy**

The first step in this study is to determine the hot corrosion behavior of IN738 base alloy and then compare it with hot corrosion results from brazed samples using 100% regular brazing filler alloy. The purpose is to investigate the effect of brazing on hot corrosion resistance of IN738 samples. Inconel 738 which was used as the base alloy in this research, generally consists of a gamma matrix with an extensively dispersed gamma prime intermetallic phase, MC carbides and gamma-gamma prime eutectics, as shown in Figures 4.1 and 4.2.

The hot corrosion experiment was performed by using the immersion method with 25% NaCl + 75% Na<sub>2</sub>SO<sub>4</sub> salt mixture, which is considered as the most widely used type of salt to evaluate the corrosion resistance of superalloys [13] [17] [120] [132] [133] [134]. The addition of NaCl to Na<sub>2</sub>SO<sub>4</sub> is because in the alloy studied, the Cr content is high and consequently will result in the formation of very protective Cr<sub>2</sub>O<sub>3</sub> scales during the hot corrosion tests. Therefore, a severe test medium is selected in this study. The hot corrosion experiment was done isothermally at 900°C in a furnace in air atmosphere for different exposure times. Figure 4.3 shows the hot corrosion behavior of IN738 base metal. It was observed that up to 110 hours exposure time used in this study, the IN738 base alloy did not show any considerable amount of weight-loss. After carrying out a visual inspection, a thin layer of protective oxide scale was observed on the surface of the IN738 base alloy. Figure 4.4 shows the SEM-EDS x-ray mapping from the oxide scale formed on



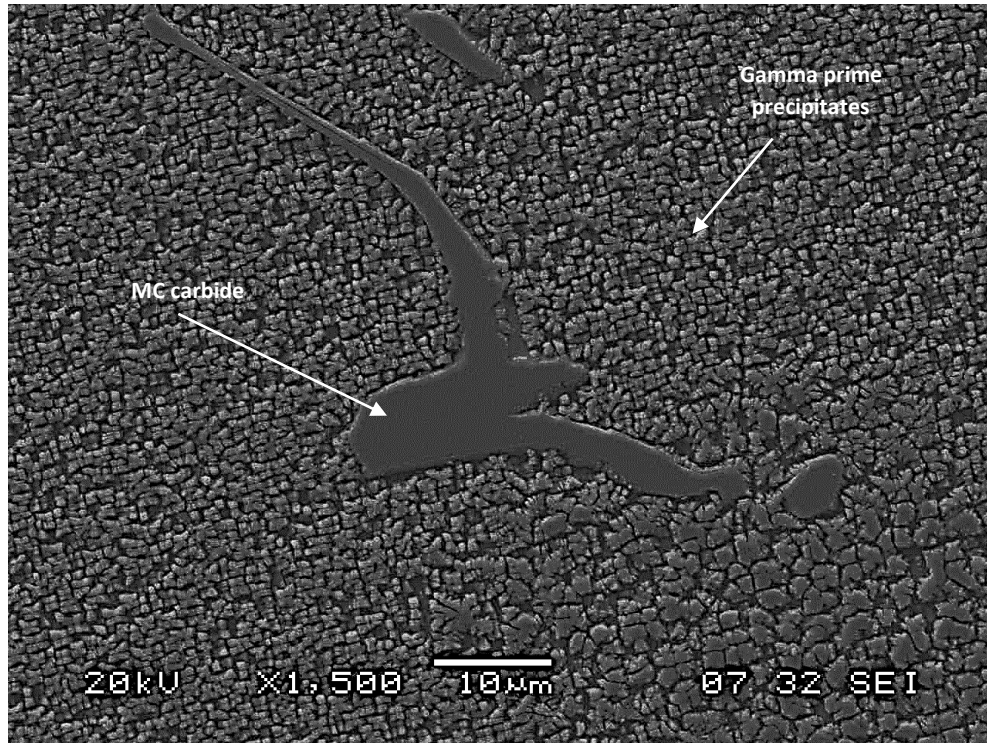


Figure 4.1 – SEM micrograph of Mc carbide in cast IN738.

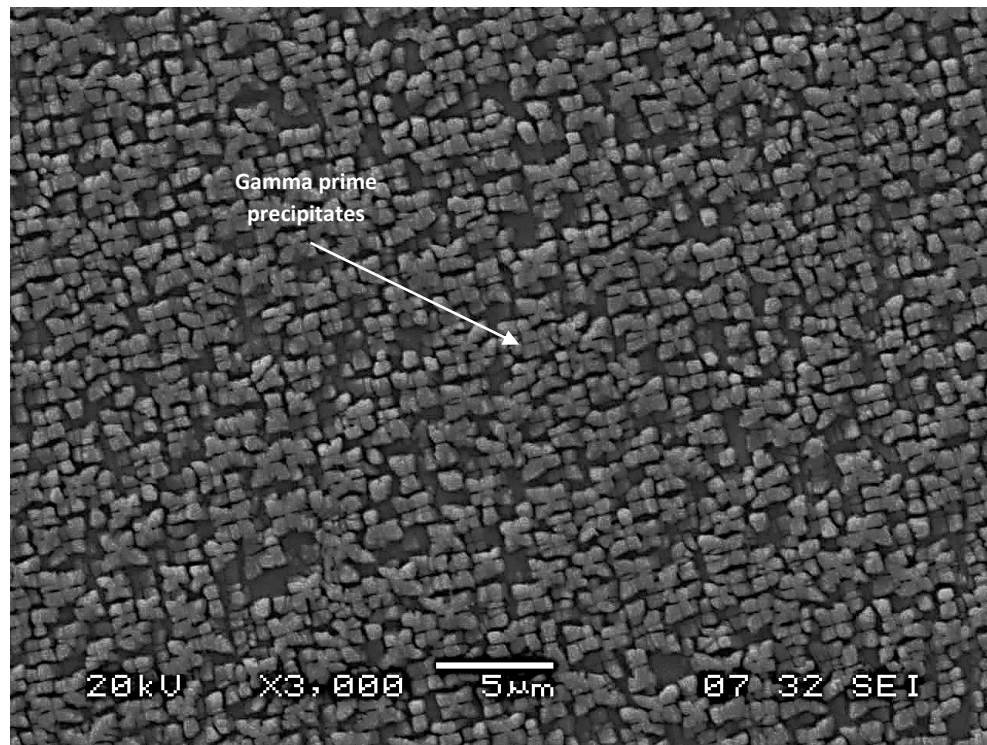
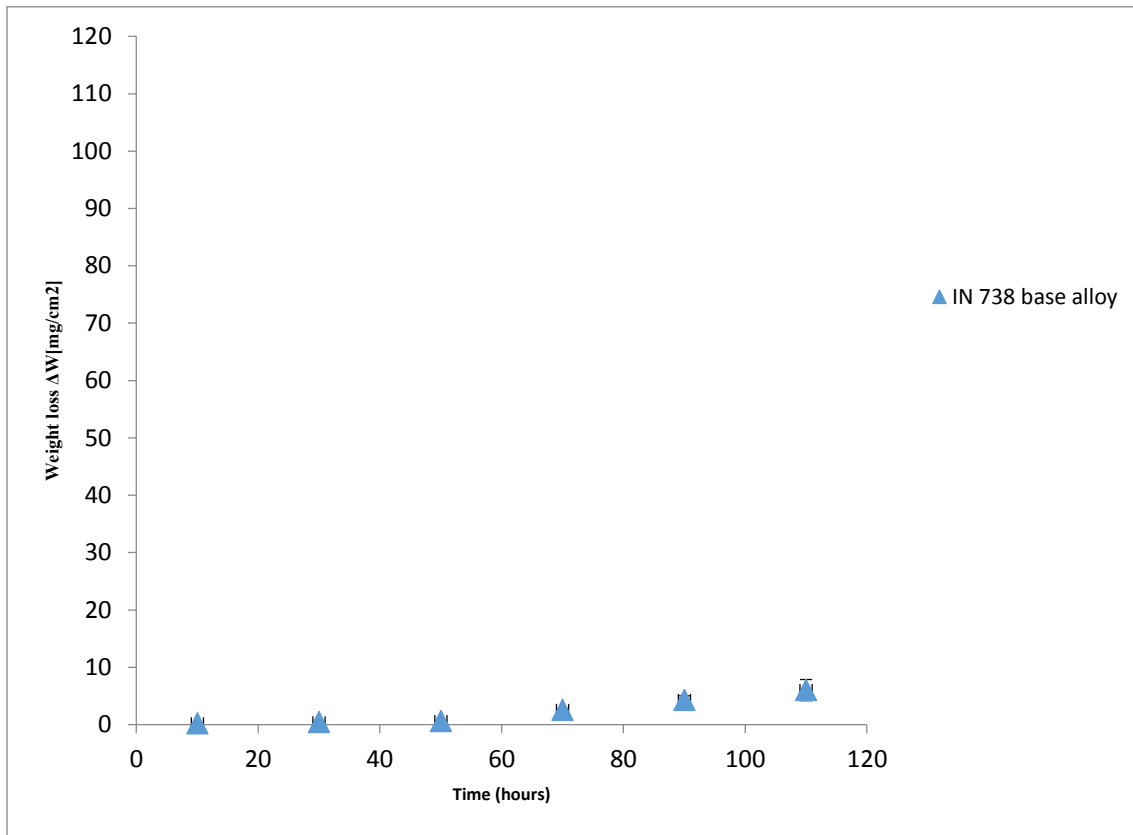
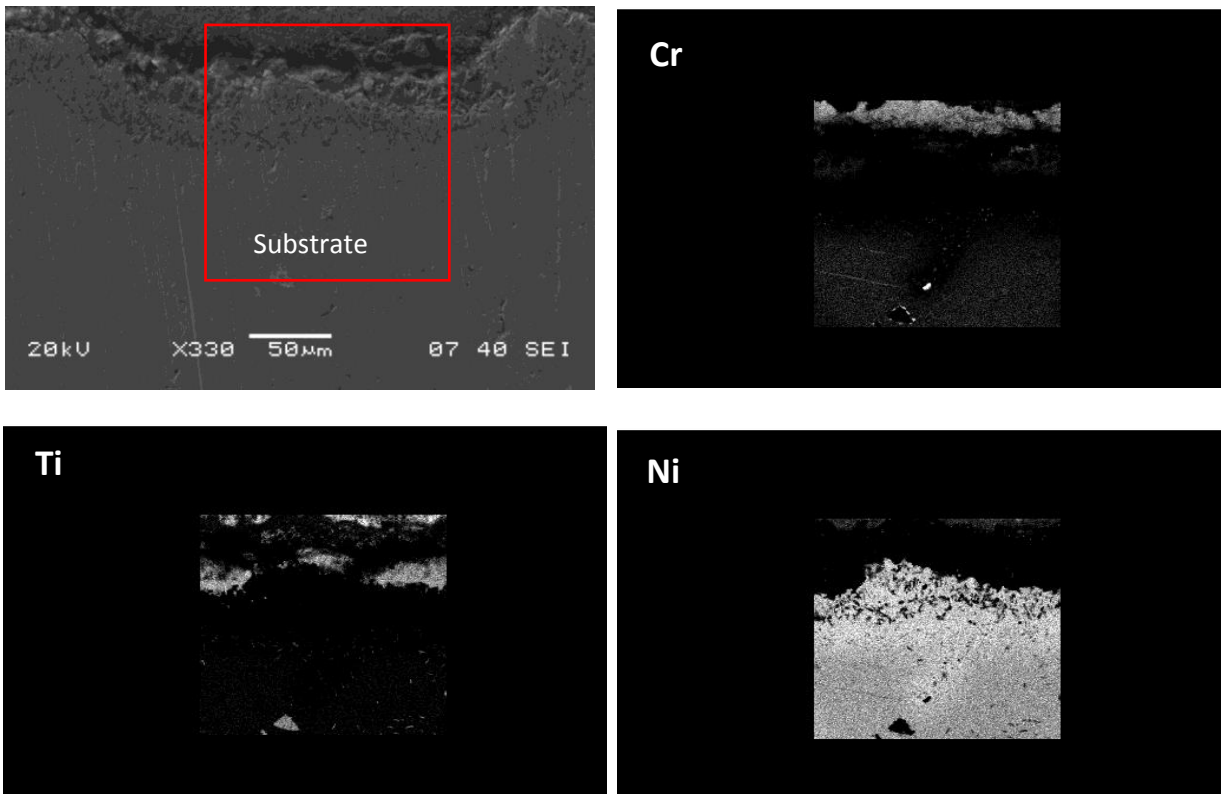


Figure 4.2 – SEM micrograph of gamma prime precipitates on gamma matrix.

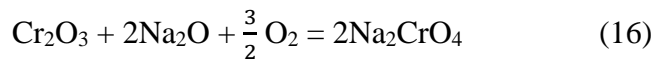


*Figure 4.3 - Hot corrosion behavior of IN738 base metal. The maximum weight-loss, which was observed at 110 hours exposure time, was less than 10 mg/cm<sup>2</sup>.*



*Figure 4.4 – SEM-EDS x-ray mapping from oxide scale on IN738 base alloy. The oxide scale is rich in Cr and Ti.*

the surface of the IN738 base alloy which shows that the oxide scale is rich in Cr and Ti. The hot corrosion behavior of Inconel 738 has been studied by a number of researchers [62] [67] [68] [81] [82] [135]. Considering that the nature and composition of oxide scales, which form on the surface of a material during hot corrosion, depends on the composition of the alloy, it has been well established that IN738 which contains 16% Cr and 3% Ti produces protective and dense Cr<sub>2</sub>O<sub>3</sub> and TiO<sub>2</sub> oxide scales. The good resistance of IN738 superalloy to hot corrosion is due to its protective Cr oxide scale. Cr is considered as the most beneficial alloying element to prevent hot corrosion. This is because of some reasons. The first reason is that unlike other alloying elements, basic dissolution of Cr<sub>2</sub>O<sub>3</sub> (chromia) depends on oxygen activity [101]. This is due to the valence change of Cr in reaction (16) [101]. Chromia solubility increases with increasing oxygen activity [52]. Therefore, chromia is always more soluble at the more oxidizing interface (salt/gas) than at a more reduced interface (oxide/salt). This results in the inability of chromia to satisfy Rapp and Goto negative solubility criterion [106]. The Rapp and Goto negative solubility criterion is satisfied if solubility of the protective oxide scale is greater at the oxide/salt interface and decreases towards the salt/gas interface [106]. Therefore, the protective oxide scale will dissolve at the oxide/salt interface and precipitate as non-protective oxide scale at the salt/gas interface, where the solubility is lower.



Second specific feature of Cr is that chromate ions are able to precipitate back to solids of NaCrO<sub>2</sub> or Cr<sub>2</sub>O<sub>3</sub> which deposit and block oxide grain boundaries and flaws at the metal/salt interface [109]. This can seal the alloy and provide protection. Moreover, Cr also inhibits detrimental effects produced by sulfur in some alloys by forming Cr sulfides. This prevents the formation of other deleterious sulfide phases such as Al sulfide or liquid NiS [92]. Based on these references [62]

[67] [68] [81] [82] [135], the hot corrosion attacks against Inconel 738 are initiated by basic fluxing followed by acidic fluxing of the protective oxide scales. Initially,  $\text{Cr}_2\text{O}_3$  and  $\text{TiO}_2$  react with  $\text{Na}_2\text{SO}_4$  to form  $\text{Na}_2\text{CrO}_4$  and  $\text{Na}_2\text{O}(\text{TiO}_2)_n$  and gaseous  $\text{SO}_3$ . Therefore, a large portion of the protective oxide scale is removed. This results in the inability of the alloy to reproduce protective oxide scales because of the large depletion of Cr from the region adjacent to the oxide scale. As the oxidation process proceeds, non-protective oxide scales instead of continuous and protective scales are formed. This is due to the removal of Cr from the alloy through a fluxing reaction, which in turn gives rise to non-protective scales on the surface of the alloy. Therefore, the oxidation of the base material increases, and sulfides form underneath the oxide scales. At the same time,  $\text{MoO}_3 - \text{WO}_3$  build up along the oxide-alloy interface and gradually  $\text{MoO}_3$  reacts with  $\text{Na}_2\text{CrO}_4$  and  $\text{Na}_2\text{O}(\text{TiO}_2)_n$  to form  $\text{Na}_2\text{MoO}_4$  which reduces the melting point of the  $\text{MoO}_3 - \text{WO}_3$  areas. Large areas of molten  $\text{MoO}_3 - \text{WO}_3 / \text{Na}_2\text{MoO}_4$  result in acidic fluxing of the oxide scales and consequently catastrophic attacks on the alloy.

Brazing was done by the use of 100% conventional brazing filler alloy (Ni-15Cr-3.5B) with the brazing cycle shown in Figure 3.2. Figures 4.5 and 4.6 (a and b) show the microstructure of the joint region with the use of 100% filler alloy taken by optical microscope and SEM respectively. Ohsasa et al. [136] used Scheil simulation to numerically model the transient liquid phase bonding process of Ni by using an Ni-Cr-B ternary filler metal. They reported that during the solidification of the residual liquid in the sample held at  $1100^\circ\text{C}$ , segregation of the alloying elements take place and an Ni base solid solution FCC phase formed as the primary phase followed by a eutectic reaction  $\text{L} \rightarrow \text{FCC} + \text{Ni}_3\text{B}$  at  $1042^\circ\text{C}$ . Solidification was reported to be completed with a ternary eutectic reaction  $\text{L} \rightarrow \text{FCC} + \text{Ni}_3\text{B} + \text{CrB}$  at  $997^\circ\text{C}$ .

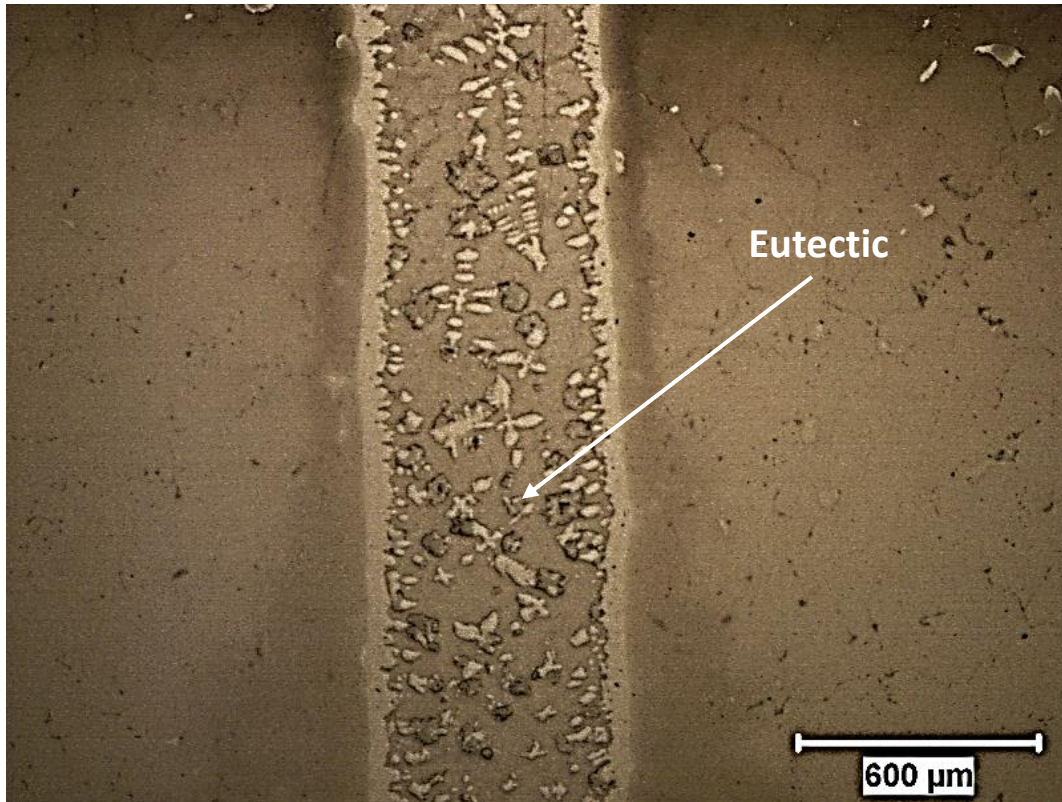


*Figure 4.5 – Optical micrograph showing eutectic constituents in joint region of wide-gap brazed sample with 100% regular brazing filler alloy.*

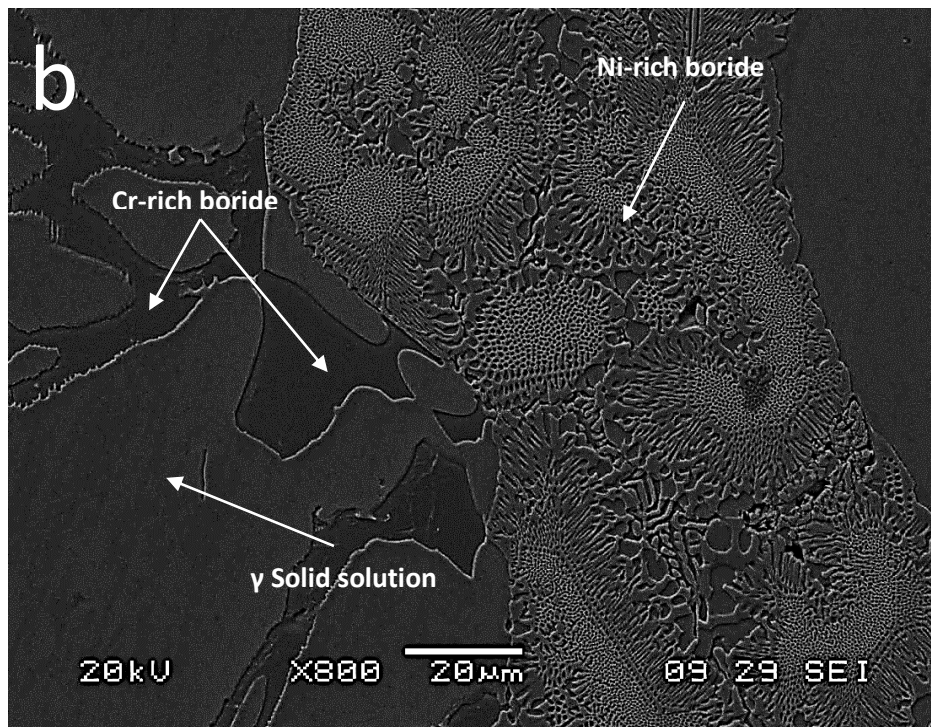
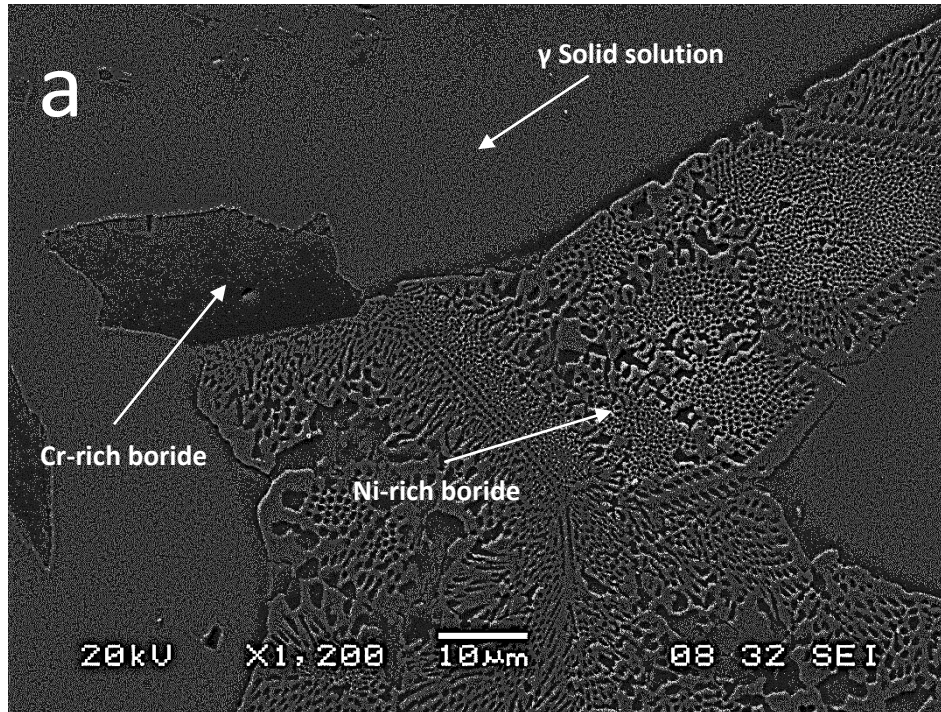


Figure 4.6 – (a and b) SEM micrographs of eutectic constituents in joint region of brazed sample with 100% conventional brazing filler alloy.

It is important to mention that the amount and width of the eutectic constituents depend on the amount of liquid found in the joint region during brazing. In this study, the regular brazing filler alloy with a melting point of 1050°C completely melted at the bonding temperature with the use of 100% conventional brazing (Ni-15Cr-3.5B) filler alloy, thus providing a complete liquid interlayer which solidified during cooling. It can be seen from Figure 4.5 that the joint microstructure consists of eutectic constituents which were found to be an Ni-base gamma solid solution, and Ni-rich and Cr-rich boride phases (presence of boron was qualitatively detected in these phases but not quantified because the energy dispersive x-ray spectrometry (EDS) analytical software was not able to quantify this light element due to low atomic number of Boron (less than 5) [35]). Their semi-quantitative EDS compositional analyses are provided in Table 4.1.

The hot corrosion experiment for brazed samples was performed using the same condition that was used for the base alloy. Figure 4.7 shows the hot corrosion behavior of the Inconel 738 samples that were brazed by using ‘100% conventional brazing filler alloy’. As discussed in Chapter 2, the duration of the initiation stage can determine the susceptibility of an alloy to hot corrosion attacks and eventually, the transition from the initiation stage to the propagation stage takes place due to the breakdown of the protective oxide scales [52]. Therefore, the length of the initiation stage highly depends on the protectiveness of the oxide scales which form on the substrate [57]. It has been considered that the length of the initiation period is somewhat arbitrarily defined [81]. Moreover, Fryburg et al. [81] reported that the initiation period is mostly defined as the time when an abrupt change occurs in the slope of the corrosion curve. Therefore, materials have slow linear oxidation behavior during the initiation stage and a sharp change in the slope of the plot of the weight-loss vs. time can determine the transition from the initiation stage to the propagation stage.



*Table 4.1-SEM-EDS semi-quantitative metallic composition of eutectic constituents in the wide-gap brazed joint with 100% conventional brazing filler alloy.*

<b>Element</b>	<b>Nickel rich boride phase (Wt.%)</b>	<b>Chromium rich boride phase (Wt.%)</b>	<b><math>\gamma</math> solid solution phase (Wt.%)</b>
<b>Ni</b>	<b>80</b>	<b>4.8</b>	<b>69.55</b>
<b>Cr</b>	<b>5.6</b>	<b>83.55</b>	<b>14.66</b>
<b>Ti</b>	<b>4.33</b>	<b>1.07</b>	<b>1.93</b>
<b>Al</b>	<b>0.66</b>	<b>0</b>	<b>3.97</b>
<b>Mo</b>	<b>0</b>	<b>4.1</b>	<b>1.08</b>
<b>W</b>	<b>0.28</b>	<b>1.42</b>	<b>2.67</b>
<b>Nb</b>	<b>1.3</b>	<b>0</b>	<b>0</b>
<b>Ta</b>	<b>1</b>	<b>0</b>	<b>1.5</b>
<b>Co</b>	<b>3.2</b>	<b>0.8</b>	<b>4.65</b>
<b>Fe</b>	<b>0</b>	<b>0</b>	<b>0</b>

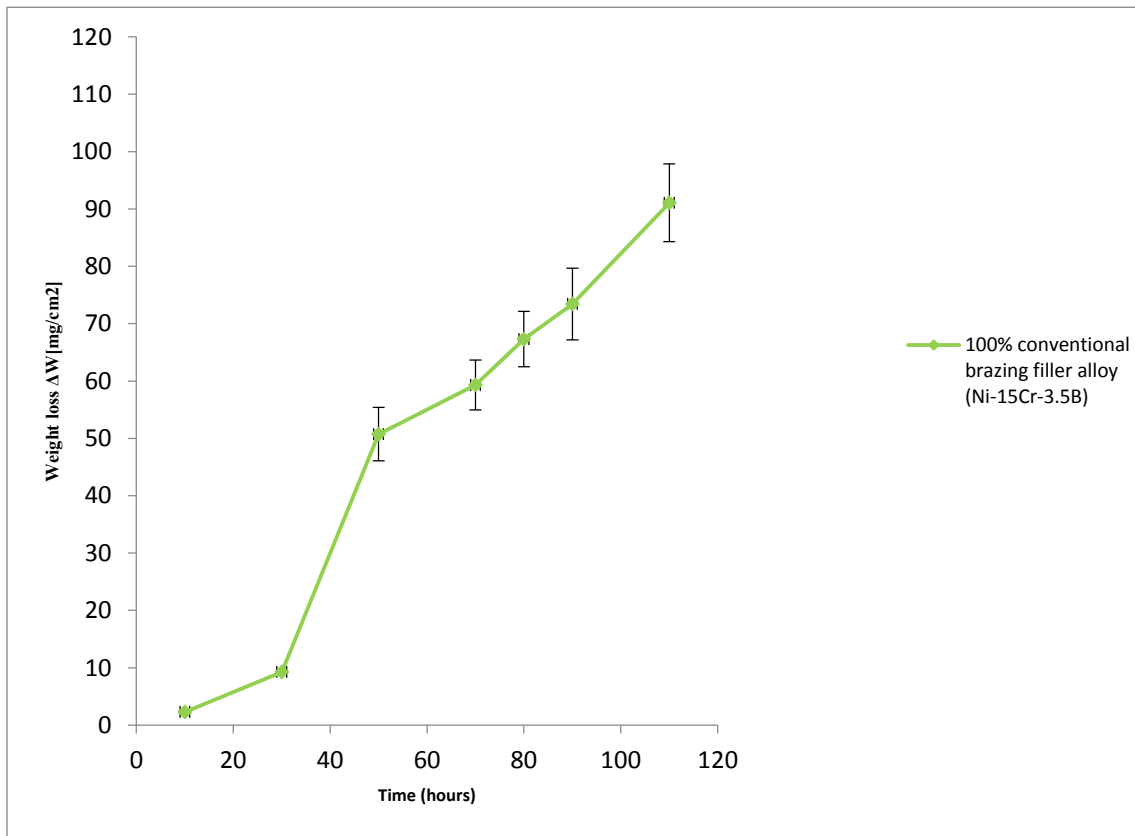


*Figure 4.7 – Hot corrosion behavior of brazed IN738 with 100% conventional brazing filler alloy (Ni-15Cr-3.5B). The duration of initiation stage is 30 hours long.*

Based on this explanation, the initiation stage of the brazed joint made from the 100% conventional filler alloy powder is about 30 hours long, such that, the coupon shows slow linear oxidation and the amount of weight loss is insignificant. After carrying out a visual inspection, a thin layer of protective oxide scales was observed on the surface of the brazed sample after 30 hrs of exposure in the hot corrosion experiment. The transition from the initiation to the propagation stage took place after this time frame (50 hours) with concomitant significant amount of weight-loss (around 50 mg/cm<sup>2</sup>) due to the oxide scale being no longer protective. The visual inspection of a brazed sample after 50 hrs of exposure showed that the corrosion attack primarily occurs within the brazed region, and this region is covered with porous thick greenish-black oxide while the base alloy material does not experience any obvious hot corrosion attack. This localized hot corrosion attack in the joint region was observed for all the hot corrosion experiments. Consequently, the initiation stage of the brazed joint made from the 100% filler alloy powder is about 30 hours long while initiation stage for IN738 base alloy was up to 110 hours or more, see Figure 4.7 and 4.3. This observation signifies that brazing caused reduction in hot corrosion resistance of IN738 samples.

From the point of view of hot corrosion resistance, it is important to remember that in the literature, Cr is the most effective alloying element used to address hot corrosion due to the formation of highly protective Cr<sub>2</sub>O<sub>3</sub> scales. However, if the Cr content in Ni-base superalloys are less than about 15%, the Cr<sub>2</sub>O<sub>3</sub> scale may no longer be sufficiently protective [49] [137]. Therefore, the main phase in this microstructure that can significantly contribute to the low hot corrosion resistance of the bonded samples is the Ni-rich boride phase due to the low amounts of Cr found in this phase; that is, Cr < 10%, see Table 4.1. It should be noted that although the filler alloy used for the brazing contains adequate concentration of Cr (15%), however, due to melting of the filler

and subsequent elemental segregation that occurs during its solidification, a Cr-deficient Ni-rich boride phase was produced in the joint region. The formation of the Cr-lean Ni-rich boride phase within the brazed joint, is thus, key factor that can explain the lower resistance of brazed joint to hot corrosion compared to the base-alloy material.

## **4.2 Microstructure and Hot Corrosion Behavior of Brazed Samples with (Nicrogap 108) Additive Powder**

According to the literature, additive powder is a good product to use because it might not melt completely during brazing and can provide the necessary capillary force to keep the molten filler in the gap, reduces the liquid phase erosion of the base alloy and enhances the joint properties by enriching the joint with the necessary alloying elements [8] [39]. However, the effects of additive powder in terms of hot corrosion resistance of the brazed joint have not been discussed comprehensively. Therefore, the next step in this study is to determine the effects of using additive powder in terms of the hot corrosion resistance of the wide-gap brazed joint. Accordingly, Figure 3.2 shows the brazing cycle which was carried out at 1100°C for 1 hour by using composite powder mixture ratio of: 70 Wt. % conventional brazing filler alloy (Ni-15Cr-3.5B) + 30 Wt. % Nicrogap 108 as the additive powder. It is important to note that the composition of the interlayer alloy, specifically, the Cr content, can significantly affect the hot corrosion behavior of the brazed joints as discussed in Chapter 2. Consequently, Nicrogap 108 was used as the additive powder as it has a similar composition as the conventional brazing filler alloy. The purpose is to compare these results to the previous ones in section 4.1 which was for brazed joints with 100% conventional

brazing filler alloy. Therefore, both 100% conventional brazing filler alloy and composite powder mixture as the interlayers have the same composition, and the only difference is the presence of the additive powder with a mix ratio of R<sub>7:3</sub> in the composite powder mixture. Figures 4.8 show the microstructure of the joint region with the use of composite powder mixture (partially melted Nicrogap 108 as the additive powder) taken by an optical microscope. In the case of using a composite powder mixture (R<sub>7:3</sub>), the interlayer alloy completely melted while the additive powder remained largely unmelted. Therefore, the microstructure of the brazed region is composed of unmelted additive powders that are uniformly distributed in the eutectic constituents. It was observed that since there is less liquid found in the joint region during brazing, the amount of eutectic constituents, particularly, Ni-rich boride phase, are considerably less than the case when 100% conventional brazing filler alloy is used. Figure 4.9 shows the hot corrosion behavior of the Inconel 738 samples that were brazed by using ‘70% filler alloy (Ni-15Cr-3.5B) + 30% Nicrogap 108 additive powder’ as the interlayer alloy and the hot corrosion test condition was the same as the one used in section 4.1. When the brazed joint was produced with a composite powder mixture, the initiation stage was observed to be around 80 hours with a small change in weight of around 10 mg/cm<sup>2</sup>. After carrying out a visual inspection, it is determined that only a thin layer of oxide scales formed on the surface of the joint and no major hot corrosion attack was observed. The transition to the propagation stage took place after 80 hours with a sharp change in the slope of the plot and the corresponding weight loss after 90 hours of exposure time is 54.5 mg/cm<sup>2</sup> which indicates a severe hot corrosion attack. After a visual inspection of the coupon, it was confirmed that the joint region is significantly corroded. Consequently, based on Figures 4.7 and 4.9, the shorter duration of the initiation stage of the joint with 100% filler alloy compared to that with a

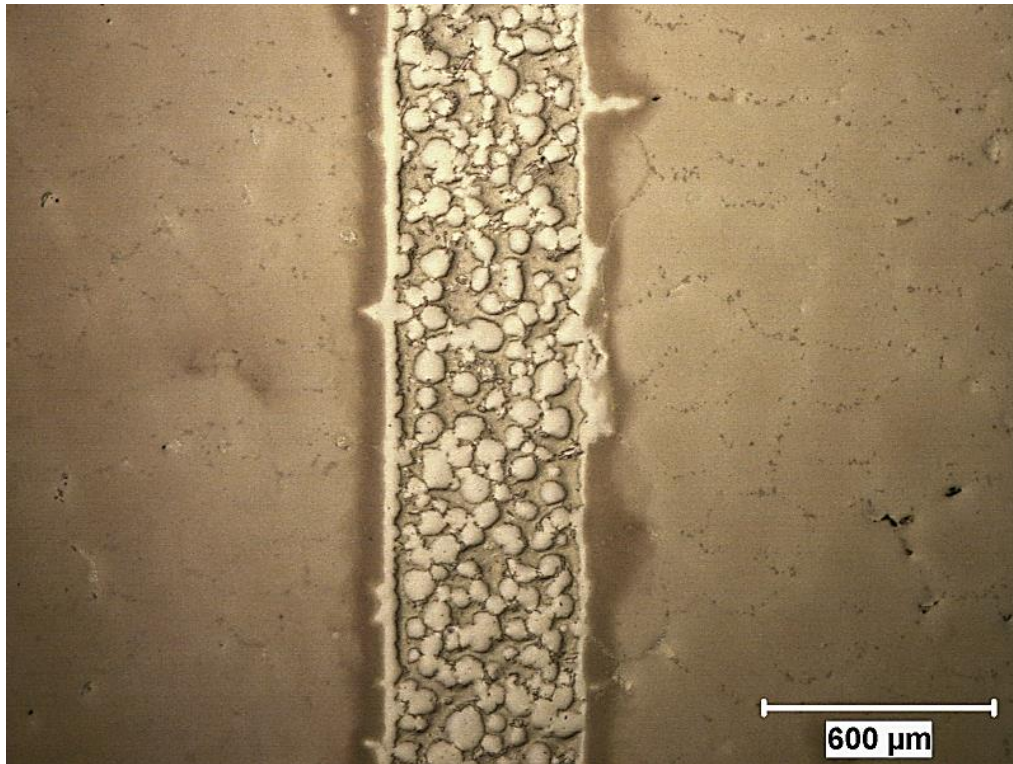


*Figure 4.8 – Optical micrograph shows the microstructure of the joint region with the use of composite powder mixture of ‘70% conventional brazing filler alloy (Ni-15Cr-3B) + 30% Nicrogap 108 additive powder’. The uniform distribution of partially melted Nicrogap 108 additive powders is shown in the joint region.*

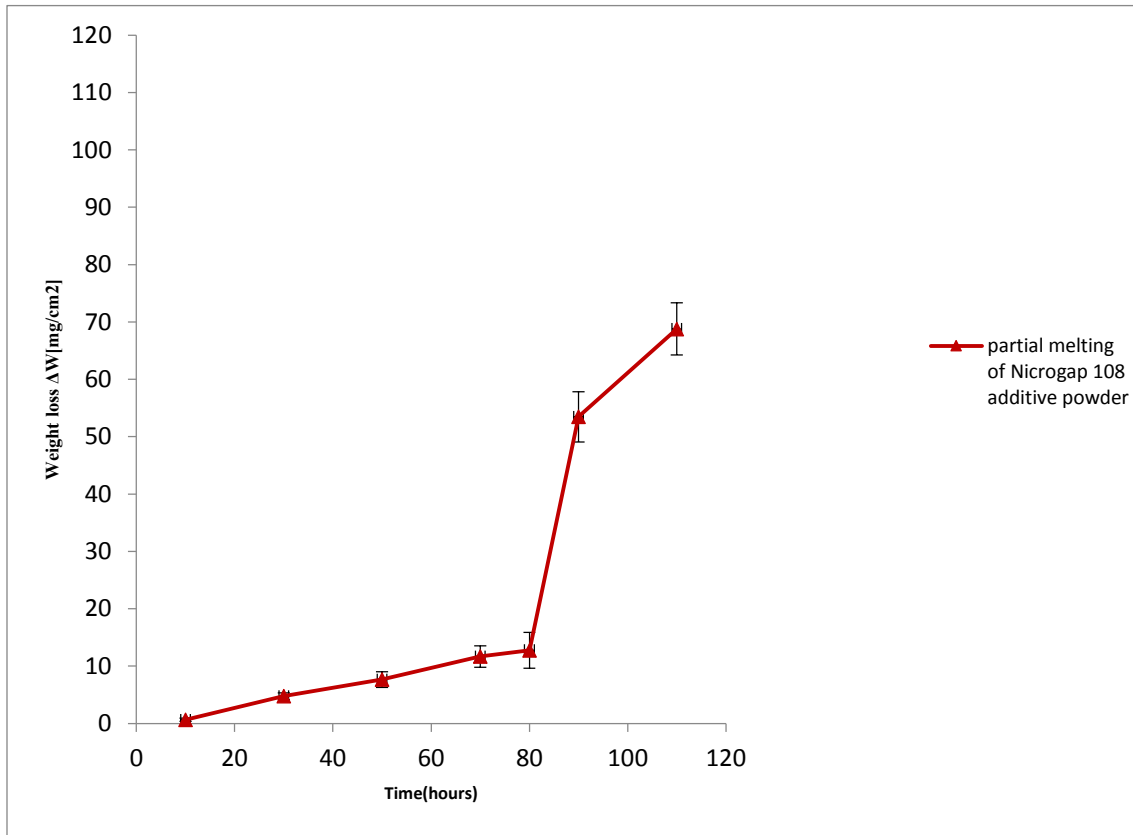


*Figure 4.9 - The hot corrosion behavior of IN738 samples which were brazed using the '70% conventional brazing filler alloy (Ni-15Cr-3B) + 30% Nicrogap 108 additive powder' as the interlayer alloy.*

composite powder mixture suggests that the use of additive powder increases the hot corrosion resistance of brazed joints. This cannot be attributed to the composition of the interlayers because the composition of both interlayers was purposely selected to be the same. Therefore, based on a visual inspection of the samples which clearly showed that hot corrosion attacks were localized in the joint region, the reason for the difference in hot corrosion resistance can be determined from the microstructure in the joint region.

The high corrosion resistance of the joint with a composite powder mixture (R<sub>7:3</sub>) is due to the lower volume of liquid found during brazing. This results in fewer eutectic constituents, particularly, Ni-rich boride, which is depleted in Cr. In addition, the uniformly distributed unmelted additive powders with 15% Cr also contribute to the high corrosion resistance of these brazed joints. Consequently, the use of additive powder is beneficial for the hot corrosion resistance of brazed samples.

### **4.3 Microstructure and Hot Corrosion Behavior of Brazed Samples with other Additive Powders (IN738 and Haynes 282)**

The next step in this study is to determine whether the type of additive powder in the composite powder mixture has any effects on the hot corrosion resistance of the brazed coupon. Therefore, Inconel 738 (AMDRY 7380) and Haynes 282 were used as the additive powder with an R<sub>7:3</sub> mix ratio using the same conventional brazing filler alloy (Ni-15Cr-3.5B). The brazing cycle and hot corrosion experiment conditions were the same as that in the section 4.2. Figures 4.10 and 4.11



show the microstructure of the joint region with partially melted Inconel 738 and Haynes 282 respectively taken by an optical microscope. When these micrographs are compared to that in Figure 4.8 which shows the brazed joint with partially melted Nicrogap 108 as the additive powder, it is found that in all three cases, the unmelted additive powders are uniformly distributed in the joint region. Figure 4.12 and 4.13 show the hot corrosion curve for brazed samples with partially melted Inconel 738 and Haynes 282 as the additive powder respectively. The initiation stage for brazed samples with Nicrogap 108, Inconel 738 and Haynes 282 additive powder (see Figures 4.9, 4.12, 4.13 respectively) are the same and lasts up to 80 hours. After 80 hours, the slope changes significantly for weight-loss vs time for all three additive powders and even the amount of weight loss after moving to the propagation stage is comparable. A visual inspection of all three samples also showed the same degradation behavior.

The three different additive powders used in these experiments have different compositions; however, all of them contain at least 15% Cr. Consequently, as long as an adequate amount of Cr is in the additive powder, the hot corrosion resistance of the brazed coupons is the same. Therefore, to have good hot corrosion resistance of the brazed samples, it is not necessary to use a highly alloyed additive powder such as Haynes 282 which is very expensive. A brazed sample with a low alloy additive powder such as Nicrogap 108 with 15% Cr can also provide the same hot corrosion resistance.

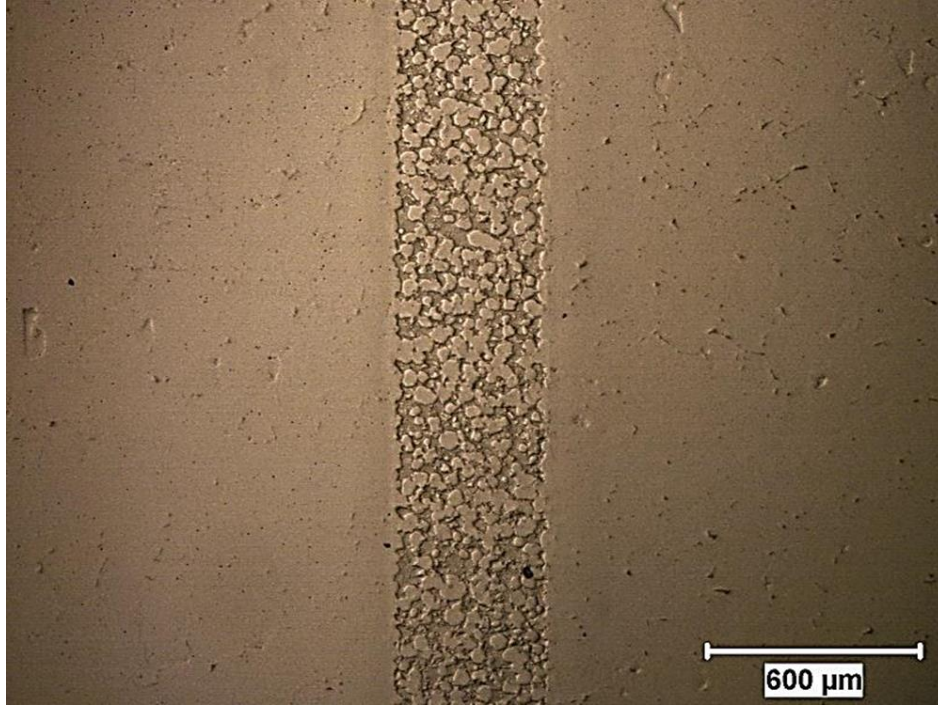


*Figure 4.10 – Optical micrograph showing uniform distribution of partially melted IN 738 additive powder in joint region.*

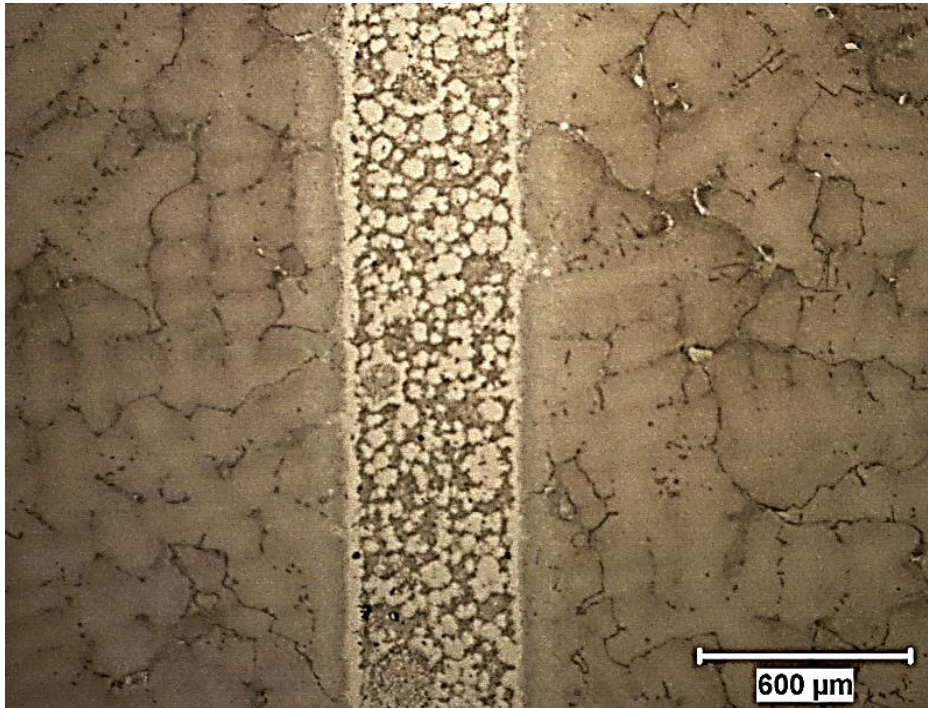


*Figure 4.11 - Optical micrograph showing uniform distribution of partially melted Haynes 282 additive powder in joint region.*

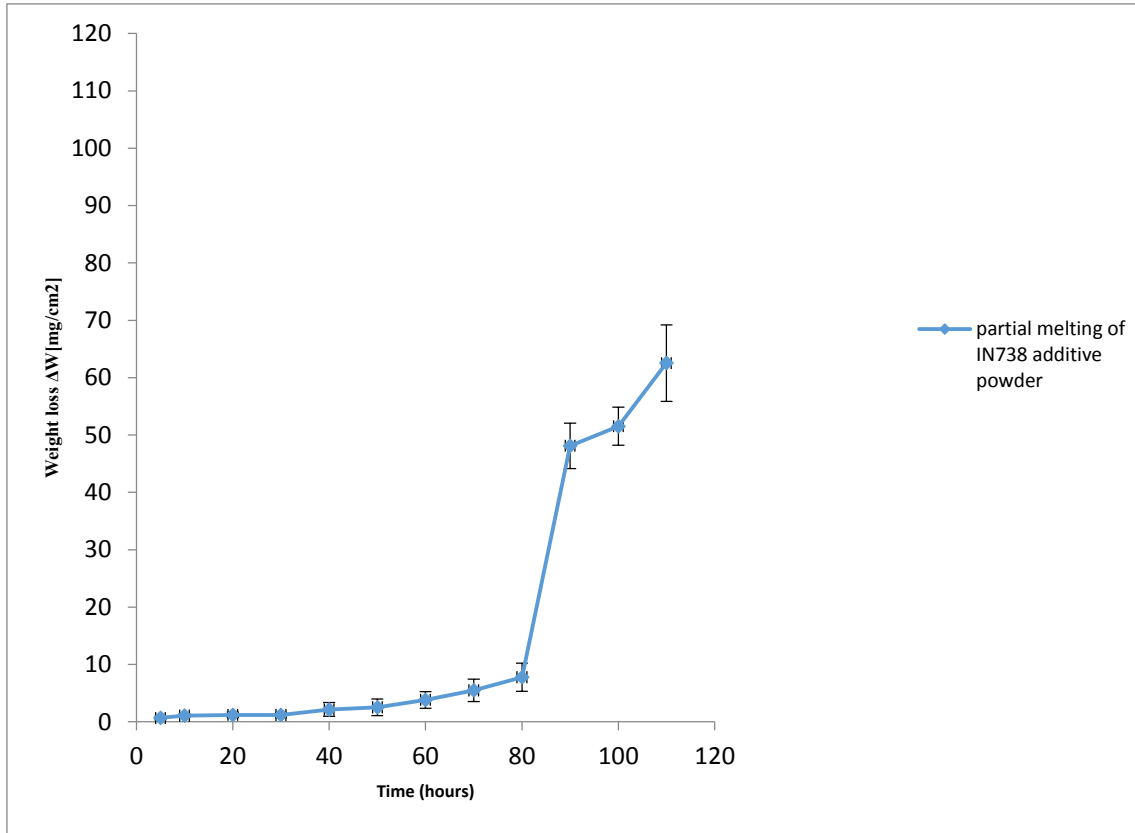
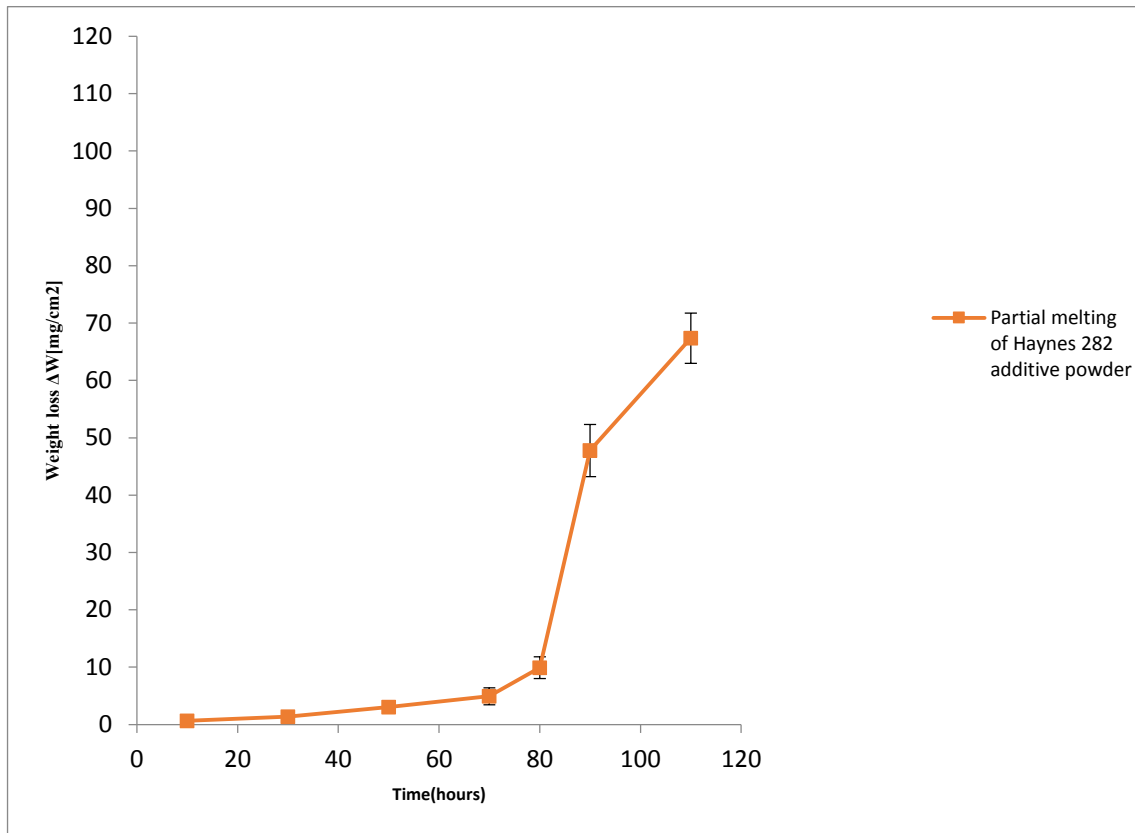


Figure 4.12 – Hot corrosion behavior of brazed IN738 with 70 wt. % conventional brazing filler alloy powder (Ni-15Cr-3.5B) + 30 wt. % IN738 additive powder.



*Figure 4.13 – Hot corrosion behavior of brazed IN738 with 70 wt. % conventional brazing filler alloy powder (Ni-15Cr-3.5B) + 30 wt. % Haynes 282 additive powder.*

#### **4.4 Microstructure and Hot corrosion Behavior of Brazed Samples with Completely Melted Additive Powder (IN738)**

It is found in this work that the use of additive powder is beneficial in terms of hot corrosion resistance of the brazed coupon and the type of additive powder does not matter as long as it contains at least 15% Cr. However, as found in the literature review, it is important to consider that under specific conditions, complete melting of additive powder is possible during brazing. Therefore, experiments were conducted to determine the effects of completely melted additive powder on the hot corrosion resistance of the brazed samples. Inconel 738 (AMDRY 7380) was used as the additive powder with a mix ratio of R<sub>7:3</sub> and the same conventional brazing filler alloy (Ni-15Cr-3.5B) was used. Two different brazing cycles were applied. One is the same as that shown in Figure 3.2 which resulted in partial melting of Inconel 738 additive powder. To obtain complete melting of Inconel 738 additive powder, the brazing temperature was increased to 1160°C. The brazing cycle is shown in Figure 3.3. The microstructure of the partially melted and completely melted Inconel 738 additive powder is shown in Figures 4.10 and 4.14 respectively. Complete melting of Inconel 738 powder provided the joint with a greater volume of liquid compared to the partially melted Inconel 738 powder. This resulted in more eutectic constituents. The SEM-EDS analysis of the joint region of the completely melted Inconel 738 showed the presence of an Ni-base gamma solid solution, and Cr and Ni-rich boride phases which are the same as Figure 4.6 (a and b). Table 4.1 can also represents their composition.

The hot corrosion experiment conditions were the same as the earlier experiments. Figure 4.12 and 4.16 show the hot corrosion results for partially melted and completely melted Inconel 738

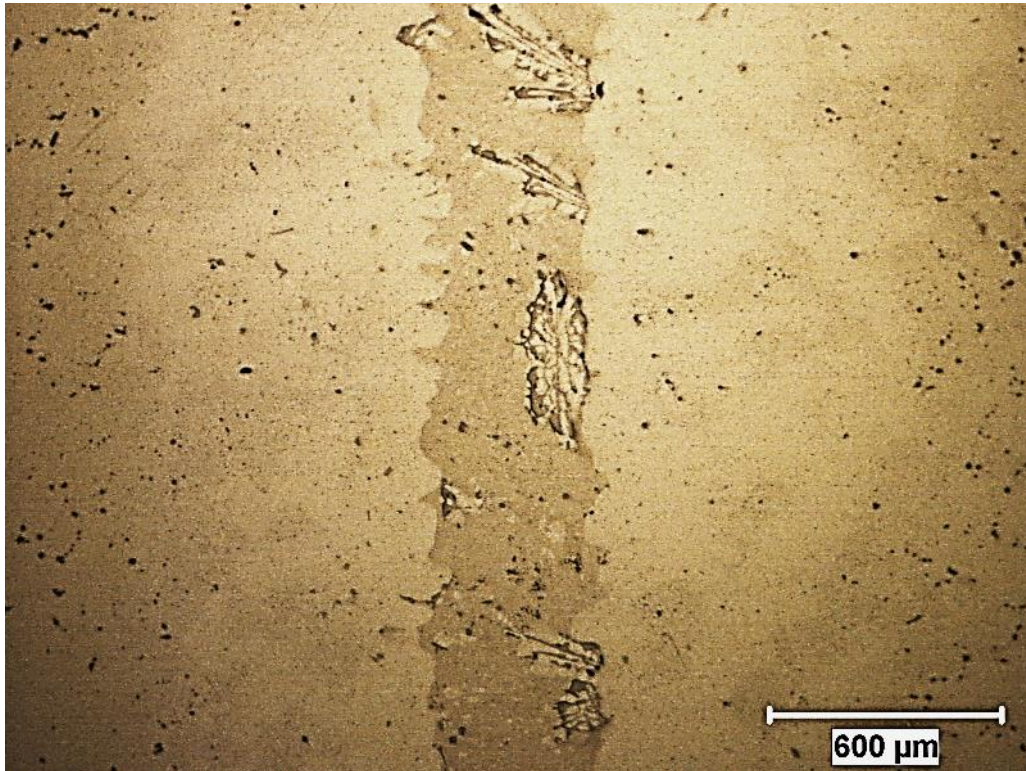


*Figure 4.14 – Optical micrograph showing eutectic constituents in joint region of completely melted IN 738 additive powder.*

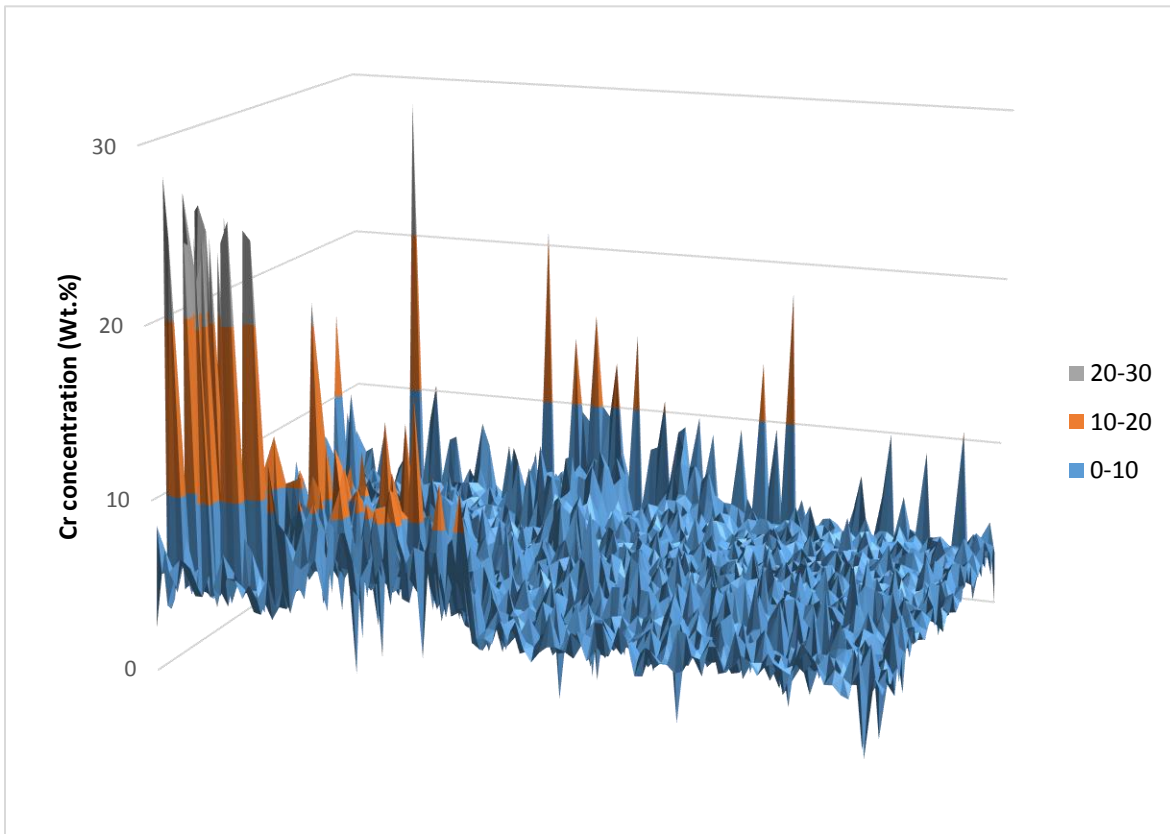


*Figure 4.15– Quant map analysis showing Cr distribution in the joint microstructure of completely melted IN 738 additive powder. The depletion of Cr in extensive region of Ni-rich boride phase is shown.*

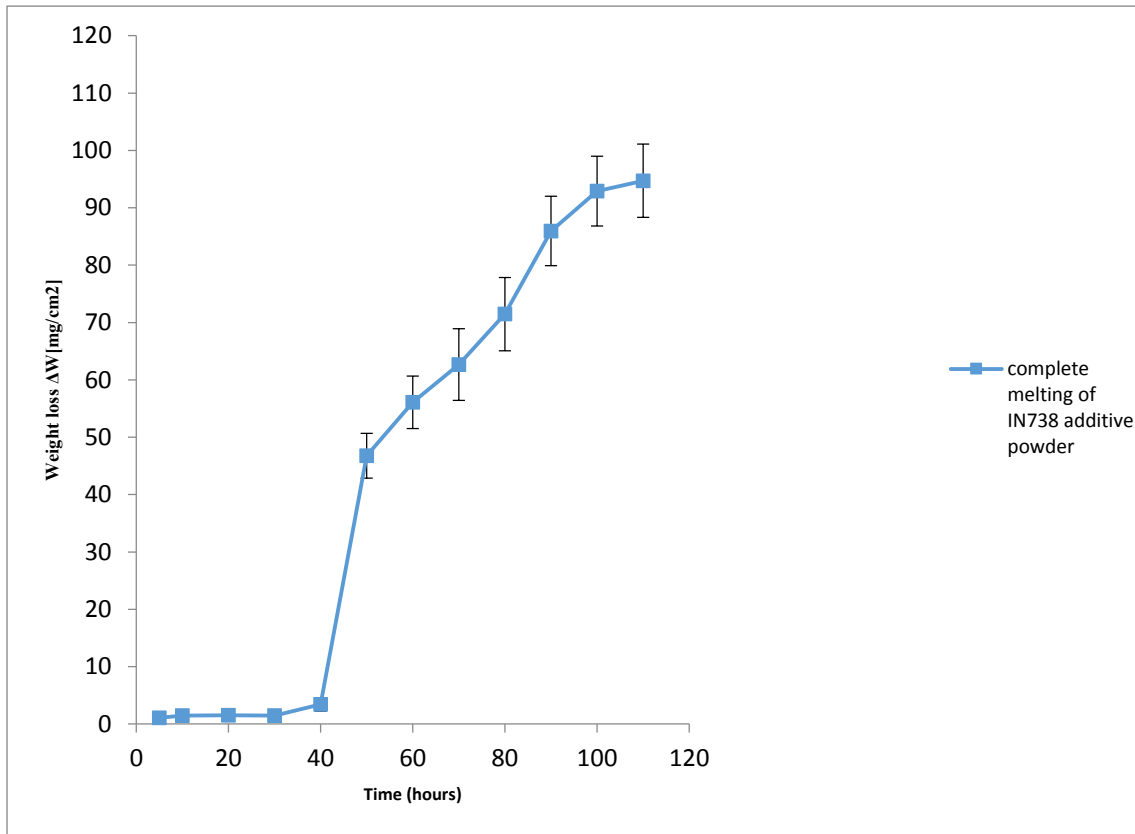


*Figure 4.16 – Hot corrosion behavior of brazed IN738 with 70 wt. % conventional brazing filler alloy powder (Ni-15Cr-3.5B) + 30 wt. % IN738 additive powder. The IN738 additive powder is completely melted.*



additive powder in the brazed joint respectively. The duration of the initiation stage for the partially melted additive powder was 80 hours and then the propagation stage ensued (see Figure 4.12). Consequently, a severe hot corrosion attack in the joint region took place, which was revealed by visual inspection. For the completely melted Inconel 738 additive powder, the initiation stage was 40 hours which is half of that of the initiation stage for partially melted Inconel 738 additive powder. The brazed sample started to severely corrode at about 50 hours and a visual inspection showed a localized attack in the joint region which increased in severity with increased exposure time. Therefore, a considerably shorter initiation stage for completely melted Inconel 738 additive powder indicates that if the additive powder melts completely during brazing, it can significantly reduce the hot corrosion resistance of the brazed sample.

The reason can be explained from the microstructure changes that take place when the additive powder is completely melted. Complete melting of additive powder provides the joint with a larger volume of liquid compared to the partially melted additive powder. This results in the formation of more eutectic constituents. Stringer [49] indicated that as far as alloy composition is concerned, the main factor in determining the resistance to hot corrosion is the Cr content. Therefore, it can be understood that the depletion of Cr (< 10%) in the Ni-rich phase results in the inability of the material to produce protective, coherent and continuous Cr<sub>2</sub>O<sub>3</sub> scales, so its corrosion resistance is significantly reduced and the joint experiences severe hot corrosion attacks. Consequently, even though, the use of additive powder is found to aid resistance to hot corrosion, if the additive powder completely melts, which can happen during brazing, the hot corrosion resistance of the brazed sample is considerably reduced. This finding has not been previously reported in the literature and it is crucial to the use of additive powder for enhancing the properties of brazed materials.

## **4.5 Effect of Salt Mixture on Hot Corrosion Behavior of Brazed Samples with Completely and Partially Melted IN738 Additive Powder**

As mentioned in the literature review, one of the factors that can greatly affect the hot corrosion behavior of materials and, particularly, the length of the initiation stage is the composition of the salt deposits. To investigate the effect of the salt composition on the hot corrosion behavior of brazed joints, brazing was performed with Inconel 738 as the additive powder with the same conventional brazing filler alloy (Ni-15Cr-3.5B), powder mixture ratio (R<sub>7:3</sub>). In one case, the brazing cycle in Figure 3.2 was used which resulted in partial melting of Inconel 738 additive powder and in another case, the brazing cycle in Figure 3.3 was used which resulted in complete melting of Inconel 738 additive powder.

The hot corrosion experiments were the same as earlier sections except for the salt composition. A series of hot corrosion experiments were carried out with 100% Na<sub>2</sub>SO<sub>4</sub> salt and also to investigate the effect of NaCl, experiments were carried out with 50% NaCl + 50% Na<sub>2</sub>SO<sub>4</sub>. The results were compared with the results from sections 4.3 and 4.4 which used a 25%NaCl + 75% Na<sub>2</sub>SO<sub>4</sub> salt mixture (see Figures 4.12 and 4.16) for partially melted and completely melted IN738 additive powder respectively. Figure 4.17 provides the hot corrosion results with 100% Na<sub>2</sub>SO<sub>4</sub> salt. Na<sub>2</sub>SO<sub>4</sub> is considered as a mild environment for chromia forming oxide scale alloys like IN738. Therefore, it can be seen that the duration of the initiation stage for both completely and partially melted Inconel 738 additive powder lasted for 110 hours, which is the maximum exposure time used in this work. A number of researchers have studied the Na<sub>2</sub>SO<sub>4</sub> hot corrosion of Inconel 738

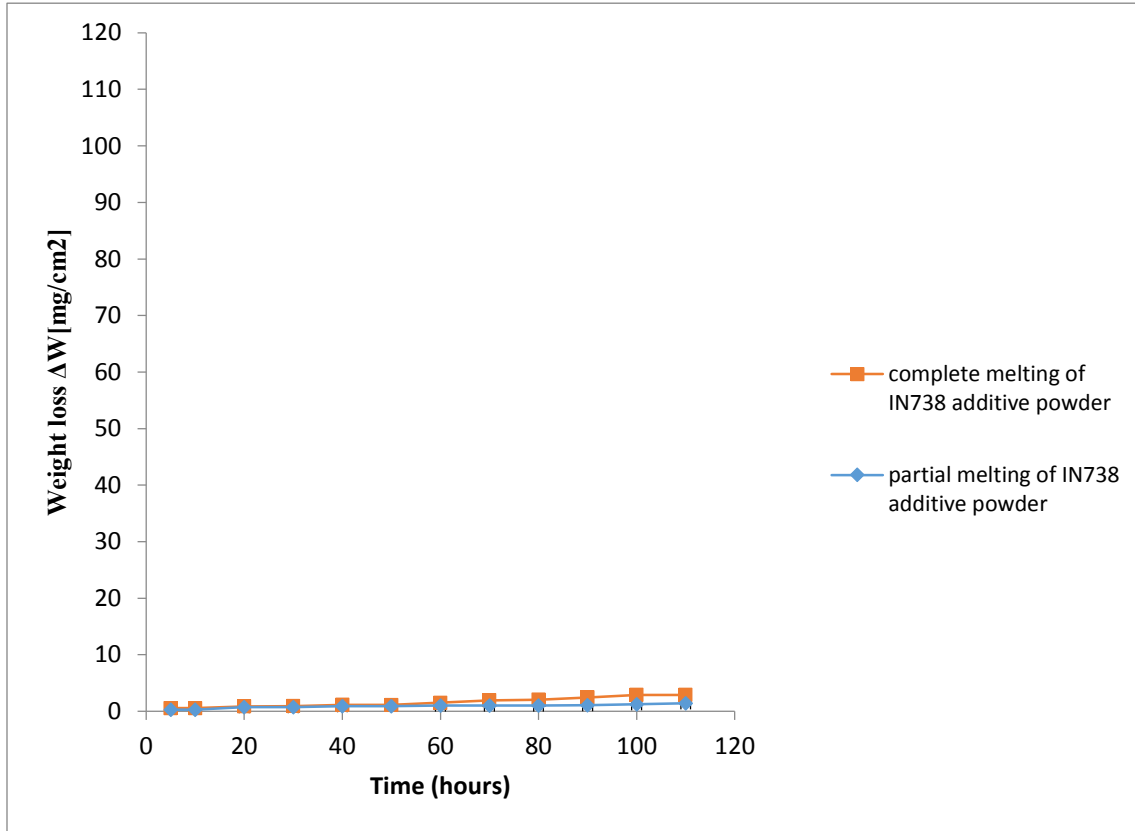


Figure 4.17 – Hot corrosion results for brazed samples with partially melted and completely melted Inconel 738 additive powder in 100% Na<sub>2</sub>SO<sub>4</sub> salt.

and other  $\text{Cr}_2\text{O}_3$  forming alloys at different temperatures by using different experimental methods. The results show that, under the test conditions, either the alloy does not show hot corrosion at all, or there is a delay of several hundred hours before the commencement of severe attacks [67] [84] [135] [138] [139] [140] [141] [142] [143] [144]. Consequently, NaCl is added to  $\text{Na}_2\text{SO}_4$  because it is more aggressive on  $\text{Cr}_2\text{O}_3$  type scales [145].

Figure 4.18 shows the hot corrosion results with the use of 50% NaCl + 50%  $\text{Na}_2\text{SO}_4$ . When these results are compared to those of the experiment carried out with 25% NaCl + 75%  $\text{Na}_2\text{SO}_4$  (Figures 4.12 and 4.16), it can be found that increasing the amount of NaCl causes a significant reduction in the length of the initiation stage for both the completely and partially melted Inconel 738 additive powder. The duration of the initiation stage of the partially melted Inconel 738 additive powder is 80 hours with a 25% NaCl + 75%  $\text{Na}_2\text{SO}_4$  salt mixture, see Figure 4.12. When the amount of NaCl is increased to 50%, the initiation stage is reduced to 40 hours, see Figure 4.18. This means that an increase in the amount of NaCl in the salt mixture significantly reduces the hot corrosion resistance of the brazed samples. The same effect was observed for the brazed sample with completely melted Inconel 738 powder. The duration of the initiation stage is 40 hours with the use of a 25% NaCl + 75%  $\text{Na}_2\text{SO}_4$  salt mixture (Figure 4.16), and when NaCl is increased to 50%, the length of the initiation stage is reduced to 20 hours (Figure 4.18). This is supported by previous work, as many researchers have indicated that the addition of NaCl to  $\text{Na}_2\text{SO}_4$  has a significant influence on the hot corrosion resistance of superalloys [for example, [13] [120] [123] [145] [146] [147] [148]]. As Johnson et al. [149] put it: “Although Cr is a useful alloying element in promoting oxidation resistance of nickel-base superalloys, its oxide can be attacked in a sodium chloride contaminated environment. Even high chromium alloys which produce coherent  $\text{Cr}_2\text{O}_3$

oxides are susceptible to attack...” That is, chloride can selectively remove certain elements such as Cr from an alloy. This process involves the formation of highly volatile gaseous chloride species, which form voids and pits in the oxide scales, thus resulting in a porous chromia scale and providing an easy path for the flow of corrosive salts [57] [64] [87].

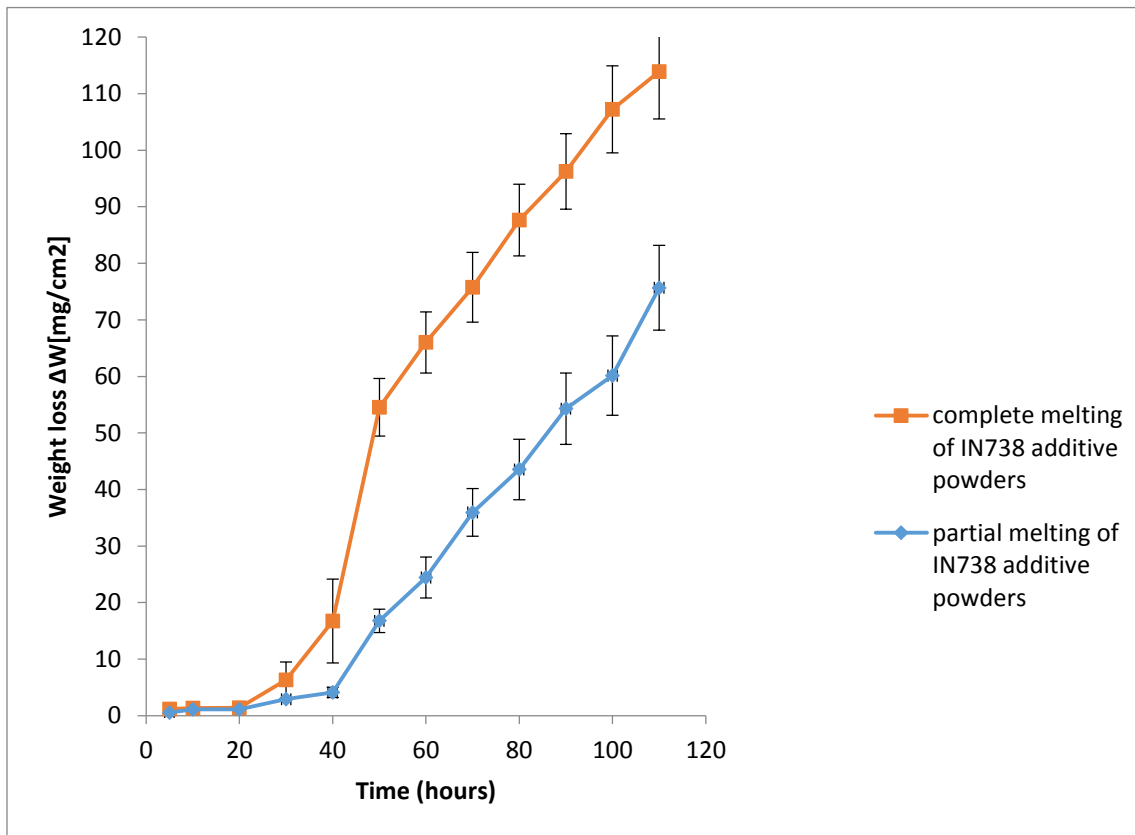


Figure 4.18 – Hot corrosion results for brazed samples with partially melted and completely melted Inconel 738 additive powder in 50%NaCl + 50% Na<sub>2</sub>SO<sub>4</sub> salt mixture.

## **4.6 Effect of Temperature on Hot Corrosion Behavior of Brazed Samples with Completely and Partially Melted IN738 Additive Powder**

Another factor which affects the resistance of materials to hot corrosion attacks is the temperature. To investigate the effect of temperature, hot corrosion experiments were conducted with a 25% NaCl + 75% Na<sub>2</sub>SO<sub>4</sub> salt mixture at 950°C and 1000°C for brazed samples with completely melted and partially melted Inconel 738 additive powder. Figure 4.19 shows the hot corrosion results at 950°C. The duration of the initiation stage for partially melted Inconel 738 additive powder is 50 hours and the transition to propagation stage takes place afterwards which results in a weight loss of 58.2 mg/cm<sup>2</sup> that corresponds to 70 hours of exposure time. In the case of the completely melted Inconel 738 powder, the initiation stage lasts only 10 hours. After 10 hours, the transition to the propagation stage takes place. The weight loss after 30 hours of exposure is 30 mg/cm<sup>2</sup>. Figure 4.20 shows the hot corrosion results at 1000°C. The duration of the initiation stage for the partially melted Inconel 738 powder is 30 hours and afterwards, the propagation stage takes place. The weight loss which corresponds to 50 hours of exposure time is 40 mg/cm<sup>2</sup>. In the case of the completely melted Inconel 738 powder, the duration of the initiation stage is the same as that at 950°C which is 10 hours. However, the corresponding weight loss after 30 hours of exposure time is much higher, at about 56 mg/cm<sup>2</sup>.

A comparison of the results of the hot corrosion experiments carried out at 900°C, 950°C and 1000°C (see Figures 4.12, 4.16, 4.19, 4.20) clearly shows that with increases in the temperature, the duration of the initiation stage is reduced and the amount of weight loss is significantly increased. These results are in a good agreement with other works. According to work in the

literature, increasing the temperature reduces the initial oxide thickness and also the duration of the initiation stage [150] because at higher temperatures, the chemical reaction rate is increased [135] and  $\text{Cr}_2\text{O}_3$  will oxidize to a gaseous species ( $\text{CrO}_3$ ) [49]. Therefore, its protectiveness is significantly reduced. Consequently, the corrosion rate generally increases with increasing temperatures [117].

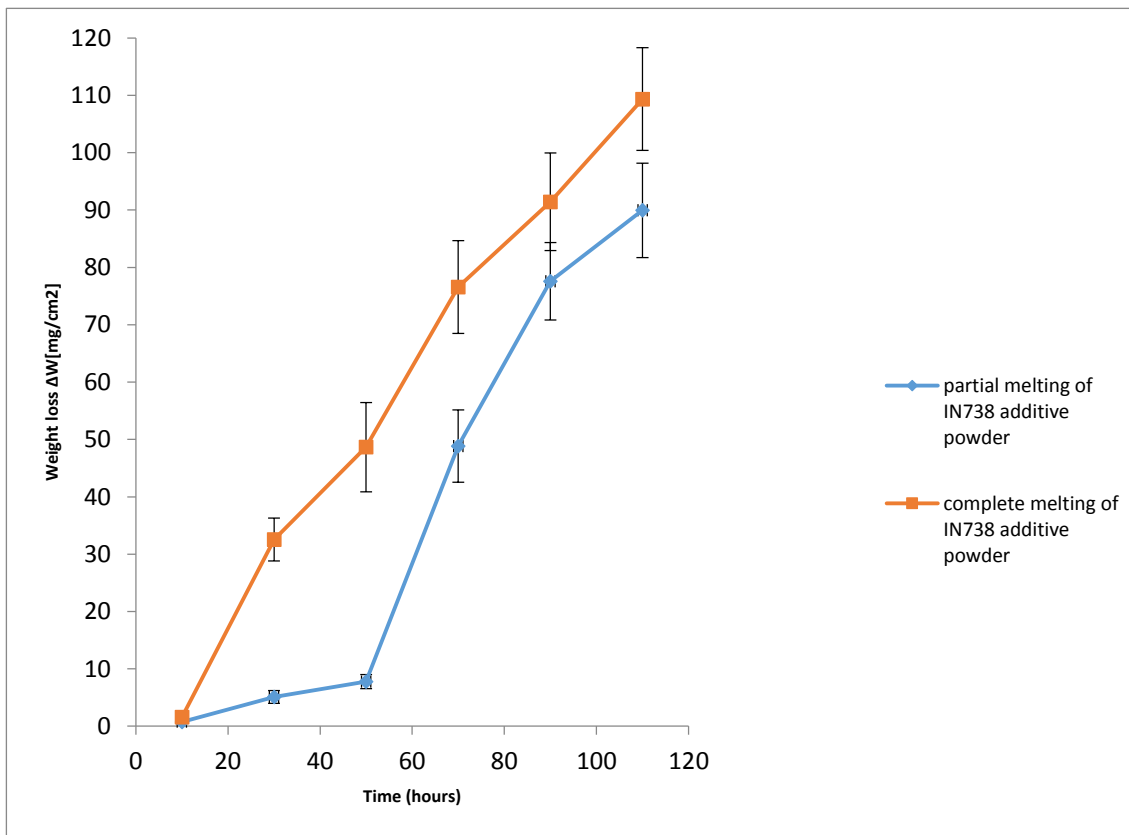


*Figure 4.19 – Hot corrosion results for brazed samples with completely melted and partially melted Inconel 738 additive powders at 950°C.*

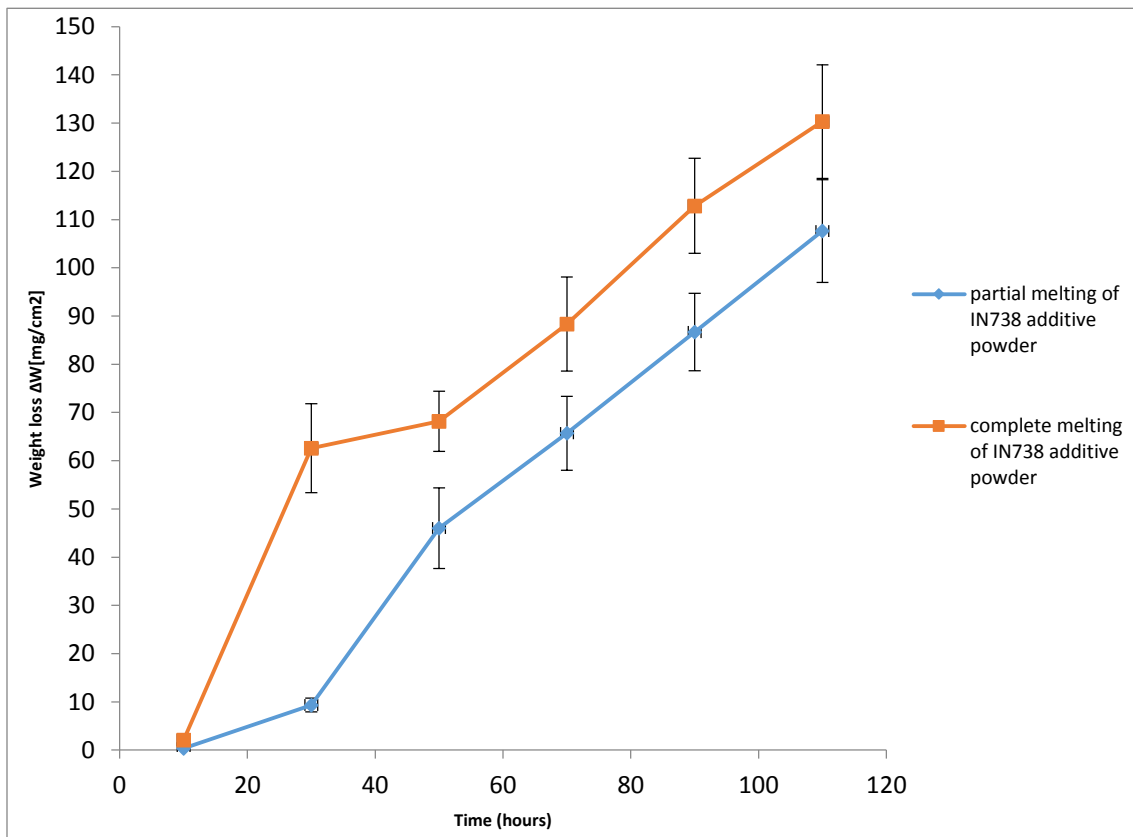


Figure 4.20 - Hot corrosion results for brazed samples with completely melted and partially melted Inconel 738 additive powder at 1000°C.



## **4.7 Effect of Completely Melted Additive Powder Containing High Amount of Cr (Haynes 282) on Hot Corrosion Behavior of Brazed Samples**

The results outlined in Section 4.4 demonstrate that completely melted additive powder can reduce the hot corrosion resistance of brazed joints. This leads to the question that if the selected additive powder has a very high amount of Cr, and even if it completely melts, can it produce protective oxide scales and avoid a reduction in the hot corrosion resistance of the brazed sample? Therefore, experiments were performed with the use of Haynes 282 as the additive powder, as it contains a high amount of Cr (20%). The same conventional brazing filler alloy (Ni-15Cr-3.5B) and powder mix ratio (R<sub>7:3</sub>) as in the section 4.4 were used. To achieve completely melting of Haynes 282, the brazing temperature was increased to 1200°C, the brazing cycle is shown in Figure 3.4. Figure 4.21 show OM micrograph of a brazed region with completely melted Haynes 282. The micrograph shows the eutectic constituents in the joint region which were found to be gamma solid solution, Ni-rich and Cr-rich boride phases with the same composition shown in Table 4.1.

The hot corrosion experiments were carried out at 900°C with a 25% NaCl + 75% Na<sub>2</sub>SO<sub>4</sub> salt mixture. Figure 4.22 shows the hot corrosion results of completely melted Haynes 282. The results were then compared with those in Section 4.4 (complete melting of Inconel 738 additive powder; see Figure 4.16). The results show that, in both cases (Figure 4.16 and 4.22), the initiation stage lasted for 30 hours and after that, significant weight loss of about 50 mg/cm<sup>2</sup> was observed which corresponds to 50 hours of exposure time for both cases.

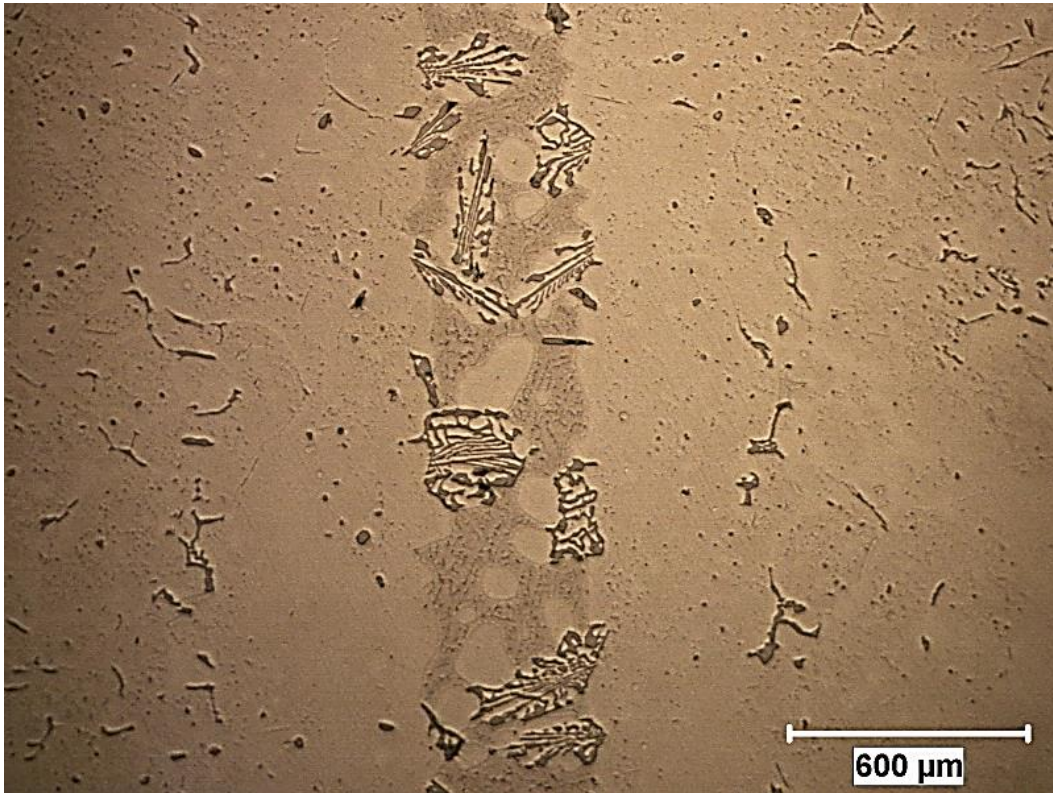


*Figure 4.21 – Optical micrograph shows eutectic constituents in joint microstructure of completely melted Haynes 282 additive powder.*

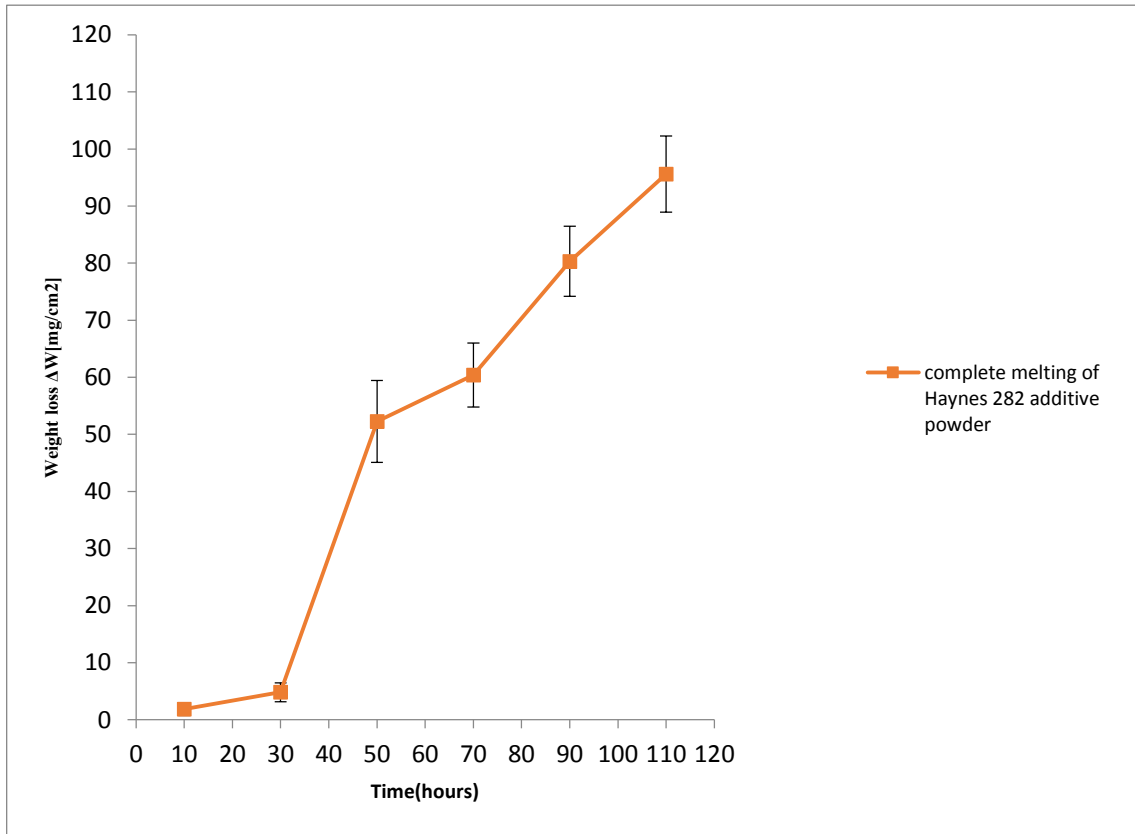


*Figure 4.22 – Hot corrosion results for brazed samples with completely melted Haynes282 additive powders.*

Therefore, despite that there is more Cr content in Haynes 282 compared to Inconel 738 additive powder, both cases show similar hot corrosion behavior. As discussed in Section 4.1, the only phase in the brazed joint that significantly lowers the hot corrosion resistance of the brazed sample is the Ni-rich boride phase, due to its low Cr content. The higher amount of Cr in Haynes 282 compared to IN738 additive powder results in less volume fraction of Ni-rich boride phase in joint microstructure of completely melted Haynes 282 compared to the joint microstructure of completely melted IN738. However, results show that the hot corrosion behavior is comparable in both cases. Therefore, even a high content of Cr in an additive powder cannot avoid the significant reduction of hot corrosion resistance in a brazed joint, if the additive powder melts completely.

#### **4.8 Effect of Brazing Cycles on Hot Corrosion Behavior of IN738 Base Metal**

In this section, experiments which were carried out to determine the effect of the brazing cycles used in this investigation on the hot corrosion behavior of Inconel 738 as the base metal are discussed. Three brazing cycles (see Figures 3.2, 3.3, 3.4) were used as the heat treatment for Inconel 738 as the base material without any brazing.

The hot corrosion experiments were performed at 900°C with a 25% NaCl + 75% Na<sub>2</sub>SO<sub>4</sub> salt mixture. Figure 4.23 shows the hot corrosion results. It can be observed that the brazing cycles at different temperatures performed in this study do not affect the hot corrosion resistance of the base metal. Although in these three heat treatments the maximum temperature is different, the last part of the heat treatment is the same for all of them (at 1100°C for 1 hour). This was purposely chosen to keep the material in the same condition at the end of each heat treatment for all the three cases.

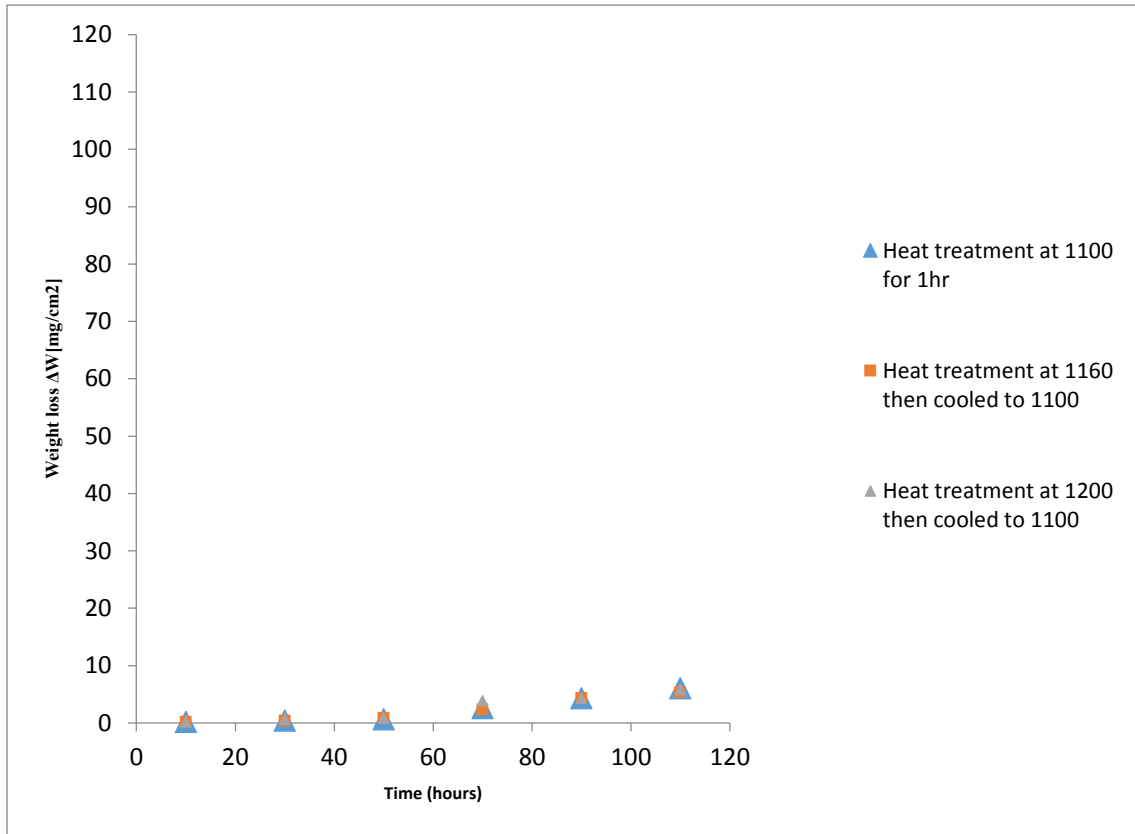


*Figure 4.23 – Hot corrosion results for un-bonded IN738 base alloy with different heat treatments.*

In the case of Inconel 738 superalloy, different heat treatments may result in dissolution of gamma-prime precipitates into the gamma matrix and then reprecipitation of gamma prime precipitates with different size, morphology and distribution depending on the heat treatment process [151]. However, heat treatments would not result in segregation of elements such as Cr and, consequently, it does not affect the hot corrosion resistance of the Inconel 738 base alloy.

## **CHAPTER 5 - CONCLUSIONS AND SUGGESTIONS FOR FUTURE WORK**

### **5.1 Summary and conclusions**

The following are the summary of the main results and conclusions from the research;

1. Brazed samples with 100% conventional brazing filler alloy showed lower hot corrosion resistance compared to the unbrazed IN738 base metal. Although the conventional brazing filler alloy contains a large amount of Cr (15%), the segregation of the alloying elements which causes the depletion of Cr in the Ni-rich boride phase results in lower hot corrosion resistance of brazed samples.
2. Utilization of a mixture of additive powder and conventional brazing filler alloy enhanced the hot corrosion resistance of brazed IN738 samples compared to brazed samples with 100% conventional brazing filler alloy due to reduced formation of Cr-depleted Ni-rich boride phase. Therefore, additive powder is beneficial in terms of hot corrosion resistance of brazed IN738 samples.
3. The beneficial effect of the use of additive powder in composite mixture was observed with the use of 3 different additive powders IN738, Nicrogap 108 and Haynes 282. The fact that Nicrogap 108 which is not as highly alloyed as IN738 and Haynes 282 provides similar resistance to hot corrosion indicates that an expensive highly alloyed additive powder is not required to obtain good hot corrosion resistance of brazed joints. As long as an adequate amount of Cr is found in the additive powder, the hot corrosion resistance is the same.
4. The use of an additive powder contributes to the hot corrosion resistance of wide-gap brazed joints. However, if the additive powder completely melts, which is possible during

brazing, this can significantly reduce the hot corrosion resistance of the brazed joint. This is due to the higher volume of liquid and correspondingly, more Ni-rich boride phases, which are depleted in Cr. This finding has not been previously reported in the literature and it is crucial to the use of additive powder for enhancing the properties of brazed materials.

5. The hot corrosion resistance of Inconel 738 brazed samples with 100% Na<sub>2</sub>SO<sub>4</sub> salt is comparatively higher than the case where NaCl is found in the salt mixture. This is because Na<sub>2</sub>SO<sub>4</sub> provides a mild environment for Cr<sub>2</sub>O<sub>3</sub> to form oxide scales, while adding NaCl to Na<sub>2</sub>SO<sub>4</sub> has a significant influence on the hot corrosion resistance of the superalloys. It is observed that NaCl is strongly aggressive on Cr<sub>2</sub>O<sub>3</sub> type oxide scales.
6. As the temperature is increased, the duration of the initiation stage is reduced, and the amount of weight loss is significantly increased. Therefore, increasing the temperature can produce a more aggressive hot corrosion environment and consequently reduce the hot corrosion resistance of brazed samples.
7. The different brazing cycles used in this study do not affect the hot corrosion resistance of the base material.

## **5.2 Suggestions for future work**

The following are some recommendations for future work based on the work in this thesis.

1. The effects of completely melted additive powders on the mechanical properties of brazed joints should be further studied.
2. The effects of brazing parameters on hot corrosion behavior of brazed joints under thermal cyclic conditions should be investigated.



3. The effect of brazing parameters on hot corrosion behavior of brazed samples under the combination of stress and load conditions should also be studied.

# Bibliography

- [1] W. F. Smith, Structure and properties of engineering alloys, Professor of engineering University of central Florida: McGraw-Hill book company series in material science and engineering, 1981.
- [2] E. Bradley, Superalloys: A technical guide, OH, United states: ASM international, 1988.
- [3] W. Miglietti, "Ductile wide gap braze repairs using precious meals for stationary gas turbine engine components," in *in proceedings of the 4th international brazing and soldering conference*, Orlando, FL, 2009.
- [4] C. Sims, Superalloys: Genesis and character, Wiley-interscience, John Wiley and Sons, 1987, pp. 3-26.
- [5] C. MA, K. SHI, Z. Y and P. XU, "Correlation between brazed joint elevated strength, microstructure and brazing processing parameter of Inconel superalloy," *Acta Metallurgica Sinica (English letters)*, vol. 24, no. 3, pp. 205-212, Jun 2011.
- [6] B. Jahnke and J. Demny, "Microstructural investigations of a nickel-based repair coating processed by liquid phase diffusion sintering," *Thin Solid Films, Metallurgical and protective coatings*, vol. 110, no. 3, pp. 225-235, 1983.
- [7] L. Zhang, J. Feng and P. He, "Brazing temperature and time effects on the mechanical properties of TiC cermet/Ag-Cu-Zn/Steel joints," *Material science and engineering: A*, vol. 428, no. 1-2, pp. 24-33, 2006.
- [8] L. Osoba and O. Ojo, "Influence of solid state diffusion during equilibration on microstructure and fatigue life of superalloy wide-gap brazements," *Metallurgical and materials transactions A, Communication*, vol. 44A, no. 9, pp. 4020-4024, 2013.
- [9] M. Donachie and S. Donachie, Superalloys: a technical guide, 2nd edn, Materials Park,OH: ASM international, 2002.
- [10] A. Ghoneim, Numerical simulation and experimental study of transient liquid phase bonding of single crystal superalloys, winnipeg, manitoba: department of mechanical and manufacturing engineering, 2011.
- [11] J. F. Hunedy, Influence of base alloy composition on processing time during transient liquid phase bonding of nickel base superalloys, Winnipeg, Manitoba: Master of Science, Department of Mechanical and Manufacturing Engineering, 2013.
- [12] O. Ojo, "on an effective approach for reducing TLP bonding time in single crystal superalloys," *Journal of materials science*, vol. 47, no. 3, pp. 1598-1602, 2012.

- [13] L. Zheng, Z. Maicang and D. Jianxin, "hot corrosion behavior of powder metallurgy Rene95 nickel-based superalloy in molten NaCl-Na<sub>2</sub>SO<sub>4</sub> salts," *Materials and Design*, vol. 32, no. 4, pp. 1981-1989, April 2011.
- [14] R. A. Rapp, "Hot corrosion of materials: a fluxing mechanism ?," *Corrosion science*, vol. 44, no. 2, pp. 209-221, February 2002.
- [15] S. H. Cho, J. M. Hur, C. S. Seo, J. S. Yoon and S. W. Park, "Hot corrosion behavior of Ni-base alloys in a molten salt under an oxidizing atmosphere," *Journal of alloys and compounds*, vol. 468, no. 1-2, pp. 263-269, January 2009.
- [16] C. Zeng and J. Lia, "Electrochemical impedance studies of molten (0.9Na,0.1K)<sub>2</sub>SO<sub>4</sub>-induced hot corrosion of the Ni-based superalloy M38G at 900 °C in air," *Electrochimica Acta*, vol. 50, no. 28, pp. 5533-5538, September 2005.
- [17] D. Deb, S. R. Iyer and V. Radhakrishnan, "A comparative study of oxidation and hot corrosion of a cast nickel base superalloy in different corrosive environments," *Materials letters*, vol. 29, no. 1-3, pp. 19-23, November 1996.
- [18] T. Sidhu, S. Prakash and R. Agrawal, "Evaluation of hot corrosion resistance of HVOF coatings on a Ni-based superalloy in molten salt environment," *Materials science and engineering: A*, vol. 430, no. 1-2, pp. 64-78, August 2006.
- [19] S. Zhao, X. Xie, G. D. Smith and S. J. Patel, "Research and Improvement on structure stability and corrosion resistance of nickel-base superalloy Inconel alloy 740," *Materials and design*, vol. 27, no. 10, pp. 1120-1127, 2006.
- [20] J. Gonzalez-Rodriguez, S. Haro, A. Martinez-Villafane, V. Salinas-Bravo and J. Porcayo-Calderon, "Corrosion performance of heat resistant alloys in Na<sub>2</sub>SO<sub>4</sub>-V<sub>2</sub>O<sub>5</sub> molten salts," *Materials science and engineering: A*, Vols. 435-436, pp. 258-265, November 2006.
- [21] M. Uusitalo, P. Vuoristo and T. Mantyla, "High temperature corrosion of coatings and boiler steels below chlorine-containing salt deposits," *Corrosion science*, vol. 46, no. 6, pp. 1311-1331, June 2004.
- [22] S. D. Nelson, S. Liu, S. Kottilingam and J. C. Madeni, "Spreading and solidification behavior of nickel wide-gap brazes," *Welding in the world*, vol. 58, no. 4, pp. 593-600, July 2014.
- [23] G. Hoppin and T. F. Berry, "Activated diffusion bonding," *Weld J*, vol. 49, no. 11, p. 505, 1970.
- [24] R. Decker, Strengthening mechanisms in nickel-base superalloys, paper from steel strengthening mechanisms, Climax Molybdenum Co., Greenwich, Conn., 1970.
- [25] C. Sims, N. Stoloff and W. Hagel, *Superalloys II: Fundamental of strengthening*, United States: Wiley-Interscience, New York, NY, 1987.
- [26] M. Durand-Charre, *The microstructure of superalloys*, CRC Press, 1998.

- [27] H. Chen, J.-M. Gong and S.-T. Tu, "Numerical modelling and experimental investigation of diffusion brazing SS304/BNi-2/SS304 joint," *Science and technology of welding and joining*, vol. 14, no. 1, pp. 32-41, 2009.
- [28] K. A. Ellison, P. Lowden and J. Liburdi, "Powder metallurgy repair of turbine components," in *ASME International Gas Turbine and Aeroengine Congress and Exposition; Manufacturing Materials and Metallurgy; Ceramics; Structures and Dynamics*, Germany, 1992.
- [29] S. Kou, *Welding metallurgy*, Second ed., Hoboken: Wiley interscience, John Wiley and sons, 2003, pp. 3-32.
- [30] K. Ferjutz and J. R. Davis, *welding, brazing and soldering*, vol. 6, ASM International, Materials Park, OH: ASM handbook, 1993.
- [31] J. N. Sanghvi, *A microstructural study of HAZ cracking in conventionally and directionally cast polycrystalline and single crystal IN-738 LC*, Winnipeg, Manitoba: University of Manitoba, 2014.
- [32] H. G. a. D. Jacobson, "Principles of soldering and brazing," in *ASM international*, Ohio, USA, 1996.
- [33] M. Haafkens and J. Matthey, "A new approach to the weldability of nickel-base As-cast and power metallurgy superalloys," *Weld. J.*, vol. 61, no. 25, pp. 25-30, 1982.
- [34] O. O. Akande, *Transient liquid phase bonding of dissimilar single crystal superalloys*, Winnipeg: University of Manitoba, 2016.
- [35] O. A. Ojo, *The effect of brazing parameters on microstructure and properties of diffusion brazed joint of IN-738 superalloy*, Winnipeg: University of Manitoba, 2002.
- [36] K. B. Grove, "Braze repair of aero engine components," *Metals and materials*, vol. 5, no. 6, pp. 341-345, 1989.
- [37] P. R. Mobley and G. S. Hopping, "Wide-gap brazing for high-temperature service," *Welding J*, vol. 40, no. 6, pp. 610-619, 1961.
- [38] S. K. Tung and L. C. Lim, "Wide gap brazing with prepacks of nickel base braze mixes," *Materials science and technology*, vol. 11, no. 9, pp. 949-954, 1995.
- [39] X. Wu, R. S. Chandel, H. P. Seow and H. Li, "Wide gap brazing of stainless steel to nickel-based superalloy," *Journal of materials processing technology*, vol. 113, no. 1-3, pp. 215-221, June 2001.
- [40] S. K. Tung and L. C. Lim, "Void formation in wide gap brazing using prepacks of nickel base braze mixes," *Materials science and technology*, vol. 10, no. 5, pp. 364-369, 1994.
- [41] F. P. L. Kavishe and T. J. Baker, "Influence of joint gap width on strength and fracture toughness of copper brazed steels," *Materials science and technology*, vol. 6, no. 2, pp. 176-181, 1990.

- [42] W. D. Zhuang and T. W. Eagar, "High temperature brazing by liquid infiltration," *Welding Journal-Including Welding Research*, vol. 76, no. 12, pp. 526-531, 1997.
- [43] J. Zhu, X. Qu and H. He, *Hunan Metall*, vol. 11, no. 6, 2004, (in Chinese).
- [44] L. C. Lim, W. Y. Lee and M. O. Lai, "Nickel base wide gap brazing with pre placement technique, Part 1 - Effect of material and process parameters on formation of microvoids," *Materials science and technology*, vol. 11, pp. 955-960, 1995.
- [45] K. A. Ellison, P. Lowden and J. Liburdi, "Repair joints in nickel -based superalloys with improved hot corrosion resistance," *The American Society of Mechanical Engineers (ASME)*, 1993.
- [46] W. F. Gale, D. A. Butts, T. Zhou and M. D. Ruscio, "Microstructure and mechanical properties of titanium aluminide wide-gap, transient liquid-phase bonds prepared using a slurry-deposited composite interlayer," *Metallurgical and materials transactions A*, vol. 33, no. 10, pp. 3205-3214, 2002.
- [47] W. D. Zhuang and a. T. W. Eagar, "Transient liquid-phase bonding using coated metal powders," *Welding Journal-Including Welding Research Supplement*, vol. 76, no. 4, p. 157s, 1997.
- [48] Y. Kwon, J. Kim, J. Moon and M. Suk, "Transient liquid phase bonding process using liquid phase sintered alloy as an interlayer material," *Journal of materials science*, vol. 35, no. 8, pp. 1917-1924, 2000.
- [49] J. Stringer, "High temperature corrosion of superalloys," *Materials science and technology* , vol. 3, no. 7, pp. 482-493, 1987.
- [50] U. F. A. Administration, "Figure 14-1. Basic components of a gas turbine engine.," *Airplane Flying Handbook*, U.S. Government Printing Office, U.S. Federal Aviation Administration FAA-8083-3A, Washington D.C.: U.S, 2004.
- [51] D. Driver, D. W. Hall and G. W. Meetham, "The development of gas turbine materials," *Applied science publishers Ltd*, pp. 1-30, 1981.
- [52] M. N. Task, The effects of composition and microstructure on the reaction behavior of MCrAlY alloys under a variety of aggressive environmental conditions, University of Pittsburgh swanson school of engineering, 2009.
- [53] N. Bornstein and W. Allen, "The Chemistry of Sulfidation Corrosion-Revisited," *Materials Science Forum*, Vols. 251-254, pp. 127-134, 1997.
- [54] N. S. Bornstein and M. A. DeCrescente, "Formation and Reactivity Thermodynamics of Sodium Sulfate with Gas Turbine Alloys.," *CORROSION*, vol. 24, no. 5, pp. 127-133, 1968.
- [55] H. Hanby and J. Beer, "Salt Deposition and Corrosion in Marine Gas Turbines.," 1969-1970.

- [56] C. Mccreath, "Hot Corrosion Site Environment in Gas Turbines," *Materials science and technology*, vol. 3, no. 7, pp. 494-500, 1987.
- [57] F. Pettit, "Hot corrosion of metals and alloys," *oxidation of metals*, vol. 76, no. 1, pp. 1-21, August 2011.
- [58] D. A. Shores and W. C. Fang, "Transport of Oxidant in Molten  $\text{Na}_2\text{SO}_4$  in  $\text{O}_2$  -  $\text{SO}_2$  -  $\text{SO}_3$  Environments," *The Electrochemical Society*, vol. 128, no. 2, pp. 346-348, 1981.
- [59] W. C. Fang and R. A. Rapp, "Electrochemical Reactions in a Pure  $\text{Na}_2\text{SO}_4$  Melt," *The Electrochemical Society*, vol. 130, no. 12, pp. 2335-2341, 1983.
- [60] H. Numata, A. Nishikata and S. Haruyama, "Electrochemical studies of corrosion of iron, nickel and nickel alloys in alkali sulfate melt," *Japan Institute of Metals, Transactions*, vol. 24, pp. 303-310, 1983.
- [61] X. Zheng and R. A. Rapp, "Electrochemical Impedance of a Platinum Electrode in Fused  $\text{Na}_2\text{SO}_4$  Melts in  $\text{SO}_2$ - $\text{O}_2$  Environments," *Journal of the Electrochemical Society*, vol. 140, no. 10, pp. 2857-2862, 1993.
- [62] F. S. Pettit and G. H. Meier, "Oxidation and hot corrosion of superalloys," *Superalloys 1984, The Metal Society AIME*, pp. 651-687, 1984.
- [63] G. Janz, *Molten Salts Handbook*, New York: Academic Press, 1967.
- [64] I. Gurrappa, "Hot Corrosion Behavior of CM 247 LC Alloy in  $\text{Na}_2\text{SO}_4$  and NaCl Environments," *oxidation of metals*, vol. 51, no. 5, pp. 353-382, June 1999.
- [65] J. Conde, E. Erdos and P. Huber, High temperature alloys for gas turbines (eds.), The Netherlands: R. Brunetaud et al., D. Reidel publishing Co., 1982, p. 99.
- [66] P. Patnaik, High temperature oxidation and hot corrosion of nickel and cobalt based superalloys, Ottawa, Canada: national research council canada (National Aeronautical Establishment), October, 1985.
- [67] R. Haque, F. Kohl, G. Fryburg, C. Stearns and W. Fielder, "Effects of temperature and oxide scale thickness on the hot corrosion of IN-738," in *InProc. of the Symp. on High Temperature Materials Chemistry, Electrochem Soc*, Denver, Colorado, 1981.
- [68] C. Giggins and F. Pettit, Hot Corrosion Degradation of Metals and Alloys - A Unified theory, No. PWA-FR-11545. Pratt and Whitney aircraft middletown ct materials engineering and research lab, 1979.
- [69] R. A. Rapp and N. Otsuka, "Effects of Chromate and Vanadate Anions on the Hot Corrosion of Preoxidized Ni by a Thin Fused  $\text{Na}_2\text{SO}_4$  Film at  $900^\circ\text{C}$ ," *Journal of electrochemical society*, vol. 137, no. 1, pp. 53-60, 1990.

- [70] R. A. Rapp, "Chemistry and electrochemistry of hot corrosion of metals," *Materials science and engineering*, vol. 87, pp. 319-327, 1987.
- [71] R. A. Rapp, "High temperature corrosion of aerospace alloys," *Neuilly-sur-seine, NATO advisory group for aerospace research and development*, pp. 147-153, 1973.
- [72] R. Burgel, J. Greossmann, O. Iusebrink, H. Mughrabi, F. Pyczak, R. Singer and A. Volek, "Development of a new alloy for directional solidification of large industrial gas turbine blades," *Superalloys*, pp. 25-34, 2004.
- [73] Y. Murata, R. Hashizume, A. Yoshinari, N. Aoki, M. Morinaga and Y. Fukui, "Alloying effects on surface stability and creep strength of nickel based single crystal superalloys containing 12 mass% Cr," *In Ninth International Symposium on Superalloys*, pp. 285-294, 2000.
- [74] E. GL, "The development of the CMSX-11B and CMSX-11C alloys for industrial gas turbine application," *Eighth International Symposium on Superalloys (Superalloys 1996)*, pp. 22-26, Sept 1996.
- [75] J. Zhang, Z. Hu, Y. Murata, M. Morinaga and N. Yukawa, "Design and development of hot corrosion resistant nickel-base single-crystal superalloys by the d-electrons alloy design theory.1.characterization of the phase-stability," *metallurgical transactions A*, vol. 24, pp. 2443-2450, 1993.
- [76] I. Okada, T. Torigoe, K. Takahashi and D. Izutsu, "Development of Ni base superalloy for industrial gas turbine," *Superalloy2004*, pp. 707-712, 2004.
- [77] J. S. Zhang, Z. Q. Hu, Y. Murata, M. Morinaga and N. Yukawa, "Design and development of hot corrosion-resistant Nickel-base single-crystal superalloys by the d-Electrons alloy design theory: Part 2. Effects of refractory metals Ti, Ta, and Nb on microstructures and properties," *Metallurgical transactions A*, vol. 24, no. 11, pp. 2451-2464, November 1993.
- [78] K. Peters, D. W. and J. S. , "Oxidation and hot corrosion of nickel-based alloys containing molybdenum," *Corrosion science*, vol. 16, no. 11, pp. 791-796, 1976.
- [79] T. Sidhu, R. Agrawal and S. Prakash, "Hot corrosion of some superalloys and role of high-velocity oxy-fuel spray coatings—a review," *Surface and Coatings Technology*, vol. 198, no. 1-3, pp. 441-446, 2005.
- [80] A. Misra, "Mechanism of  $\text{Na}_2\text{SO}_4$  - Induced Corrosion of Molybdenum Containing Nickel-Base Superalloys at High Temperatures 1. corrosion in atmospheres containing  $\text{O}_2$  only," *Journal of electrochemical society*, vol. 133, no. 5, pp. 1029-1038, 1986.
- [81] G. Fryburg, F. Kohl and C. Stearns, "Chemical Reactions Involved in the Initiation of Hot Corrosion of IN-738," *Journal of the electrochemical society*, vol. 131, no. 12, pp. 2985-2997, 1984.

- [82] Y. Zuo, R. Zhu and M. Guo, "Hot Corrosion of Some Nickel-Base Superalloys Containing Niobium," *Corrosion, the journal of science and engineering*, vol. 43, no. 1, pp. 51-55, 1987.
- [83] N. S. Bornstein, M. A. DeCrescente and H. A. Roth, "The relationship between relative oxide ion content of Na<sub>2</sub>SO<sub>4</sub>, the presence of liquid metal oxides and sulfidation attack," *Metallurgical transactions*, vol. 4, no. 8, pp. 1799-1810, August 1973.
- [84] D. Johnson, D. Whittle and J. Stringer, "Mechanisms of Na<sub>2</sub>SO<sub>4</sub>-induced accelerated oxidation," *Corrosion science*, vol. 15, no. 6-12, pp. 721-739, 1975.
- [85] T. Sidhu, S. Prakash and R. Agrawal, "Hot corrosion performance of a NiCr coated Ni-based alloy," *Scripta Materialia*, vol. 55, no. 2, pp. 179-182, July 2006.
- [86] Z. Kejun, J. Zhanpeng and H. Peiyun, "Effect of Nb on the hot corrosion behavior of Ni-base superalloy," *Zeitschrift fuer Metallkunde/Materials Research and Advanced Techniques*, vol. 80, no. 2, pp. 129-134, 1989.
- [87] I. Gurrappa, I. Yashwanth, I. Mounika, H. Murakami and S. Kuroda, "Chapter 3: the importance of hot corrosion and its effective prevention for enhanced efficiency of gas turbines," in *Gas Turbines- Materials, Modeling and performance*, INTECH (World's largest Science, Technology & Medicine Open Access book publisher), 2015, pp. 55-102.
- [88] L. F. Aprigliano, "Burner-Rig Simulation of Low-Temperature Hot Corrosion," November 1977.
- [89] N. S. Bornstein and M. A. DeCrescente, "The relationship between compounds of sodium and sulfur and sulfidation," *Transactions of the Metallurgical Society of AIME* 245, no. 9, pp. 1947-52, 1969.
- [90] D. Inman and N. S. Wrench, "Corrosion in fused salts," *British Corrosion Journal*, vol. 1, no. 6, pp. 246-250, 1966.
- [91] J. A. Goebel and F. S. Pettit, "Alloy-molten slag reactions associated with hot corrosion of alloys," *The electrochemical society*, pp. 693 in metal-slag-gas reactions and processes, 1975.
- [92] J. A. Goebel, F. S. Pettit and G. W. Goward, "Mechanisms for the hot corrosion of Nickel-base alloys," *Metallurgical transactions*, vol. 4, pp. 261-278, 1973.
- [93] A. U. Seybolt, "Sulfur diffusion through Cr<sub>2</sub>O<sub>3</sub> at 1000 degrees C," *Transactions of the metallurgical society of AIME* 242, no. 4, p. 752, 1968.
- [94] E. L. Simons, G. V. Browning and H. A. Liebhafsky, "Sodium Sulfate in Gas Turbines," *Corrosion, the journal of science and engineering*, vol. 11, no. 12, pp. 17-26, 1995.
- [95] G. J. Danek, "State-of-the-Art Survey on Hot Corrosion in Marine Gas Turbines," *Naval Engineers Journal*, vol. 77, no. 6, pp. 859-869, 1965.



- [96] A. Seybolt, "Contribution to the Study of Hot Corrosion," *Trans. Met. Soc. AIME*, 242, pp. 1955-1961, Sept. 1968.
- [97] J. A. Goebel and F. S. Pettit, "Na<sub>2</sub>SO<sub>4</sub>-induced accelerated oxidation (hot corrosion) of nickel," *Metallurgical transactions*, vol. 1, no. 7, pp. 1943-1954, July 1970.
- [98] D. Gupta and R. Rapp, "The Solubilities of NiO, Co<sub>3</sub>O<sub>4</sub> and Ternary Oxides in Fused Na<sub>2</sub>SO<sub>4</sub> at 1200°K," *Journal of the Electrochemical Society*, vol. 127, no. 10, pp. 2194-2202, 1980.
- [99] Y. Zhang and R. Rapp, "Solubility of α-Fe<sub>2</sub>O<sub>3</sub> in fused Na<sub>2</sub>SO<sub>4</sub> at 1200 K," *Journal of the Electrochemical Society*, vol. 132, no. 3, pp. 734-735, 1985.
- [100] Y. Zhang and R. Rapp, "Solubilities of α-Fe<sub>2</sub>O<sub>3</sub> and Fe<sub>3</sub>O<sub>4</sub> in Fused Na<sub>2</sub> SO<sub>4</sub> at 1200 K," *Journal of the Electrochemical Society*, vol. 132, no. 10, pp. 2498-2501, 1985.
- [101] Y. Zhang, "Solubilities of Cr<sub>2</sub>O<sub>3</sub> in Fused Na<sub>2</sub>SO<sub>4</sub> at 1200 K," *Journal of the Electrochemical Society*, vol. 133, no. 3, pp. 655-657, 1986.
- [102] P. Jose, D. Gupta and R. Rapp, "Solubility of α-Al<sub>2</sub>O<sub>3</sub> in fused Na<sub>2</sub>SO<sub>4</sub> at 1200 K," *Journal of the Electrochemical Society*, vol. 132, no. 3, pp. 735-737, 1985.
- [103] D. Shi and R. Rapp, "The Solubility of SiO<sub>2</sub> in Fused Na<sub>2</sub>SO<sub>4</sub> at 900°C," *Journal of electrochemical society*, vol. 133, pp. 849-580, 1986.
- [104] M. Deanhardt and K. Stern, "Solubility Products of Metal Oxides in Molten Salts by Coulometric Titration of Oxide Ion Through Zirconia Electrodes," *Journal of electrochemical society*, vol. 128, pp. 2577-2582, 1982.
- [105] N. Birks, G. Meier and F. Pettit, Introduction to the High Temperature Oxidation of metals, 2. ed., Ed., New York: Cambridge University Press, 2006.
- [106] R. A. Rapp and K. S. Goto, "The hot corrosion of metals by molten salts," *Physical Electrochemistry Division, Electrochemical Society*, vol. 81, no. 10, p. 159, 1981.
- [107] N. S. Bornstein and M. A. DeCrescente, "The Role of Sodium in the Accelerated Oxidation Phenomenon termed Sulfidation," *Metallurgical Transactions*, vol. 2, no. 10, pp. 2875-2883, 1971.
- [108] R. A. Rapp and N. Otsuka, "The Role of Chromium in the Hot Corrosion of Metals," *ECS transactions*, vol. 16, no. 49, pp. 271-282, 2009.
- [109] D. Shi and R. Rapp, "Electrochemical studies of Na<sub>2</sub>CrO<sub>4</sub>-Na<sub>2</sub>SO<sub>4</sub> melts at 1200 K," *Materials and corrosion*, vol. 41, no. 5, p. 215–226, May 1990.
- [110] N. Bornstein, M. DeCrescente and H. Roth, "Accelerated Corrosion in Gas Turbine engines," in *Gas Turbine Materials Conference*, Washington, D.C., 1972.

- [111] J. Conde and G. Wareham, "Aspects of the Mechanisms of Hot Corrosion in Marine gas turbines," in *The 2nd Conference on Gas Turbine Materials in a Marine environment*, 1974.
- [112] K. L. Luthra, "Low temperature hot corrosion of cobalt-base alloys: Part II. Reaction mechanism," *Metallurgical Transactions A*, vol. 13, no. 10, p. 1647 and 1843, 1982.
- [113] R. H. Barkalow and F. S. Pettit, "On the oxidation mechanisms for hot corrosion of CoCrAlY coatings in marine gas turbines," in *Proceedings of the 14th Conference on Gas Turbine Materials in a Marine Environment*, (Naval Sea Systems Command, Annapolis, MD), 1979.
- [114] K. T. Chiang, F. S. Pettit and G. H. Meier, "High Temperature Corrosion," *NACE-6*, p. 519, 1983.
- [115] K. Luthra and D. Shores, "Mechanism of Na<sub>2</sub>SO<sub>4</sub> Induced Corrosion at 600°-900°C," *Journal of electrochemical society*, vol. 127, no. 10, pp. 2202-2210, 1980.
- [116] D. Wortman, R. Fryxell and I. Bessen, "A Theory for Accelerated Turbine Corrosion at intermediate temperatures," in *The 3rd Conference on Gas Turbine Materials in a Marine environment*, 1976.
- [117] D. W. McKee, D. A. Shores and K. L. Luthra, "The effect of SO<sub>2</sub> and NaCl on high temperature hot corrosion," *Journal of the Electrochemical Society*, vol. 125, no. 3, pp. 411-419, 1978.
- [118] L. Yang, C. Bo, W. Junwei, W. Zhiping and L. Wensheng, "Corrosion behavior of Cr, Fe and Ni based superalloy in molten NaCl," *rare metal materials and engineering*, vol. 43, no. 1, pp. 17-23, 2014.
- [119] X. Wang, L. Xin, F. Wang, S. Zhu, H. Wei and X. Wang, "Influence of sputtered nanocrystalline coating on oxidation and hot corrosion of a nickel-based superalloy M951," *Journal of Materials Science & Technology*, vol. 30, no. 9, pp. 867-877, 2014.
- [120] L. Yuan and H. M. Wang, "Hot corrosion behaviors of a Cr<sub>13</sub>Ni<sub>5</sub>Si<sub>2</sub>-based metal silicide alloy in Na<sub>2</sub>SO<sub>4</sub>+ 25wt.% K<sub>2</sub>SO<sub>4</sub> and Na<sub>2</sub>SO<sub>4</sub>+ 25wt.% NaCl molten salts," *Intermetallics*, vol. 18, no. 3, pp. 324-329, 2010.
- [121] I. Gurrappa, "Protection of titanium alloy components against high temperature corrosion," *Materials Science and Engineering: A*, vol. 356, no. 1, pp. 372-380, 2003.
- [122] I. Gurrappa, "Mechanism of degradation of titanium alloy IMI 834 and its protection under hot corrosion conditions," *Oxidation of metals*, vol. 59, no. 3-4, pp. 321-322, 2003.
- [123] I. Gurrappa, "Influence of alloying elements on hot corrosion of superalloys and coatings: necessity of smart coatings for gas turbine engines," *Materials science and technology*, vol. 19, no. 2, pp. 178-183, 2003.
- [124] I. Gurrappa, "Effect of aluminum on hot corrosion resistance of MCrAlY-based bond coatings," *Journal of materials science letters*, vol. 20, no. 24, pp. 2225-2229, 2001.

- [125] I. Gurrappa, "Identification of hot corrosion resistant MCrAlY based bond coatings for gas turbine engine applications," *Surface and coatings technology*, vol. 139, no. 2, pp. 272-283, 2001.
- [126] I. Gurrappa, "Hot corrosion of protective coatings," *Materials and Manufacturing Processes*, vol. 15, no. 5, pp. 761-773, 2000.
- [127] I. Gurrappa, "Overlay coatings degradation—an electrochemical approach," *Journal of materials science letters*, vol. 18, no. 21, pp. 1713-1717, 1999.
- [128] I. Gurrappa, "Thermal barrier coatings for hot corrosion resistance of CM 247 LC superalloy," *Journal of materials science letters*, vol. 17, no. 15, pp. 1267-1269, 1998.
- [129] I. Gurrappa, "Hot corrosion behavior of Nimonic-75," *High temperature and materials science*, vol. 38, no. 2-3, pp. 137-144, 1997.
- [130] I. Gurrappa, "Surface engineering for hot-corrosion resistance," *Corrosion prevention & control*, vol. 44, no. 6, pp. 151-178, 1997.
- [131] I. Milošev and B. Navinsek, "A corrosion study of TiN (physical vapour deposition) hard coatings deposited on various substrates," *Surface and Coatings Technology*, vol. 63, no. 3, pp. 173-180, 1994.
- [132] G. Liua, F. Yu, J. Tian and J. Ma, "Influence of pre-oxidation on the hot corrosion of M38G superalloy in the mixture of Na<sub>2</sub>SO<sub>4</sub>-NaCl melts," *Materials Science and Engineering: A*, vol. 496, no. 1-2, pp. 40-44, 2008.
- [133] Z. Bao, Q. Wang, W. Li, X. Liu, J. Gong, T. Xiong and C. Sun, "Preparation and hot corrosion behaviour of an Al-gradient NiCoCrAlYSiB coating on a Ni-base superalloy," *Corrosion Science*, vol. 51, no. 4, pp. 860-867, 2009.
- [134] G. Liua, M. Li, Y. Zhou and Y. Zhang, "Hot corrosion behavior of Ti<sub>3</sub>SiC<sub>2</sub> in the mixture of Na<sub>2</sub>SO<sub>4</sub>-NaCl melts," *Journal of the European Ceramic Society*, vol. 25, no. 7, pp. 1033-1039, 2005.
- [135] G. El-Awadi, S. Abdel-Samad and E. S. Elshazly, "Hot corrosion behavior of Ni based Inconel 617 and Inconel 738 superalloys," *Applied Surface Science*, vol. 378, pp. 224-230, 2016.
- [136] K. Ohsasa, T. Narita and T. Shinmura, "Numerical modeling of the transient liquid phase bonding process of Ni using Ni-B-Cr ternary filler metal," *Journal of Phase Equilibria*, vol. 20, no. 3, pp. 199-206, 1999.
- [137] C. T. Sims and W. C. Hagel, *The Superalloys - vital high temperature gas turbine materials for aerospace and industrial power*, New York: John Wiley & Sons, 1972.
- [138] J. M. Ferguson, "Hot corrosion of some nickel based alloys in a laboratory test (Dean test)," Central electricity research laboratories, 1980.

- [139] K. Page and R. Taylor, "Turbine corrosion - Rig evaluation and engine experience," *Deposition and corrosion in gas turbines*, pp. 350-375, 1973.
- [140] Y. Bourhis and C. John, "Na<sub>2</sub>SO<sub>4</sub> - and NaCl - induced hot corrosion of six nickel base superalloys," *Oxidation of Metals*, vol. 9, no. 6, pp. 507-528, 1975.
- [141] G. C. Fryburg, F. J. Kohl and C. A. Stearns, "Hot corrosion studies of four nickel-base superalloys: B-1900, NASA-TRW VIA, 713C and IN738," in *NASA-TM-X-73479*, Jan 01, 1976.
- [142] E. Erdoes and E. Denzler, "On the oxidation and hot corrosion of IN 713 LC, IN 738 LC, and IN 939. Behaviour of high temperature alloys in aggressive environments," *Metals Society*, pp. 455-463, 1979.
- [143] P. Cavallotti, U. Ducati, D. Colombo and G. Donzelli, "Some Mechanisms of Scale Degradation in Hot Corrosion Experiments. In Behaviour of High Temperature Alloys in Aggressive Environments," The Netherlands, 1979.
- [144] C. J. Grant, "Electrochemical corrosion measurements on IN738 and FSX 414 gas turbine alloys in molten sulphates," *British corrosion journal*, vol. 14, no. 1, pp. 26-32, 1979.
- [145] M. Kawakami, K. Goto, R. Raba and M. Kajiyama, "Mechanism of Accelerated Oxidation of Heat Resistant Super Alloys Induced by Molten Salt Deposition," *Tetsu-to-Hagane*, vol. 65, no. 7, pp. 811-819, 1979.
- [146] S. Y., "Accelerated oxidation rate of chromium induced by sodium chloride," *Oxidation of Metals*, vol. 27, no. 5-6, pp. 315-332, 1987.
- [147] M. Li, X. Sun, W. Hu, H. Guan and S. Chen, "Hot Corrosion of a Single Crystal Ni-Base Superalloy by Na-Salts at 900°C," *Oxidation of Metals*, vol. 65, no. 1, p. 137-150, February 2006.
- [148] W. J.M., D. P.H. and L. Y, "An investigation of the oxidation dynamics of an Fe-Cr-Ni-Ti superalloy," *Journal of Chinese Society of Corrosion and Protection*, vol. 6, no. 2, p. 149, 1986.
- [149] J. Johnson, J. Nicholls, R. Hurst and P. Hancock, "The mechanical properties of surface scales on nickel-base superalloys—II. Contaminant corrosion," *Corrosion Science*, vol. 18, no. 6, pp. 543-553, 1987.
- [150] T. T. Huang and G. H. Meier, "An investigation of the initiation stage of hot corrosion in Ni-base alloys," NASA technical reports server (NTRS), United States, Jan 01, 1979.
- [151] I. Guzmán, A. Garza, F. Garcia, J. Acevedo and R. Méndez, "Effect of Heat Treatment Solution on the Size and Distribution of Gamma Prime ( $\gamma'$ ) of Super-alloy INCONEL 738," in *In MRS Proceedings*, Cambridge University Press, 2012.